COMPUTER AIDED ENGINEERING OF AN UNMANNED UNDERWATER VEHICLE

A THESIS SUBMITTED TO
THE GRADUATE SCHOOL OF NATURAL AND APPLIED SCIENCE
OF
MIDDLE EAST TECHNICAL UNIVERSITY

BY

NECMETTİN CEVHERİ

IN PARTIAL FULFILLMENT OF THE REQUIREMENTS
FOR
THE DEGREE OF MASTER OF SCIENCE
IN
MECHANICAL ENGINEERING

JULY 2009

Approval of the thesis:

COMPUTER AIDED ENGINEERING OF AN UNMANNED UNDERWATER VEHICLE

submitted by **NECMETTİN CEVHERİ** in partial fulfillment of the requirements for the degree of **Master of Science in Mechanical Engineering Department, Middle East Technical University** by,

Prof. Dr. Canan Özgen _______________
Dean, Graduate School of **Natural and Applied Science**

Prof. Dr. Suha Oral _______________
Head of Department, **Mechanical Engineering**

Prof. Dr. M. Haluk Aksel _______________
Supervisor, **Mechanical Engineering Dept., METU**

Prof. Dr. S. Kemal İder _______________
Co-Supervisor, **Mechanical Engineering Dept., METU**

Examining Committee Members:

Instr. Dr. Tahsin Çetinkaya _______________
Mechanical Engineering Dept., METU

Prof. Dr. M. Haluk Aksel _______________
Mechanical Engineering Dept., METU

Prof. Dr. S. Kemal İder _______________
Mechanical Engineering Dept., METU

Asst. Prof. Dr. Cüneyt Sert _______________
Mechanical Engineering Dept., METU

Prof. Dr. M. Kemal Leblebicioğlu _______________
Electrical and Electronics Engineering Dept., METU

Date: _______________

PLAGIARISM

I hereby declare that all information in this document has been obtained and presented in accordance with academic rules and ethical conduct. I also declare that, as required by these rules and conduct, I have fully cited and referenced and results that are not original to this work.

Name, Last Name : NECMETTİN CEVHERİ

Signature :

ABSTRACT

COMPUTER AIDED ENGINEERING OF AN UNMANNED UNDERWATER VEHICLE

Cevheri, Necmettin
M.Sc., Department of Mechanical Engineering
Supervisor: Prof. Dr. M. Haluk Aksel
Co-Supervisor: Prof. Dr. S. Kemal İder

July 2009, 150 pages

Hydrodynamic and thermal analyses performed during the conceptual design of an unmanned underwater vehicle are presented in this study. The hull shape is determined by considering alternative shapes and the dimensions are determined from the internal arrangement of components. Preliminary thermal analyses of the watertight section are performed with a commercial software called FLUENT to check the risk of over-heating due to the heat dissipation of devices.

Performance of the proposed hull design is analyzed by FLUENT. Before simulations of the vehicle, validation studies are performed. Models 4159, 4158 and 4154 of Series 58 are chosen as the experimental reference. Their total resistance coefficients are compared with the results of the validations analyses. Mesh densities, turbulence models, near wall modeling approaches and inlet turbulence intensities are varied to understand their effects on the accuracy of predictions. A suitable turbulence modeling approach is chosen to analyze forward and vertical motions of the vehicle to check whether speed requirements are fulfilled. Hull configurations with and without appendages are used to observe their effects on total drag. It is observed that the proposed design satisfies speed requirements of the vehicle and no overheating is expected in the watertight section.

Keywords: Unmanned underwater vehicles (UUV), underwater robots, CFD, drag, FLUENT, turbulence modeling

ÖZ

BİR İNSANSIZ SUALTI ARACININ BİLGİSAYAR DESTEKLİ TASARIMI VE ÜRETİMİ

Cevheri, Necmettin
Yüksek Lisans, Makina Mühendisliği Bölümü
Tez Yöneticisi: Prof. Dr. M. Haluk Aksel
Ortak Tez Yöneticisi: Prof. Dr. S. Kemal İder

Temmuz 2009, 150 sayfa

Bir insansız sualtı aracının kavramsal tasarımı esnasında gerçekleştirilen hidrodinamik ve ısıl analizler bu tezin ana konusunu oluşturmaktadır. Gövdenin şekline çeşitli sualtı aracı şekillerinin değerlendirilmesi sonucu karar verilmektedir. Boyutlar ise cihazların gövde içine yerleşiminden sonra ortaya çıkmaktadır. Elektronik ekipmanın bulunduğu bölmenin ısınmasına dair analizler ticari bir hesaplamalı akışkanlar dinamiği yazılımı olan FLUENT yardımı ile yapılmaktadır.

Önerilen tasarımın performans analizleri de FLUENT ile yapılmaktadır. Analizlerden önce bazı doğrulama çalışmaları gerçekleştirilmiştir. Bu çalışmalarda Series 58 adı verilen bir grup gövdeden 4159, 4158 ve 4154 modelleri deneysel referans olarak alınmaktadır. Bu modellerin toplam direnç katsayıları yapılan analiz sonuçları ile kıyaslanmaktadır. Bu analizler esnasında ağ yoğunluğu, türbülans modeli, duvar yakınındaki akışı modelleme yöntemleri ve giriş türbülans yoğunluğu değiştirilerek çözümlere etkileri gözlemlenmektedir. Uygun bir türbülans modeli seçilerek aracın ileri ve yukarı yönde hareketleri incelenmekte ve verilen tasarım kıstaslarını sağlaması şartı kontrol edilmektedir. Gövde çıkıntılarının dahil edildiği ve edilmediği modeller yaratılarak bu çıkıntıların toplam sürüklenme kuvvetine etkileri gözlemlenmektedir. Analizler sonucu gövdenin istenen hız kriterlerini sağladığı ve sızdırmaz orta bölümde aşırı ısınma oluşmadığı sonucuna varılmaktadır.

Anahtar Kelimeler: İnsansız sualtı aracı, sualtı robotu, Sualtı Robotu, hesaplamalı akışkanlar dinamiği, sürüklenme, FLUENT, türbülans modelleme

Dedicated to my family and Mehtap…

ACKNOWLEDGEMENTS

I would like to express my gratitude to my thesis supervisor Prof. Dr. M. Haluk Aksel and my thesis co-supervisor Prof. Dr. S. Kemal İder for their support, guidance and criticism throughout my studies.

This thesis work is based on the Unmanned Underwater Vehicle (ULİSAR) Project. I would like to thank to Prof. Dr. M. Kemal Leblebicioğlu, the supervisor of the project, for this valuable opportunity and his leadership throughout the project. The contributions from project group members Prof. Dr. Levend Parnas, Assist. Prof. Dr. Afşar Saranlı, Emre Ege, Hüseyin Yiğitler, Kadir Isıyel, Alper Kılıç and Mine Cüneyitoğlu were invaluable for the project and for the thesis study.

This project was funded by the Scientific and Technological Research Council of Turkey. I would like to express my appreciation for their support and motivation throughout the project.

Manufacturing was performed by Barış Elektrik Endüstrisi Inc. I would like to thank to Fikret Şenel, Bora Balya, Onur Miskbay and Ergül Soyçeken for their efforts and suggestions.

I would like to express my appreciation to Emre Öztürk and Özgün Güler for their help with the CFD simulations and Necati Karaismailoğlu for his help with the format of the thesis.

I would like to thank to Mehtap Çakmak for her continuous support, faith and love. Finally I would like to express my deepest gratitude to my family for their encouragement, understanding and support during my studies.

TABLE OF CONTENTS

CHAPTERS

LIST OF TABLES

TABLES

LIST OF FIGURES

FIGURES

NOMENCLATURE

A	Area, m^2
C_d	Drag force coefficient
C_μ	Modeling constant
C_P	Surface pressure coefficient
C_t	Total resistance coefficient
D	Diameter, m
f	Body force per unit mass, m/s^2
k	Turbulence kinetic energy, m^2/s^2
k_p	Kinetic energy at point P, m^2/s^2
L	Length of the vehicle, m
l	Characteristic length, m
p	Pressure, N/m^2
p_{ref}	Reference pressure, N/m^2
R	Total resistance, N
Re	Reynolds Number
Re_y	Turbulent Reynolds number
S	Wetted surface area, m^2
t	Time, s
U	Free stream velocity, m/s
u	Velocity in x direction, m/s
u_τ	Friction velocity, m/s
u^+	Non-dimensional velocity
u'	Fluctuation of velocity in x direction, m/s
v	Velocity in y direction, m/s
v'	Fluctuation of velocity in y direction, m/s
w	Velocity in z direction, m/s
w'	Fluctuation of velocity in z direction, m/s
y_p	Distance from the point P, m

y^+	Wall yplus
y^*	Wall ystar

Greek Letters

ε	Turbulent kinetic energy dissipation rate, m^2/s^3
μ	Dynamic viscosity, kg/m.s
μ_{lam}	Laminar viscosity, kg/m.s
μ_t	Turbulent (eddy) viscosity, kg/m.s
ρ	Density of the fluid, kg/m^3
τ	Shear stress, N/m^2
ω	Turbulent kinetic energy specific dissipation rate, 1/s

CHAPTER 1

INTRODUCTION

Unmanned underwater vehicles (UUV's) can be defined simply as robots which operate underwater. These robots do not require an operator on the vehicles and depending on their level of intelligence they can operate with little or no intervention by the operator on the surface to follow a pre-defined mission. To achieve this mode of operation, these vehicles carry various equipments. They need navigation systems, sensors, energy systems, a main computer, communication devices and an appropriate mechanical design.

First of all, navigation systems are obligatory to determine the location with respect to a certain reference point. Early vehicles counted on dead reckoning which determines the position of the vehicle using the initial position, speed and time data [1]. In this method, a suitable time interval is selected and the displacement of the vehicle within this interval is found by the speed and time while the final position is derived by adding this displacement to the initial position. Inertial Navigation Systems (INS) are more commonly used in modern vehicles. These systems work similar to dead reckoning. They include motion sensors like accelerometers and gyroscopes to determine the final position and orientation by integration process. Some modern vehicles take advantage of a Global Positioning System (GPS) to determine the current position and update their INS.

Secondly, various sensors are required depending on operation requirements. In fact, sensors are very important for these vehicles because they can be critical for the functioning of the vehicle and even the purpose of the vehicle may be carrying those sensors as payloads for experimentation and research. Sensors used in these vehicles can be classified into two categories: motion sensors and underwater research/experimentation sensors [2]. Motion sensors are primarily used by the navigation systems. Accelerometers and gyroscopes are well-known examples for this category. On the other hand, experimentation and research sensors are primarily used for collecting underwater data. Radiation sensors, Conductivity/Temperature/Depth (CTD) sensors, pressure-sensitive depth sensors, digital cameras, hydrology sensors and environmental sensors are common examples for this category [3]. A sensor which is used by almost all vehicles is the side scan sonar. These sonars scan the environment in order to detect obstacles on the route of the robot and map the seabed. Later on, depending on the level of the autonomy of the robot, obstacle avoidance algorithms can be generated. Acoustic transducers are also used for mapping regions and determining obstacles which are close to the vehicle while side scan sonars are used for larger areas.

Thirdly, rechargeable energy systems are vital for these equipments to function. Unmanned underwater vehicles which are not connected to the surface ship with a tether carry their energy sources on their body so that they do not have energy transmitting underwater cables. Throughout unmanned underwater vehicles history, various types of energy sources were used. Lead acid and silver-zinc batteries were frequently used in the early history. Later on, lithium-ion and lithium-polymer batteries began to be used for current vehicles being developed. NiMH batteries are another source which is being commonly used in modern vehicles. Besides these technologies, modern techniques like fuel-cells and solar energy are investigated for future vehicles. An example of a solar-powered robot, SAUV, is developed by the Falmouth Scientific, Inc. (FSI) in cooperation with the Autonomous Undersea Systems Institute (AUSI) and Technology Systems Inc. (TSI) [4]. The vehicle possesses solar cells on the body. When the vehicle needs to recharge batteries, it surfaces and resides on the surface until the batteries are charged. This distinctive feature allows on-vehicle recharging of energy systems; therefore, the vehicle can operate for weeks to months while untethered underwater vehicles can operate for a few hours. These vehicles are convenient for long term operations like stationkeeping. For long-term operations, fuel cell technology is also being used in modern vehicles. Urashima, which is considered to be the first vehicle to be powered by fuel cells, is developed in Japan in March 2003 [5]. The vehicle is powered via Polymer Electrolyte Fuel Cell (PEFC) system. In their sea trials in 2004, they achieved a continuous autonomous operation of 43 hours at a depth of 800 m and had a journey of 220 km. They also claim that the vehicle can operate up to 300 km autonomously. It is obvious that fuel cell technology is extremely useful for long-term operations.

Almost all unmanned underwater vehicles need a communication device for human intervention no matter what the level of autonomy is. In cases where this intervention is desired to be wireless, acoustic modems are used. These modems work in pairs; one modem is placed on the vehicle while the other is placed on the surface buoy. The limitation is that these modems have narrow bandwidths and it makes is almost impossible to transmit data continuously. Receiving data when the vehicle surfaces or when it is recovered are considered as remedies for the insufficient bandwidth [6]. Nonetheless, underwater communication still remains as a major issue to be solved for the improvement of vehicles. Certainly, these robots require control units to coordinate the operation of sensors, navigations systems, communication devices and energy systems. This is accomplished with a main CPU. The main CPU is usually stacks of standard PC-104 electronic cards which are housed in a water-tight section.

Finally, a body with an appropriate mechanical design is necessary for holding all of these systems together. Mechanical design has many steps like hull design, internal design, manufacturing and testing. In this thesis, hydrodynamic and thermal simulations performed during the conceptual design of an unmanned underwater vehicle are presented.

1.1 Classification of Underwater Systems

Underwater systems can be divided into two categories as manned systems and unmanned systems [1]. This classification is seen in Table 1.1. Submarines and non-military purpose underwater vehicles are well-known examples of manned vehicles. On the other hand, unmanned systems can be divided into four categories depending on their autonomy level. First category is simple submersibles. These are simple submersibles which float separately or towed behind a ship or submarine via cable. They are simple vehicles that may carry sensors or other devices. An acoustic jammer which is used for defense against torpedoes can be given as an example for this category. The second type is Remotely Operated Vehicles which is abbreviated as ROV's. ROV's are underwater robots that are connected to a ship or submarine with a tether. This tether is used for both transmitting power to the robot and communication with the robot. In some systems the power source may be on the vehicle so no tether for power transmission is necessary. However, they may not be completely autonomous and need some type of a communication system. Such systems are called Unmanned Untetherred Vehicles. Finally, systems that carry their power on-board, that do not require any tether and that can operate autonomously without any operator intervention are called Autonomous Underwater Vehicles (AUV).

Tablo 1.1 Classification of underwater systems [1]

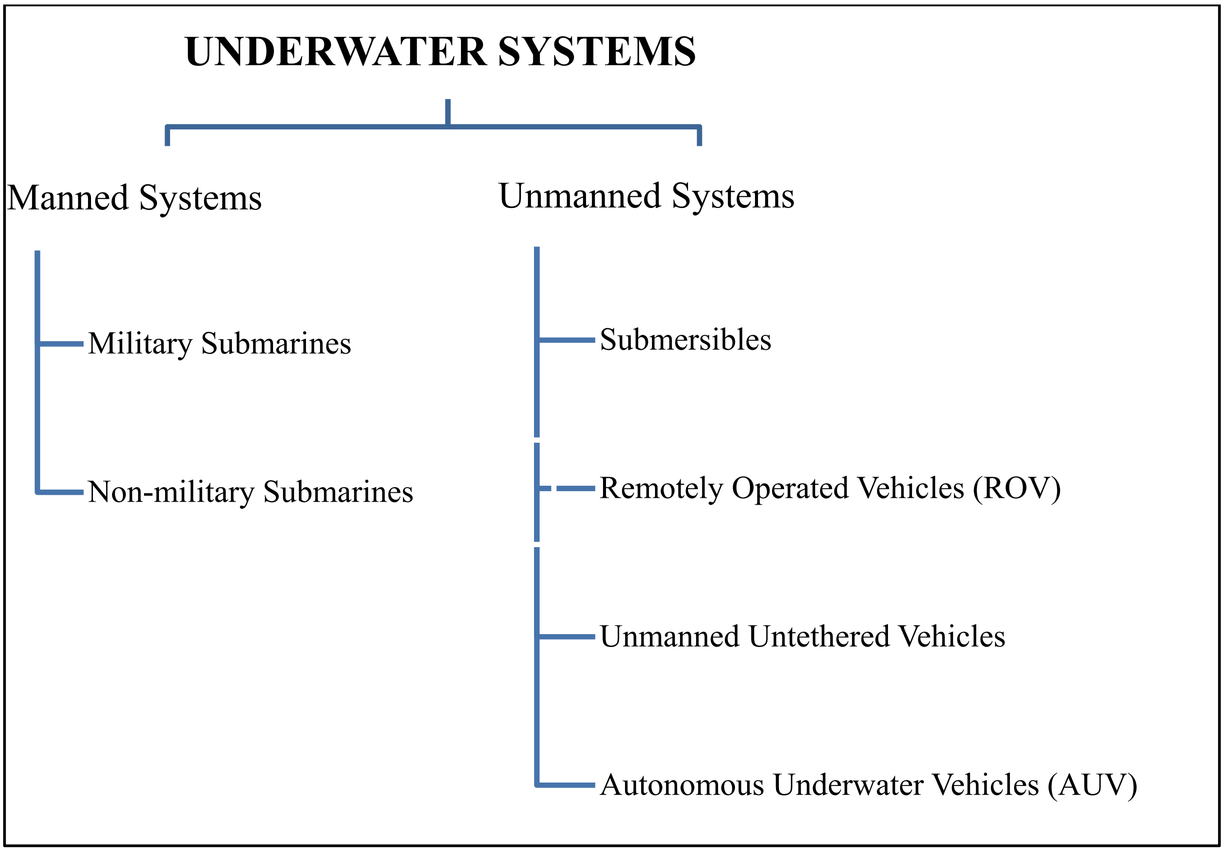

1.2 Purposes of AUV’s

Unmanned underwater vehicles are underwater robots which are capable of carrying out various underwater tasks without the need of an operator on the robot. They can be modified and equipped with tools like robot arms, cameras and research/experimentation sensors depending on the mission. ROV’s require a tether to communicate with the operator on the surface; on the other hand, AUV’s can complete a pre-defined mission autonomously without any human intervention. Nevertheless, all unmanned underwater vehicles are advantageous for underwater missions, no matter what the level of autonomy is. Today, unmanned underwater vehicles are mainly used for commercial, military and scientific purposes.

Commercial use of unmanned underwater vehicles has begun in the beginning of 2000s and has been intensifying since then. The most common commercial use is in oil and gas industry [7]. Inspection of the seabed for pipeline and underwater infrastructures along with the maintenance and repair of these structures are basic tasks that are executed. Utilization of AUV’s or ROV’s for these missions results in a significant decrease in expenditures. At present, ROV’s and deep tow systems are default tools for underwater survey operations rather than AUV’s. However, a comparison study performed in C&C Technologies by Thomas S. Chance, Art A. Kleiner, and Jay G. Northcutt exemplifies the advantage of AUV’s [8]. It is mentioned that ROV’s and especially deep tow Systems are default tools for underwater survey; however, they have serious deficiencies. Their operating depths are limited by tether length. A 10000 meter tether length not only brings up storage problems, but also limits the speed and maneuvering capabilities. On the other hand, AUV’s overcome these deficiencies. A comparison in this study exemplifies that for a 45 mile pipeline survey in Gulf of Mexico, the use of AUV instead of a deep tow system reduces survey cost from $707,200 to $291,325 which means a 59% recovery on expenses. The emphasis on the use of unmanned vehicles in oil/gas industry is also expected to increase because companies are heading towards deeper parts of the ocean to discover new oil and gas resources. Besides the oil/gas industry, telecommunication industry makes use of this technology for the inspection and installation of fiber optic cables.

Unmanned underwater vehicles are frequently used for military applications as well. The majority of military applications are mine countermeasures. These vehicles can both search for underwater mines and destruct them if detected. It is obvious that the risk of losing staff for mine destruction is minimized. Other than mine countermeasures; reconnaissance and survey are military actions that are executed. At present, they are not used directly for battles and their roles are limited. However, there is a tendency to increase their military capabilities. For this purpose, in December 2003 U.S. Navy prepared their new AUV master plan [9]. In this plan, they state that their aim is to increase the capabilities of these vehicles for future battle situations. Some of the potential military duties in the future are attacking, defense, delivering military payload, anti-submarine warfare, patrol, mine countermeasures, forming underwater communication links, surveillance and tactical oceanography.

Academic organizations have been using UUV's for scientific purposes for a long time. The aim is to gather underwater data which would be difficult to get with conventional methods. These can be oceanographic data like ocean current information, species concentration or seabed mapping. Moreover, behavior of underwater animals and plant life can be inspected. Underwater archeology is also another field where scientists make use of UUV's.

1.3 History of UUVs

Although the history of UUVs commences from 1960s, the concept of developing underwater submersibles is much older. The first example of manned submersibles is the "Turtle", the first American Submarine which was built in 1775. As the submarine technology progressed, a need for building unmanned submersibles for the purpose of launching explosives to enemies grew. As a consequence, torpedoes were developed in the late nineteenth century. Torpedoes are, in fact, assumed to be the first examples of unmanned underwater vehicles. The first self-propelled torpedo was developed by Robert Whitehead in 1866 [10]. The first torpedoes were using compressed air supply for powering and by 1870 they could maintain a cruising speed of about 6 knots. Whitehead continued his torpedo experiments in Austrian Navy. In the meantime United States Navy also started a torpedo program. Until the World War 1, military rivalry forced navies of the world to put emphasis on the improvement of torpedo technology. Depth control, gyroscope and radio guidance were added to torpedoes. Moreover, propulsion systems were improved and a cruising speed of 30 knots was achieved in 1890. Prior to World War 1, war noses and Anti-Circular Run (ACR) systems were utilized. ACR system prevented torpedoes to explode if they are headed to the ship or submarine itself. In fact, these attempts were for the sake of adding intelligence to torpedoes and they can be accepted as the first steps of "Autonomy" for torpedoes.

Another important step in adding intelligence to torpedoes was the development of the "Homing Torpedo" during the World War 2. The idea behind it is that the torpedo would try to sense any underwater noise like the noise of the propeller of a submarine before attacking. Later on when the enemy ship or submarine is detected, the torpedo would hit. For this purpose, Mine MK 24 was developed which showed good success in the latter years of the World War 2. After this point, there was a tendency to improve the homing characteristics of torpedoes in order to develop more intelligent torpedoes.

While torpedo technology was progressing, a new technology of unmanned submersibles originated in 1960s when ROV's were developed. ROV's are unmanned underwater vehicles where human intervention and power transmission is accomplished with a tether from a surface vessel where a human operator or control unit is present. Unlike torpedoes, ROV's house more thrusters in different locations and orientations; hence, have more degrees of freedom and this ability in combination with the human intervention enables ROV's to perform difficult underwater tasks. Therefore, ROV's have been used for various tasks like underwater rescue operations, underwater archeology, mine destruction and etc. since 1960's.

Even though ROV's make it possible to reach underwater locations which would have been impossible to do with human divers and performed various missions, there are several drawbacks. Underwater tethers are necessary and the operation depth is limited to tether length. The necessity of a surface vessel and continuous human intervention is also undesired. The motivation to overcome these drawbacks led to the development of AUV's.

The first example of AUV's is believed to be the Special Purpose Underwater Research Vehicle, SPURV, which was developed by the University of Washington in

1957. It had an operating depth of more than 3000 meters and could maintain a cruising speed of 4 knots. Except SPURV, it is seen in the literature that most of the early AUV’s were developed in 1970s [1]. SPURV2 was developed by the University of Washington, EAVE by the University of Hampshire, SKAT, L1 and L2 by the Russian Academy of Sciences in 1970s. Moreover, Massachusetts Institute of Technology (MIT) launched its AUV program in 1973 even though the Autonomous Underwater Vehicle Laboratory was truly established in 1988. In 1970s, several experiments with these AUV models were performed in order to learn more about AUV’s and their potential. In this era, the progress of the AUV technology was slower compared to ROV technology. The main reason is that AUV’s needed new technologies for their development more than ROV’s. AUV’s do not have tethers with which power transmission and communication can be achieved. Moreover, they need to have small, high-performance computers on the robot and complex algorithms to perform pre-defined missions. In 1980s, the advances in computer technology and energy systems paced the progress of AUV technology. The first “International Symposium on Unmanned Untethered Submersible Technology” was also held in 1980. In 1992, MIT developed the Odyssey AUV which showed great success. Until late 1990s, various new versions of Odyssey were developed and they were tested in various places like Bellinghausen Sea in Antarctica to Beaufort Sea in the Arctic. The success of Odyssey initiated a collaboration between MIT and NATO in 1998. Odyssey performed various oceanographic experiments as a result of this collaboration. This proves that in 1990s, AUVs evolved from proof of concept designs to operational vehicles. In 2000s, commercialization of AUV technology also began to take place. Many commercial AUVs like Hugin from Norway, Maridan 600 from Denmark, AQUA EXPLORER 2 from Japan, Sea Oracle and CETUS II from USA and Explorer from Canada were developed [7]. These vehicles were able to execute numerous commercial tasks. For instance Maridan 150 was used for underwater archeology and Maridan 600 was used by De Beers for diamond mining survey. Hugin vehicles were used for underwater pipeline survey. These vehicles prove that the commercial acceptance of AUVs has occurred in the beginning of 2000s.

1.4 Literature Survey – UUV Examples

In unmanned underwater vehicle technology, it is difficult to define a standard for the vehicles being designed. When the literature is searched from the view point of a mechanical engineer, it is seen that there are numerous vehicles with different subsystems, sizes, shapes, materials and capabilities. Therefore, before starting a design, one should carefully investigate previous unmanned systems and determine basic features of them. In this part of the thesis, some of the systems that were investigated throughout the literature survey will be presented.

The MAYA AUV is developed in the National Institute of Oceanography in India [11]. It is a small vehicle with a length of L = 1.742 m and a diameter of D = 0.234 m. As seen in Figure 1.1, the vehicle has a torpedo like hull shape.

Figure 1.1 The AUV – MAYA [11]

There is a cylindrical middle hull section which is water tight. This section is sealed and equipments like control unit and batteries which should be kept in a dry environment are kept located in this section. This cylindrical section is enclosed by tapered rear and forward cones. The shape of the forward cone is ellipsoidal in order to form a low-drag hull. The rear cone, on the other hand, is made more slender so as to provide appropriate flow into the thruster which is at the rear end. The forward and rear end caps are floodable. It means that these sections are not sealed and water fills these sections during service. In this wet section, sensors that should reside in water are located. The connection between the free flooding section and the waterproof region is achieved by underwater connectors which are mounted on the rear and forward end faces of the middle section. The ability to detach the end caps from the middle section also enables the user to access the devices inside the middle section which is good in terms of modularity.

The middle section is waterproof; therefore, it is expected that it will withstand high pressure values especially in case of deep submergence. The middle section is manufactured from aluminum 6082 with 6 mm of thickness and it was tested in a at a depth of 178 meters. The end caps; however, are not loaded heavily since those sections are floodable. They are manufactured from glass fiber reinforced plastic.

The MAYA AUV is propelled with a single DC brushless motor that is attached to the rear end of the vehicle. Maneuvering is accomplished by control surfaces. Two horizontal planes for vertical movement and a single rudder for horizontal movement are utilized. Symmetric NACA section profiles are used for these planes. Thruster capacity and power requirement was determined from drag tests.

Their design led to a total weight of 54 kgf while the available buoyancy was only 43.4 kgf. In order to balance the vehicle, the hull was wrapped with PVC foams. A density of 200 kg/m^3 was used for withstanding high pressures. After trimming, a net buoyancy of 0.5 kgf was attained. After these studies, the vertical distance between the centers of buoyancy and gravity were 7 mm. This value is small when compared to other AUVs in service. Detailed information about stability will be given in the following chapters.

Woods Hole Oceanographic Institute (WHOI) is one of the most important institutions in ocean science. They have been in the leading role for a long time in this field. Nereus is one of their most recent underwater vehicles [12]. The operating depth of this vehicle is 11000 meters which is considered to be a very high value. Nereus is a hybrid remotely operated vehicle (HROV): it can operate both as an AUV or ROV. In case of deep-submergence, the vehicle switches to an untethered mode, in other words AUV mode; alternatively, in case of a shallow water investigation the tethered mode, or ROV mode, is on. The switch between operating modes can even be executed during the mission in the sea. As seen in Figure 1.2, the vehicle has two hulls which are attached to the chassis. These hulls are free-flooding and two lightweight pressure hulls are placed inside them to house dry equipments. Pressure hulls are made from ceramic and titanium to withstand high pressures in deeper parts of the ocean. Buoyancy is attained by hollow ceramic spheres which are located on the top of the vehicle as seen. Junction boxes and pressurized hoses are used for underwater cabling. The vehicle has movable foils (or wings) at the aft and mid parts of the body. Two thrusters are attached to the aft foils, while another one is attached to the middle plane; therefore, the thrusters are movable and this gives the ability of vectored thrust. The vehicle has no motion in lateral direction in the AUV mode.

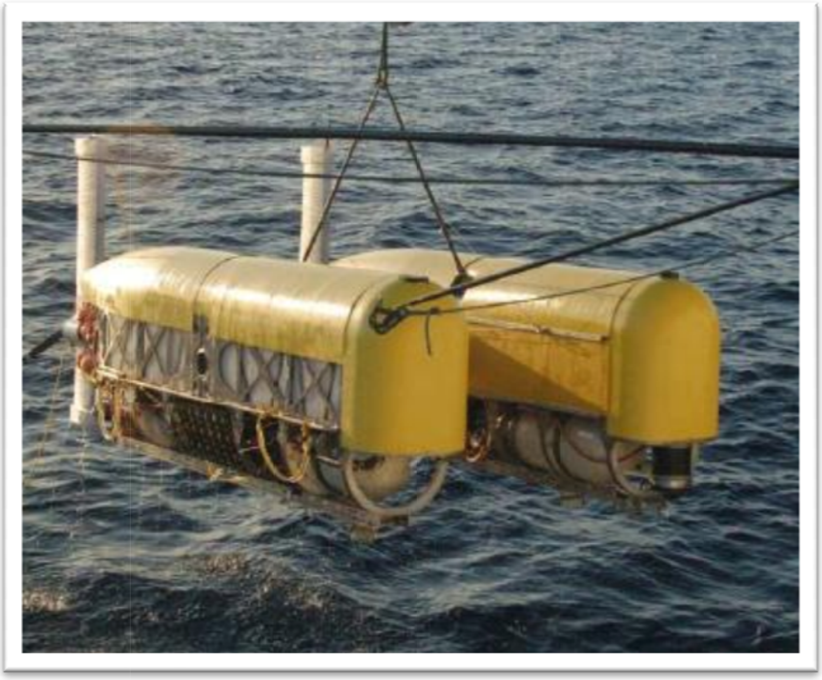

Figure 1.2 Nereus in AUV mode [12]

For AUV and ROV modes, different configurations are employed. As seen in Figure 1.3, an additional unit is attached to the bottom of the vehicle. It houses additional sensors, power source and a 6 Degrees of Freedom (DOF) robot arm. In ROV mode, lateral thrust is also available with an additional thruster.

Figure 1.3 Nereus in ROV model [12]

The Autonomous Underwater Vehicle Laboratory at MIT is one of the leading laboratories in AUV field. Hovering Autonomous Underwater Vehicle, HAUV, is an Odyssey 4 class AUV which is one of the AUV's that is being developed by the group [13]. It is designed as a relatively inexpensive vehicle which will be capable of performing deep submergence operations of about 6000 meters. Its weight is 350 kgf, length is 2.6 m, height and width are 1.3 m. As seen in Figure 1.4, the shape is different from previous examples and it does not have a torpedo shape. The vehicle has two forward looking thrusters which are attached to the body with movable foils. Their movement enables vectored thrust so three degrees of freedom are possible. An additional degree of freedom, lateral movement, is achieved by the lateral thrusters. These thrusters are placed inside a tunnel that passes through the body. Horizontal and vertical fins at the rear side of the body are fixed and they increase the roll stability of the vehicle. Like most of the designs of other MIT AUV's, HAUV has a floodable hull. Batteries and the control unit are housed in separate glass spheres as seen in Figure 1.5. These spheres are large; therefore, no buoyancy foams are needed. The vehicle is designed to be slightly buoyant. The spheres and other sensors are attached to a plastic frame which is shown in Figure 1.6. Top, bottom and side faces of the frame are covered with 1/4" ABS fairings. The vehicle's distinctive shape results in decent pitch and roll stability characteristics. The horizontal and vertical fins that are attached from behind also improve stability.

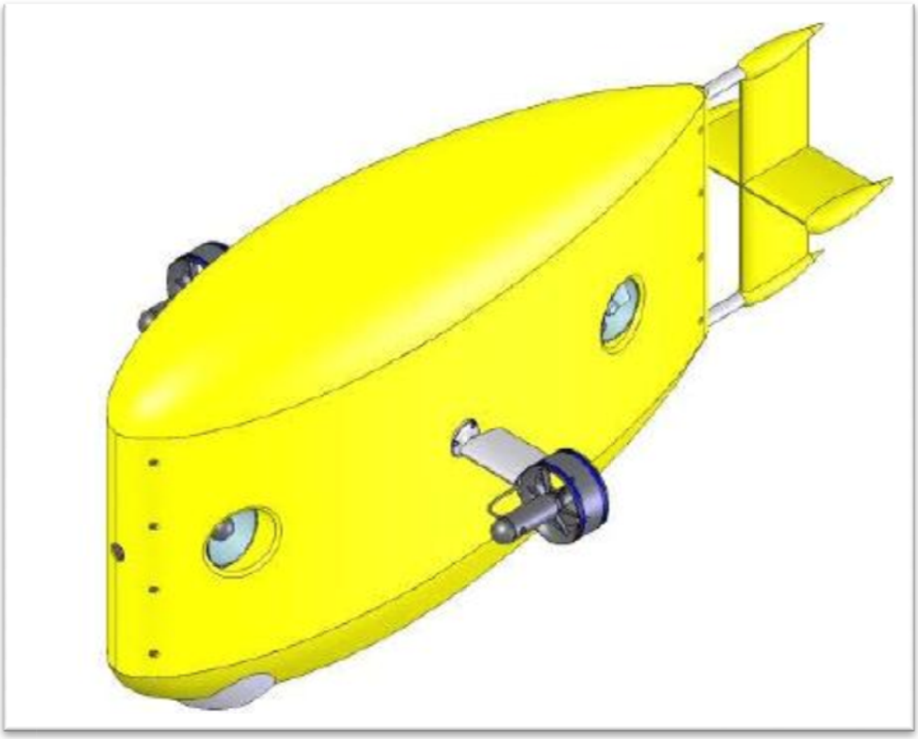

Figure 1.4 Odyssey 4 class HAUV [13]

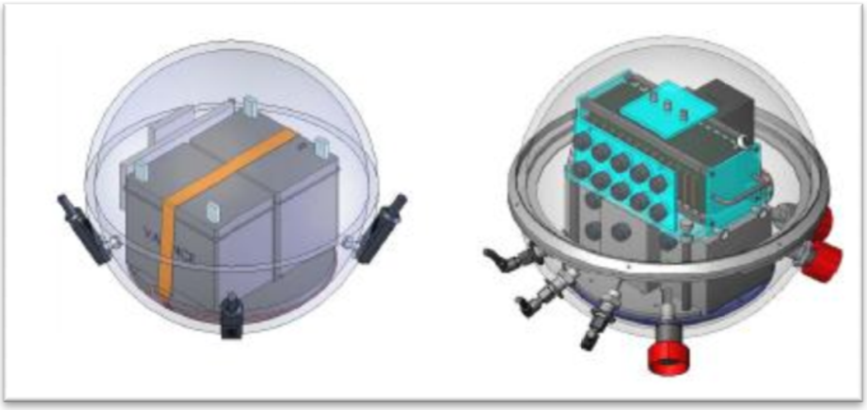

Figure 1.5 Pressure hulls of HAUV [13]

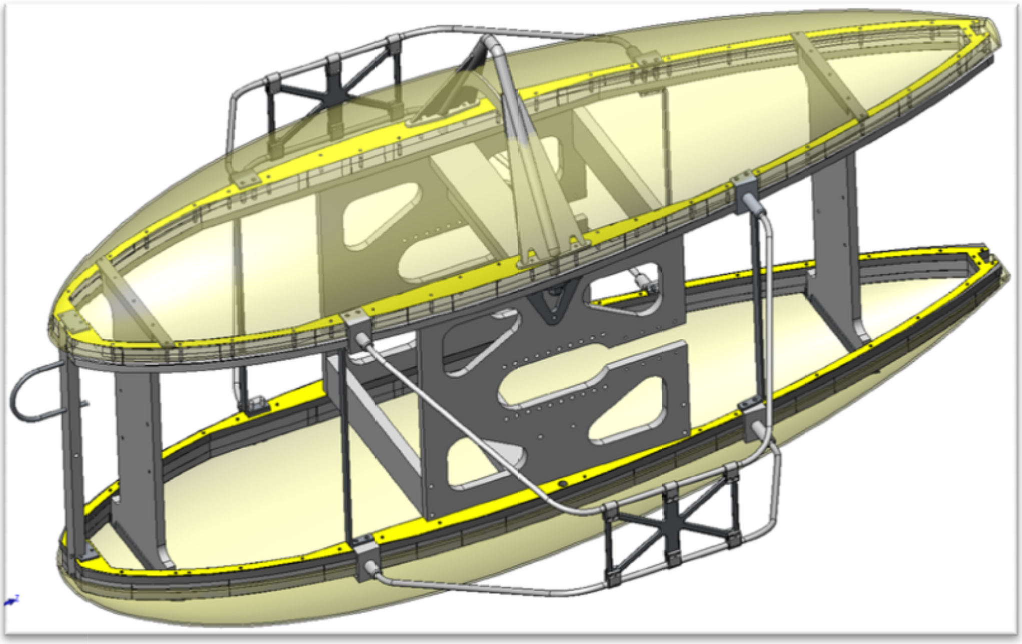

Figure 1.6 Frame of HAUV [13]

Aquabox II is an AUV which is developed by the Kyushu Institute of Technology [14]. It is a small vehicle with a length of 1.2 meters and a weight of 60 kgf. The operating depth is 50 meters. As seen from Figure 1.7 the vehicle carries two forward thrusters at the sides and a vertical thruster which is mounted to a tunnel passing through the vehicle. Two additional thrusters are mounted horizontally for swaying motion. It should be noted that all thrusters are fixed so maneuvering is accomplished by the thrust differences between opposite thrusters. The vehicle has two pressure hulls inside the body both of which are manufactured from aluminum. Communication devices, batteries and motion sensors are placed at these hulls.

Figure 1.7 Aquabox II

It should be noted that there are various unconventional unmanned underwater vehicles in literature as well. For instance, AQUA is an underwater robot based on the RHEX design as seen in Figure 1.8. It swims in water by paddling motion of six legs [15]. It also has the ability to crawl on the seabed.

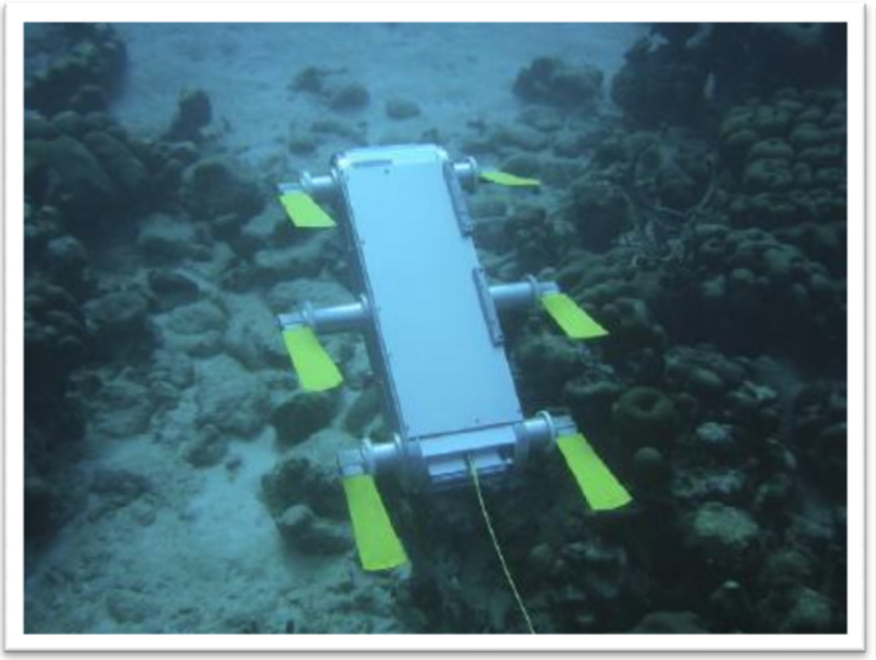

Figure 1.8 AQUA underwater robot

Besides that, unmanned vehicles that are built by inspiration from the nature, in other words biomimetics, are present. Vehicles that swim similar to turtles or sea snake are examples of such vehicles.

1.5 Basic Features of UUV's

After the literature survey, it is seen that there are numerous unmanned underwater vehicles in use. All of these systems have different properties. They vary in shape, size and material selection. They have different thruster configurations and other subsystems. Therefore, it is difficult to define standards for these vehicles. Nonetheless; it is realized that all of these vehicles have common features even though their appearances are different. They all have an appropriate hull shape to house all subsystems and satisfy an efficient hydrodynamic design. Pressure hulls or vessels are present for keeping control units and batteries in a safe and dry environment. Propulsion and maneuvering systems are used depending on the required capabilities of the vehicle. A suitable internal design is done so that all subsystems can function properly and the internal volume is used efficiently. Ballast systems are employed to maintain the balance and stability of the vehicle if necessary. Finally suitable underwater connectors and cables are used to connect separate subsystems.

1.6 Information about the Research Project ULISAR

This thesis study is performed during the design of an unmanned underwater vehicle. The vehicle is designed and manufactured in a research project sponsored by the Scientific and Technological Research Council of Turkey and named as ULİSAR Project (Ulusal İnsansız Sualtı Aracı Projesi). The primary goal of the project is to develop a prototype of an unmanned underwater vehicle that has the ability to swim steadily underwater, scan the environment, receive underwater image, store data and perform certain pre-defined missions. Later on, the level of the autonomy can be increased. New sensors or robot arms can be added for suiting different military, scientific or civilian purposes.

For achieving this, a multidisciplinary project group was formed. The project leader was Prof. Dr. M. Kemal Leblebicioğlu from the Electrical and Electronics Engineering (EEE) Department. Assistant Professor Dr. Afsar Saranli from the same department and Professors M. Haluk Aksel, S. Kemal Ider and Levend Parnas from the Mechanical Engineering (ME) Department also worked actively for the project. Three graduate students from the EEE department and one graduate student from the ME department were present. Besides the academic part, BARIŞ Electrical Industry Inc. was responsible from the manufacturing and Yenel Ltd. Company was responsible from the manufacturing of certain electronic equipments.

The project is accepted to be one of the first efforts of designing an unmanned underwater vehicle in Turkey. Besides that, the vehicle has several distinctive features. It is able to operate autonomously to accomplish a pre-defined mission and when needed, wireless communication is possible via acoustic modem. Cameras and lights are placed for getting underwater vision. Side scan sonar is used for scanning the environment and acoustic transducers are employed for detecting closer obstacles. Composite materials technology is utilized due to its novelty. The vehicle is capable of diving to 100 meters. The motion capabilities of the vehicle are surge, heave, pitch and yaw. No lateral motion is required and roll control is passive. The vehicle is expected to have a forward speed of 2 m/s.

1.7 Present Study

In this thesis hydrodynamic and thermal analyses done during the design of an unmanned underwater vehicle hull are presented. In the first chapter, an introduction to unmanned underwater vehicles is made. Their classification, history and purposes are described. Moreover, some of the recognized unmanned underwater vehicles are examined and their common characteristics are defined.

In the second chapter, the conceptual design of the hull of the vehicle is carried out. Alternative hull shapes, propulsion and maneuvering systems are discussed and appropriate selections are made. Internal arrangement of components determines the dimensions of the hull. Furthermore, hull material and production method are decided at this step. In the third chapter the heating problem of the hull is investigated. Heating analyses and tests of the pressure hull are given in this part. In the fourth chapter drag calculations are performed in order to predict the performance of the proposed hull design and check whether speed requirements are met. In the fifth chapter brief information about the manufacturing and testing of the vehicle are provided. The thesis is concluded by mentioning experiences gained throughout the project and discussing alternative solutions that would make the design better and making suggestions for future studies.

CHAPTER 2

CONCEPTUAL DESIGN OF THE HULL

As mentioned before, all unmanned underwater vehicles have common features even if they may have different shapes, sizes, materials or capabilities. An appropriate hull design is one of the most important steps in the design. The hull, sometimes referred to as the fairing, is the structure that covers the vehicle. The hull has many important functions for the vehicle. First of all, it provides the vehicle an efficient hydrodynamic structure. This hydrodynamic structure decreases the drag force exerted on the vehicle during its motion and increases its stability which in turn causes a smooth and efficient motion. Moreover, it encloses subsystems in order to protect them from damages and environmental effects. Finally for vehicles that do not have a chassis, the hull serves as the chassis and holds equipments.

In this chapter, conceptual design of the hull of the unmanned underwater vehicle is presented. In this conceptual design effort, the first step is investigating hull shape examples in the literature and defining their advantages and disadvantages. Propulsion and maneuvering systems are also investigated. After these investigations, suitable selections are made depending on requirements. The dimensions of the hull are specified after the internal arrangement of components in the hull. Finally, hull material and production method selections are made.

2.1 Theoretical Background

Before starting the conceptual design, it is beneficial to give information about parameters which are mentioned many times during the design process like skin friction drag, pressure drag, total drag force and prismatic coefficient. A body which travels underwater experiences water resistance. This resistance is called drag and it can be decomposed into two components: form (pressure) drag and skin friction drag. It should be noted that for bodies that travel close to the water surface, surface and wave effects are also significant and their effects should be considered in calculations as well.

2.1.1 Skin Friction Drag

For the flow of viscous fluids over surfaces, a thin region named as the boundary layer forms on the surface. In this tiny region the flow velocity increases from zero at the wall to free stream velocity at the outer limit of the boundary layer; therefore, velocity gradients are very large in the boundary layer. This severe velocity gradient causes excessive shear stress in the region. Skin friction drag is the resultant force due these stresses and is a direct result of the viscosity of the fluid. The flow and the boundary layer over a submarine are seen in Figure 2.1.

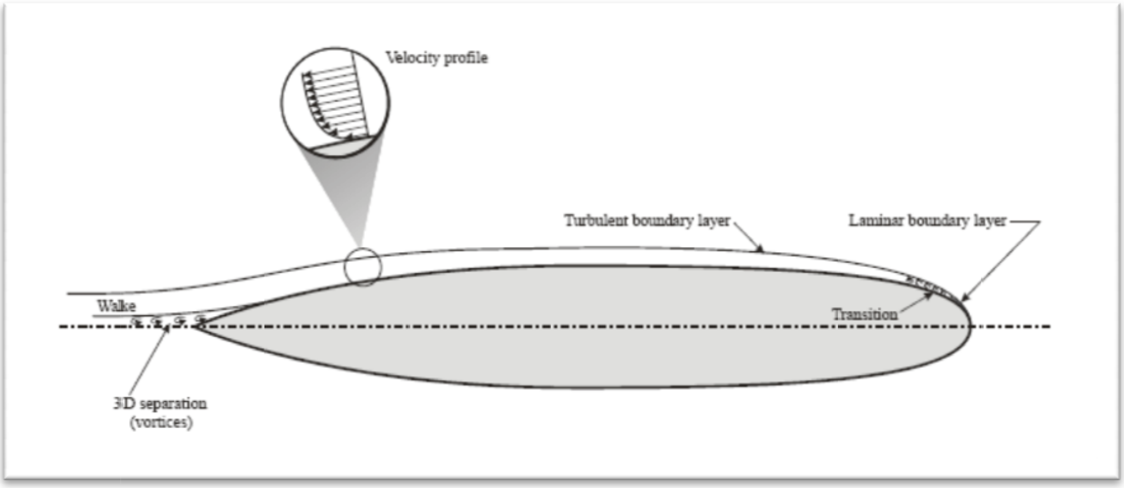

Figure 2.1 Flow around a submarine [16]

Skin friction drag value depends on the characteristics of the flow strongly. For laminar flow, thin layers of fluid slide over each other smoothly and this reduces the shear stress on the wall. On the other hand, in turbulent flows, the fluid is more chaotic with enhanced mixing, irregularities and 3D flows. As a result, velocity gradients and stresses are higher compared to laminar flow. Even though laminar flow is advantageous in terms of skin friction drag, it is hard to maintain laminar flow over the whole surface because laminar flow is very susceptible to disturbances. For almost all real flows, the flow remains laminar until a transition region and then turns into turbulent flow. This phenomenon is known as laminar to turbulent transition. Therefore, one should intend to delay transition as much as possible and increase the laminar portion of the flow on the body. At this point, it is beneficial to be able to guess the transition point and Reynolds number is used for this purpose. Reynolds number, *Re*, is a non-dimensional parameter which is the ratio of inertial forces to viscous forces.

$$Re = \frac{\rho U l}{\mu} \tag{2.1}$$

The characteristic length l is an appropriate length depending on the case. For a flow over a streamlined body, one can take l as the distance from the front end of the body. It is obvious that Reynolds number increases with the distance and after a critical Reynolds number transition happens.

Skin friction is related to the surface of the body. Due to that decreasing the surface area, which may also be referred to as the “Wetted Surface Area”, reduces the skin friction.

2.1.2 Form Drag

For a body moving in fluid, a pressure distribution forms on the body. The pressure is highest at the nose due to stagnation, decreases as the fluid accelerates on the contour of the body and is recovered at the stern. For ideal (inviscid) flows, the pressure is fully recovered and there is no pressure difference between the nose and the tail. However, for viscous flow there is a pressure difference which causes the pressure or form drag. Form drag depends strongly on the shape of the body and its pressure recovery characteristics.

An important phenomenon for form drag is the flow separation. When the fluid follows the contour of the body, it may experience pressure force against its motion and this pressure is known as adverse pressure. In such cases, the fluid is decelerated and can even be reversed at some point. At this point, the flow is not attached to the body anymore and it is separated.

Separated flows damage pressure recovery. A wake region is formed behind the body which increases the pressure difference between the nose and tail sections. For that reason, one should pay attention to prevent separation. Turbulent flows are superior over laminar flows in this aspect because they attach to the surface better. Flow over a cylinder exemplifies this situation. For laminar flow, drag coefficient, C_D is equal to 1.2 due to early separation. For turbulent flow C_D drops to about 0.3-0.4 since the flow separation is delayed.

For reducing form drag, abrupt changes in the cross-section of the body should be avoided. A streamlined body with high length-to-diameter (*L/D*) ratio is useful in this aspect. Furthermore, in critical cases designers tend to use methods like tripping the boundary layer to promote transition to turbulence and sucking the boundary layer in order to delay separation.

2.1.3 Total Drag Force

Drag force is the combination of the form drag and the skin friction drag. In order to be able to decrease the total drag force (resistance), one should understand how these drag forces contribute to the total drag.

For streamlined bodies like an airfoil, the contributions of friction drag and form drag are comparable. In this case, it will be helpful to reduce the wetted surface area. On the other hand, for bluff bodies, resistance is mainly due to form drag. One has to make the body more slender in order to reduce the form drag. However, making the body slender increases wetted surface area which in turn increases the skin friction. It can be inferred that there is an optimum aspect ratio for minimum drag. A familiar graph is given in Figure 2.2. It is seen that there is an optimum *L/D* ratio. However, this ratio is not strict and using slightly lower or higher values do not change the resistance significantly. Numerous studies have been performed to determine the

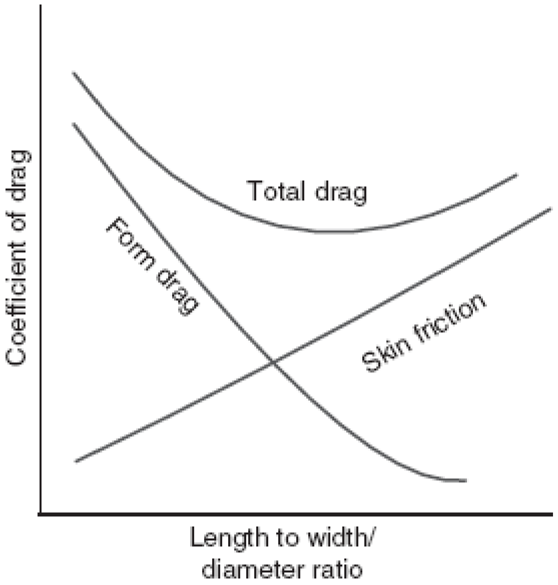

Figure 2.2: Vehicle drag curves [3]

optimum aspect ratio. One of the earliest and most well-known studies was performed by Morton Gertler at David Taylor Model Basin in 1950 [17]. Gertler tested 24 underwater bodies at various velocities to collect drag data in deep submergence. Bodies were axisymmetric and formed from sixth degree polynomials. The purpose of the research was to understand the effects of various parameters like length-to-diameter ratio, prismatic coefficient and nose diameter on resistance. When he compared the results of bodies with the same volume, he reached the conclusion that optimum aspect ratio *L/D* is 6.5. Certainly, this value is not super critical. One can use higher or lower aspect ratios depending on limitations. For instance, for a vehicle like torpedo which probably has diameter limitation, the length should be increased to obtain the same amount of volume.

For comparing performance of different vehicles a non-dimensional coefficient called the drag force coefficient is defined as:

$$C_D = \frac{F_D}{0.5\rho U^2 A} \tag{2.2}$$

F_D refers to the total drag force and A refers to the appropriate area. For bluff bodies, the area will be taken as the projected area normal to the flow direction or the frontal area, while it will be area as seen from top or the planform area for streamlined bodies.

2.1.4 Prismatic Coefficient

Prismatic coefficient is another important parameter for underwater vehicles. Prismatic coefficient is a non-dimensional value which represents the fullness of the body at the ends. It is the ratio of the volume of the body to a hypothetical volume of the prism which would be obtained by the mid-ship cross-sectional area and length. Gertler compared models with the same *L/D* ratio and varying prismatic coefficients. For both *L/D* ratio 5 and 7, he reached to the conclusion that a prismatic coefficient of 0.61 is optimum. This value is somewhat low and limits the internal space available. A solution for this problem is using a parallel mid-body [18]. In that solution, it is seen that when about half (0.495 times) of the total length is allocated as a parallel mid-body, one can achieve the same resistance as the prismatic coefficient increases from 0.682 to 0.84. The increase in prismatic coefficient means more internal space and it is obvious that it is extremely important for underwater vehicles.

2.2 Hull Requirements

Before choosing the hull shape, one needs to define hull requirements clearly. The most important function of the hull is providing the vehicle an efficient structure in terms of hydrodynamics. Form drag and skin friction drag should be minimized in order to reduce power requirements. It should also be noted that drag losses also determine the range, maximum speed and operating time of the vehicle. The hull should also allow a smooth flow over it for stable motion. These items gain importance especially for cases where speed and maneuvering criteria are strict. The hull should have a symmetric structure for rotational stability when it is stationary or moving. The size of the hull is also an important criterion. For most cases, it is not possible to try extreme values because there are restrictions in terms of size. The form drag usually limits the maximum diameter. On the other hand, minimum diameter is limited since the hull should be large enough to cover subsystems. Length of the hull should be large enough for all the subsystems to fit and small enough to minimize skin friction force and cabling requirements. The hull should be thick enough to have enough strength to withstand pressures and possible damages. If the whole hull is water tight, the thickness criterion becomes more important as the pressure force increases. Besides that, maximum length, thickness and diameter are limited to satisfy maximum weight criterion. One cannot design the hull without considering manufacturing. The design should be as simple as possible to reduce manufacturing costs and time. The hull should be ergonomic so that the users can easily carry and deploy the vehicle to water. Finally aesthetic issues become important especially for commercial uses.

These requirements are mostly determined from the project definition. It is clear that it is difficult to satisfy all of these requirements simultaneously. It should also be noted that some of these requirements may be coupled; therefore, care should be taken while changing parameters. The designer should begin with an initial design and modify that design depending on requirements. The modified design should be checked and modified again if necessary. At each step, the designer should make necessary calculations and simulations. This iterative procedure continues until the optimum design is achieved. It is important to note that feedbacks of other members of the design group should be taken into consideration for avoiding potential problems.

2.3 Hull Shape Selection

During the literature survey, it was seen that hull shapes vary significantly for different vehicles and some examples of hull shapes were presented in the previous chapter. It is difficult to make a classification for AUV shapes; however, one such classification is done by the Autonomous Undersea Vehicle Applications Center (AUVAC). According to AUVAC, autonomous underwater vehicles can have teardrop shape, torpedo shape, rectangular shape, oblate shape, open space frame and biomimetic shape [19]. Each of these shapes has advantages and disadvantages; therefore, the designer should pay attention to choose the shape that will fulfill project requirements best.

2.3.1 Teardrop Shape

Some examples of teardrop shapes vehicles can be given as the Alistar of ECA and Odyssey II of MIT AUV Laboratory. These vehicles can be seen in Figures 2.3 and 2.4. Teardrop shape is an efficient shape in terms of resistance. In fact, it is assumed to be the ideal shape since the cross-section varies continuously and slowly preventing early separation of the flow. On the other hand, there are some drawbacks. The first one is the reduction in internal space (low prismatic coefficient). Moreover, the continuously changing contour can make it difficult to house equipments and use the space efficiently. Finally, depending on the production method, manufacturing the continuously changing contour can be a difficult task.

Figure 2.3 Alistar of ECA [19]

Figure 2.4 Odyssey IIc of MIT AUV Laboratory [19]

2.3.2 Torpedo Shape

Torpedo shape is a frequently used shape for underwater vehicles. These shapes have a cylindrical mid-body, ellipsoid fore body and a parabolic after body. Some examples of such vehicles are Autosub 6000 of Subsea7 and Hugin 1000 of Kongsberg Maritime, which can be seen in Figures 2.5 and 2.6, respectively.

Figure 2.5: Autosub 6000 [19]

Figure 2.6: Hugin 1000 [19]

Torpedo shape has several advantages. First of all it gives more free space to the designer due to its cylindrical middle body. These vehicles are usually manufactured in 3 pieces. The middle, fore and aft bodies are manufactured separately and then assembled. This property provides a modular structure. The vehicle can easily be modified. Design and manufacturing is easier. Finally performance is comparable to teardrop shapes. Due to these advantages, they are commonly used for underwater vehicles, submarines and torpedoes.

2.3.3 Rectangular Shape

Rectangular shaped unmanned vehicles are very similar to torpedo shaped vehicles as it can be seen in Figure 2.7. Urashima of Japan Agency for Marine-Earth Science and can be given as an example for this category.

Figure 2.7 Urashima AUV

These vehicles have a parallel mid body enclosed by tapered ends. They may house thrusters and control planes at the tail section like torpedo shaped vehicles. One advantage over the torpedo shapes is that rectangular cross-section can be used more efficiently for placing equipments. On the other hand, performance is lower.

2.3.4 Oblate Shape

Some AUVs are designed to have a more flat structure as seen in Figure 2.8. These vehicles allow more than one thruster to be located on the vehicle as seen in Double Eagle MKII of Saab Underwater Systems. This thruster configuration provides better maneuverability. However, performance is lower due to usage of more thrusters compared to the torpedo shape where one thruster is used.

Figure 2.8: Double Eagle MKII of SAAB Underwater Systems [19]

2.3.5 Open Space Frame

In certain cases, it may be helpful to use more than one hull. These hulls are usually attached to a main frame. One example can be seen in Figure 2.9. Different equipments like electronic cards, batteries and sensors can be placed at different tubes. One major advantage is that high stability can be achieved by placing heavy components at the lower tube and light components at the lower one. Separating certain equipments may also be beneficial for their proper functioning. Besides that, the chassis allows the user to place underwater equipments easily. On the other hand, performance will be lower compared torpedo shapes. Manufacturing may also be more difficult.

Figure 2.9: SeaQuest [19]

Other than these shapes, biomimetic shapes are gaining popularity in recent years. Vehicles that are inspired from animals like penguins, fishes, snakes are being developed. Even though these technologies are promising, it is hard to tell that they are reasonable alternatives.

Every hull shape has advantages and the selection depends on the designer. For the project study, a torpedo shaped body was chosen due to certain reasons. First of all it gives one of the best performances in terms of drag amongst hull shape examples. The cylindrical middle body allows an appropriate place for placing electronic equipments and the front and rear sections are allocated for the storage of underwater equipments. Torpedo shape is the most popular hull shape which provides a larger database. For a project group who is designing such a vehicle for the first time, large database is helpful.

2.4 Propulsion and Maneuvering

The selection of the appropriate hull shape is followed by the propulsion system selection. Choosing the systems depends on various considerations. Propulsion type, configuration, efficiency, power requirement, size, thrust value and cost are primary considerations in this selection.

2.4.1 Propulsion Type

Electrical, hydraulic and jet propulsion are used by underwater vehicles [3]. Jet propulsion and hydraulic propulsion are very rarely used for special cases. During the literature survey it was seen that almost all systems rely on electrical propulsion. In this method, a shaft with propeller blades is rotated with an electric motor that can be located inside the vehicle or inside a separate casing. The rotation of propeller blades causes an increase in flow velocity across the propeller and this causes a forward thrust on the vehicle.

The efficiency of a thruster is affected by many parameters. One of the most important parameters is the quality of the flow leaving the thruster. Propeller blades create a rotational effect on the exiting flow and this effect reduces propulsion efficiency. Moreover, tip vortices are formed at the tips of propeller blades which also have negative effect on efficiency. To reduce the effects of these, underwater thrusters are enclosed by a casing named as the shroud, duct or a kort nozzle. This type of ducted propeller or kort nozzle give better performance compared to thrusters without a nozzle. One of the main reasons for this is that the tip vortices are suppressed by the duct and the flow exits axially with less swirl. On the other hand, the shroud causes an additional drag. For low speeds, the increase in propulsion overcomes this drag; however, for higher speeds the shroud begins to have a negative effect on propulsion. Therefore; ducted propellers are used for low speed applications like unmanned underwater vehicles.

Podded propulsors are a special type of a propeller where the DC motor rotating the shaft is inside a hub and the propeller blades are attached to that hub from behind. The main advantage is that these propulsors house their own motors and do not require a DC motor on the vehicle. This gives more internal space for other equipments and eliminates the risk of water leakage through propeller shaft. Furthermore, the hub provides the vehicle an axial inlet flow which in turn increases propulsion efficiency. An example of a podded propulsor with kort nozzle is seen in Figure 2.10.

Figure 2.10: Podded propulsor – BTD150 model of Seabotix

Design and manufacturing of a thruster is a very complicated issue and it is in fact a separate project topic. Consequently, in this project thrusters were purchased. Due to the advantages stated above, a podded propulsor with a shroud around it used. The details of the propulsor will be presented in the chapter on performance chapter.

2.4.2 Maneuvering

Besides the propulsion system selection, thruster configuration of the vehicle is important for maneuverability of the vehicle. Before considering alternatives, it is necessary to define required degrees of freedom of the vehicle. ULİSAR is expected to have surging motion, heave, pitch and yaw. Lateral (sway) motion and roll will not be available. In fact roll is intended to be eliminated passively. These degrees of freedom are presented in Figure 2.11.

During the literature survey, it was seen that there are various approaches for maneuvering. Generally, there are 3 means of maneuvering. The first one is using a single propeller at the aft and along with control surfaces. This is a common approach used for unmanned vehicles especially for torpedo shaped ones. Pitch and yaw motion is attained by the deflection of control planes. The advantage is that using a single propeller increases the efficiency of the system. Therefore; for long-range operations this solution is preferred. The disadvantage on the other hand is that these vehicles are maneuverable only when the vehicle is surging. They do not have the ability to do pitching, yawing and surging motion when stationary. Moreover, sealed shafts should be designed for controlling control surfaces.

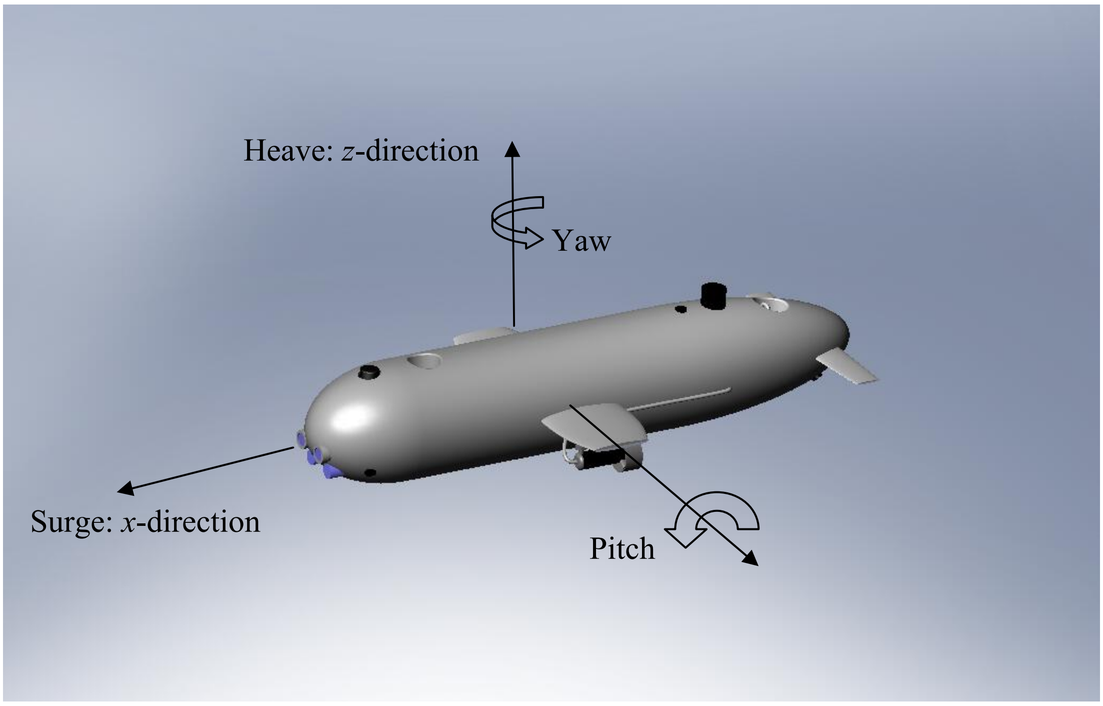

Figure 2.11: Maneuvering capabilities of the vehicle

Another alternative is vectored thrust. In this method one or more thrusters are connected to a shaft which can change the angle of the thruster. As a result, the thrust vector changes direction and vehicle can maneuver. An example is Seawolf 2, seen in Figure 2.12, which is developed by the North Carolina State University Underwater Robotics Group. This thruster arrangement is the best in terms of maneuverability. It is preferable for missions where long range is not critical. The disadvantage is that these vehicles are inefficient for surging motion and require sealed shafts for thruster control. Unmanned underwater vehicles with vectored thrust are not so common. Systems with vectored thrust have only one rotational motion for each thruster. A conceptual design of a vectored thrust system which consists of a single thruster that has 3 degrees of freedom is seen in the study of Cavallo et al. [20]. In their study, they claim that such a system can satisfy propulsion and guidance tasks.

Figure 2.12: Seawolf II of North Carolina State University

Using multiple thrusters in different arrangements is a frequently used method for maneuvering. In this method thrusters are placed symmetrical with respect to the center of mass. Maneuvering is achieved by the thrust difference and the resulting moment. The required maneuvering ability determines the number of thrusters and their arrangement. In Figure 2.13 an example of such a vehicle is seen. This vehicle has 5 thrusters. Two of these thrusters are forward thrusters, two of them are vertical and one of them is lateral. Therefore, this vehicle is capable of surge, heave, sway, pitch and yaw motions.

Multi-thruster arrangements are useful in terms of maneuvering. However, they are not efficient for long range operations since increasing the number of thrusters decreases propulsion efficiency. One other drawback of multi-thruster arrangements is the torque steering [3]. As it was stated before, flow exits with swirl from the propeller. This swirling flow induces torque on the vehicle. When two forward thrusters are working simultaneously, their effects are combined which increases the torque on the vehicle as well. Shrouds around thrusters and flow straightening blades at the exit of propellers usually suppress this effect. However, the ideal solution is employing counter-rotating thrusters. These thrusters generate opposite torques which cancel each other.

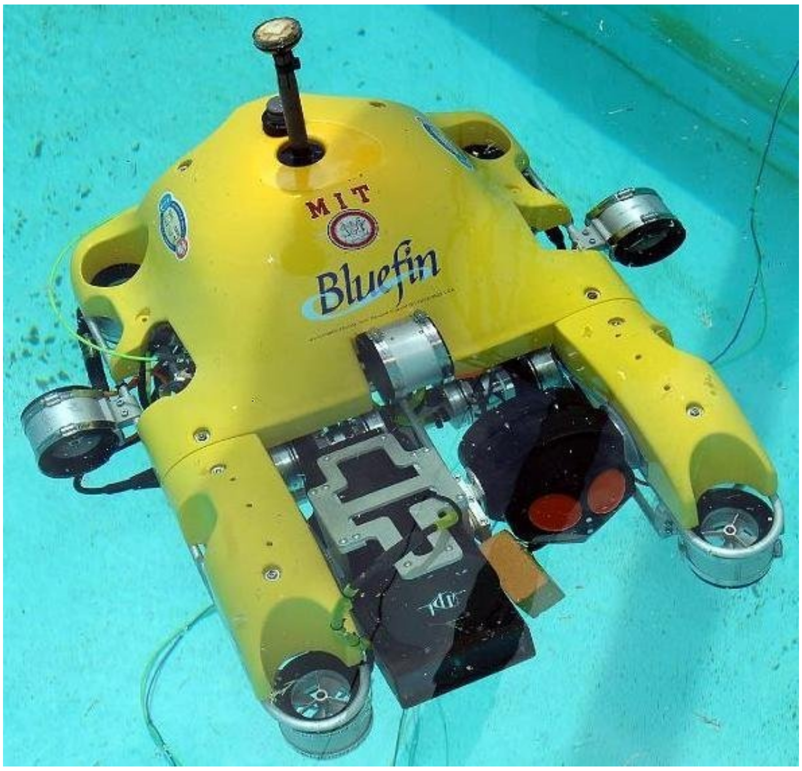

Figure 2.13: Bluefin unmanned underwater vehicle

After investigating these thruster configurations, one can deduce that the designer has to choose the appropriate one depending on project requirements. Single thruster with control surfaces is efficient and used for long range operations; however, it will be less maneuverable. On the other hand multi-thruster and vectored thrust options give maneuverability with lower efficiency. ULİSAR is the first prototype of an unmanned underwater vehicle and at this point it is not expected to have long range operations. Initial experiments will be at the pool. Considering that, maneuverability is more valuable than efficiency at this moment. Moreover, hovering motion will be beneficial for pool experiments as well. Due to these reasons, a multi-thruster configuration was chosen for propulsion and maneuvering. 4 thrusters will be used for surge, heave, pitch and yaw motions. The proposed configuration is seen in Figures 2.14 to 2.16.

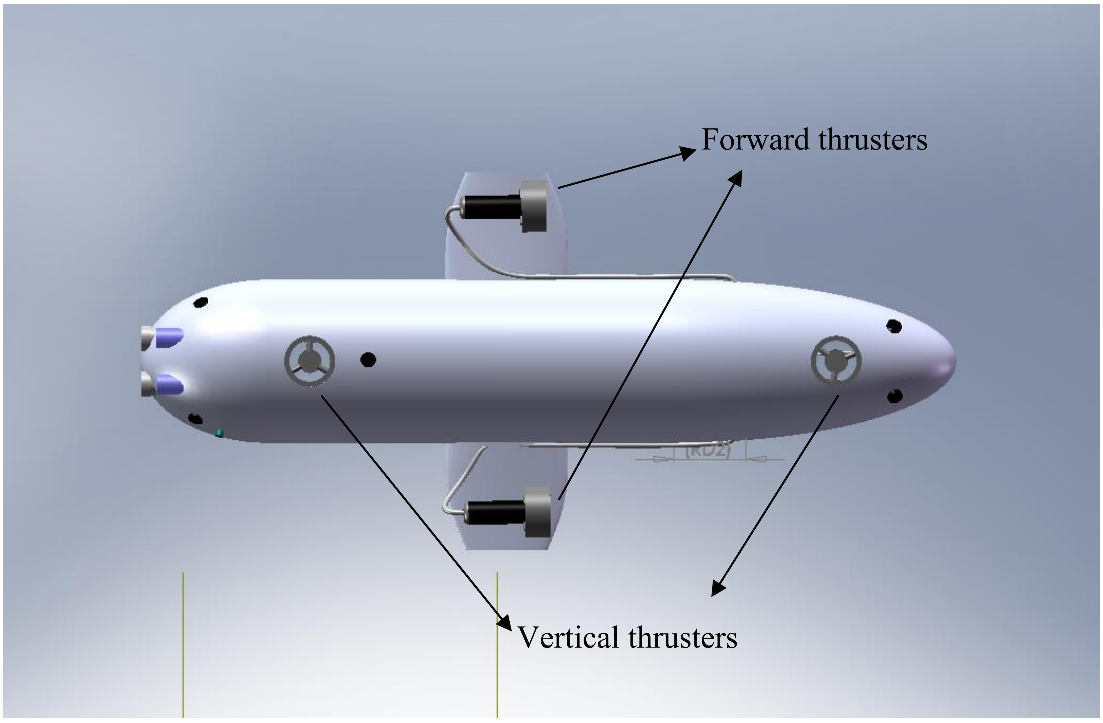

Figure 2.14: Thruster configuration – Bottom view

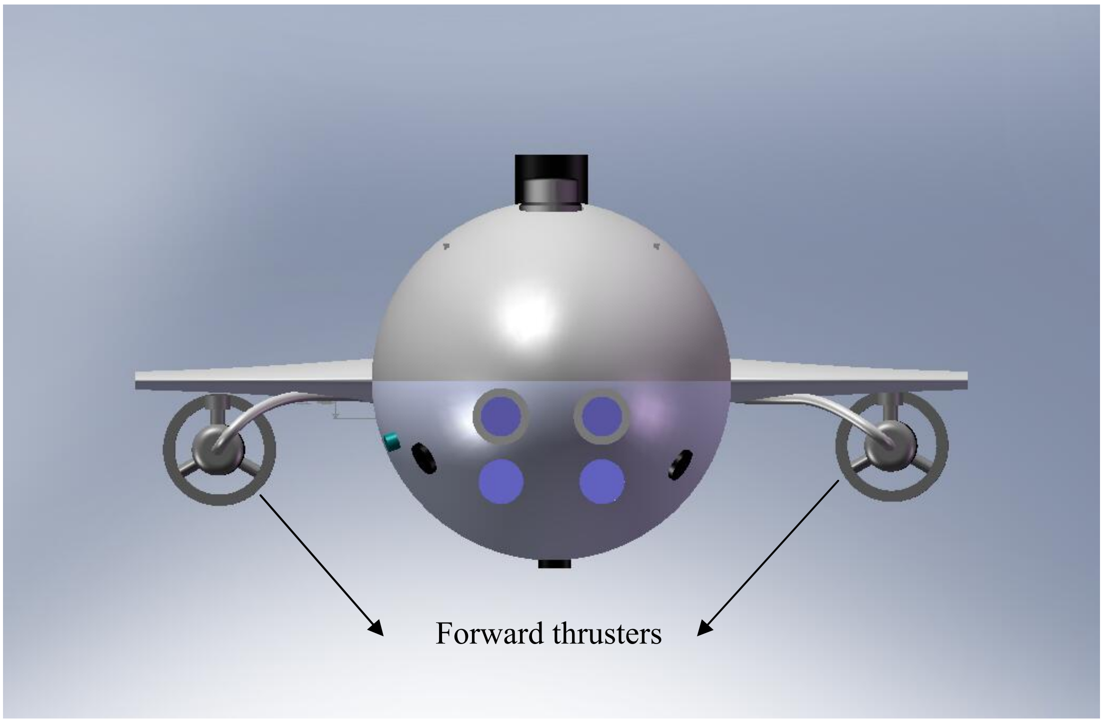

Figure 2.15: Thruster configuration – Right view

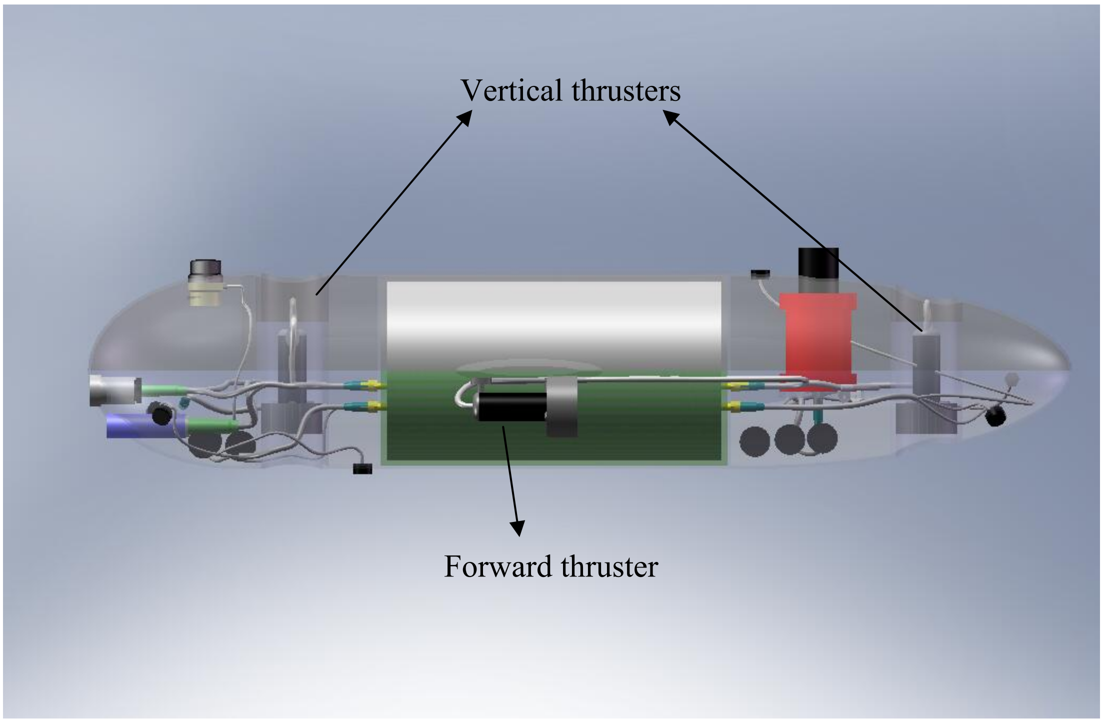

Figure 2.16: Thruster configuration – Front view

2.5 Internal Arrangement

After making a suitable selection for the hull shape and propulsion system, one has to specify the internal arrangement of the body and the dimensions of the hull. During the literature survey part of the thesis, several underwater configurations were investigated. From these investigations some conclusions were made. Firstly, almost all vehicles have floodable sections. It means that the vehicle houses electronic cards and batteries in a separate dry pressure hull while other equipments are kept in the floodable wetted sections of the vehicle. Such a design approach has benefits over a design which would have a hull that is completely sealed. The first advantage is that the sealing surfaces are reduced by this design because the waterproof region is smaller. Besides that, most of the equipments need to be in the wet section or at least must have protrusions out of the body to function properly. Acoustic modem, side-scan sonar, pressure sensor and temperature sensor are some examples of such devices. If the designer aims to seal of these protrusions, the risk of leakage will increase. The leakage of one of the systems in the design may even cause the failure of the vehicle. Finally, a floodable hull increases the wetted area of the pressure hull; hence, increases its heat removal capabilities. Due to these reasons a floodable hull is used in the design.

A floodable design was proposed as seen in Figure 2.17. It is seen that the hull consists of the upper and lower bodies. The red lines in the figure represent surfaces where sealing is applied. When these two bodies are attached properly, those sealing surfaces match and a watertight region, which may be referred to as the pressure hull, forms in the middle of the hull. Electronic equipments that should be kept inside a dry section are housed there. The sections in both sides of the pressure hull are floodable. Water enters into these sections as the vehicle is deployed to the water and drains the water when it is recovered.

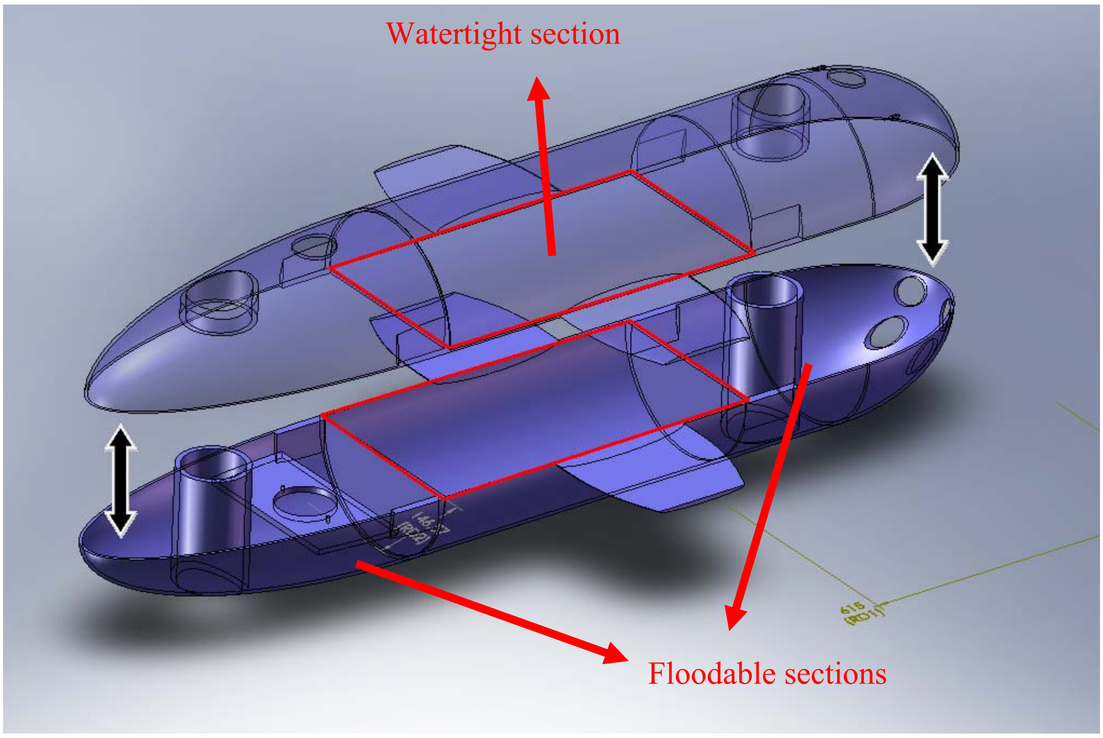

Figure 2.17 Lower and upper bodies

The idea behind designing such a two piece body was the ambition to use only one mold. As it is understood from Figure 2.17, the upper and lower bodies are exactly the same besides the internal parts. Therefore, these two bodies are produced from the same mold to reduce expenditures and manufacturing time. An alternative to this configuration may be designing three axisymmetric bodies that are attached to each other from sides. Compared to that configuration, this configuration is better in terms of strength because the upper and lower bodies are one piece solid components. Moreover, all of the connectors, electronic components and batteries are attached to the lower body. Therefore, the upper body can be detached easily and once it is detached, it makes it easy to access all of the equipments in the hull. On the other hand, this design hinders further modifications. For the three body configuration where three axisymmetric bodies are attached from the sides, it is easier to modify the vehicle by designing one of the bodies again. Conversely, for the present design, it is difficult to adjust the shape since one has to design and manufacture the whole body again.

Since the sections at the front and rear parts of the vehicle are floodable, there is no need to make the walls of those sections thick as they are not loaded under hydrostatic forces. On the other hand, the middle section resists excessive pressure forces because it is watertight. The walls of this section should be thicker to resist high pressures and create room for the seal to be attached. As a result, a variable thickness body was proposed. The details can be seen in Figure 2.18.

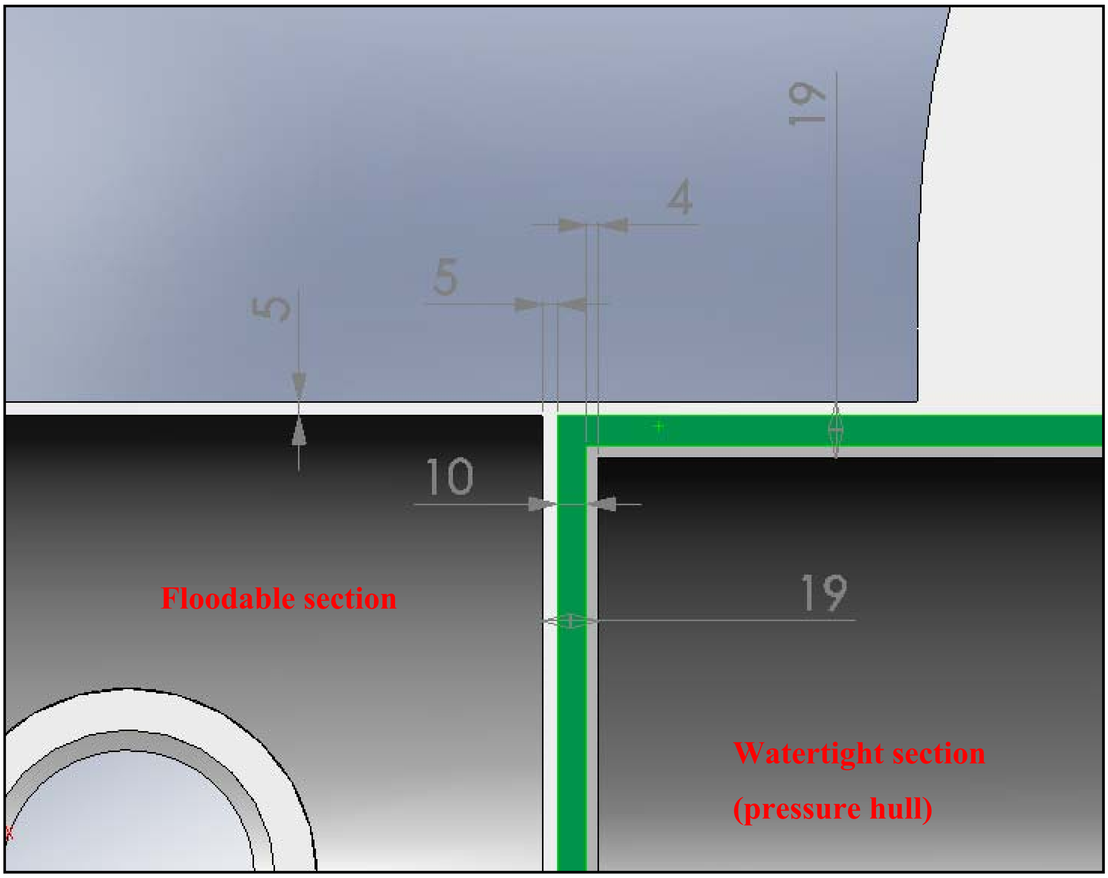

Figure 2.18 Hull thickness differences

Wall thickness values and similar other critical values for manufacturing were determined by the manufacturing company. Strength analysis for composite structures is a very detailed topic and it is out of the scope of this thesis.

2.5.1 Internal Arrangement of Devices

The dimensions of the hull are specified as the devices are located in it. The hull has two sections as stated before: floodable section and water tight section. Acoustic modem, sonar, cameras and lights, pressure sensor, thrusters and acoustic transducers are devices that are housed in the flooded section; on the other hand, electronic cards and batteries are located in the watertight section. These devices have conditions about their orientation in the hull:

- Acoustic modem which is seen in Figures 2.19 and 2.20 should remain vertical with its tip protruding out of the body.
- Sonar should remain vertical with its tip protruding out of the body. Since it is a side-scan sonar, it should be located near the front of the body to be able to scan forward.
- Cameras and lights should be located in front of the body to have forward vision. They should be separated with a distance of 4 cm.
- Vertical thrusters should be located in tunnels that pass through the body. They should be separated from each other as much as possible to increase the pitch motion capability.

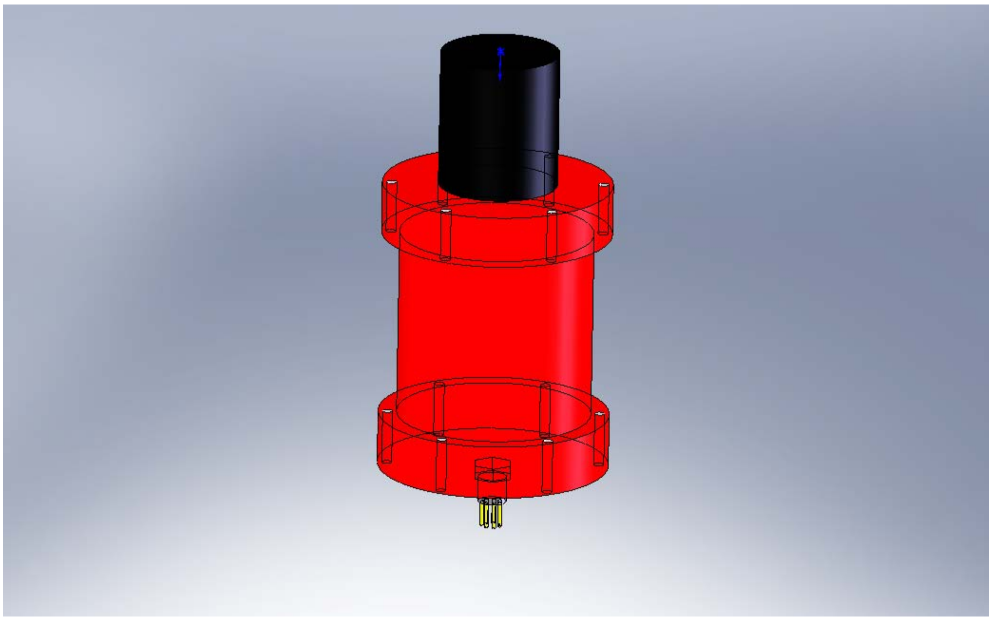

Figure 2.19 3D model of the acoustic modem

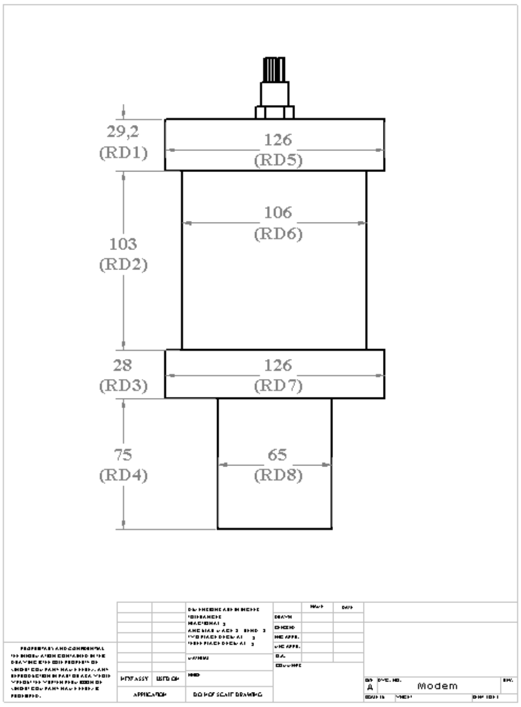

Figure 2.20 Technical drawing of the acoustic modem

Among these conditions, the most challenging device is the acoustic modem due to its dimensions (about 25 cm). In order to be able to house this device, the radius of the hull is set to be 32 cm. In order to meet location conditions of other devices, the internal arrangement seen in Figure 2.21 is proposed. Technical drawings of upper and lower bodies are also seen in Figures 2.22 and 2.23.

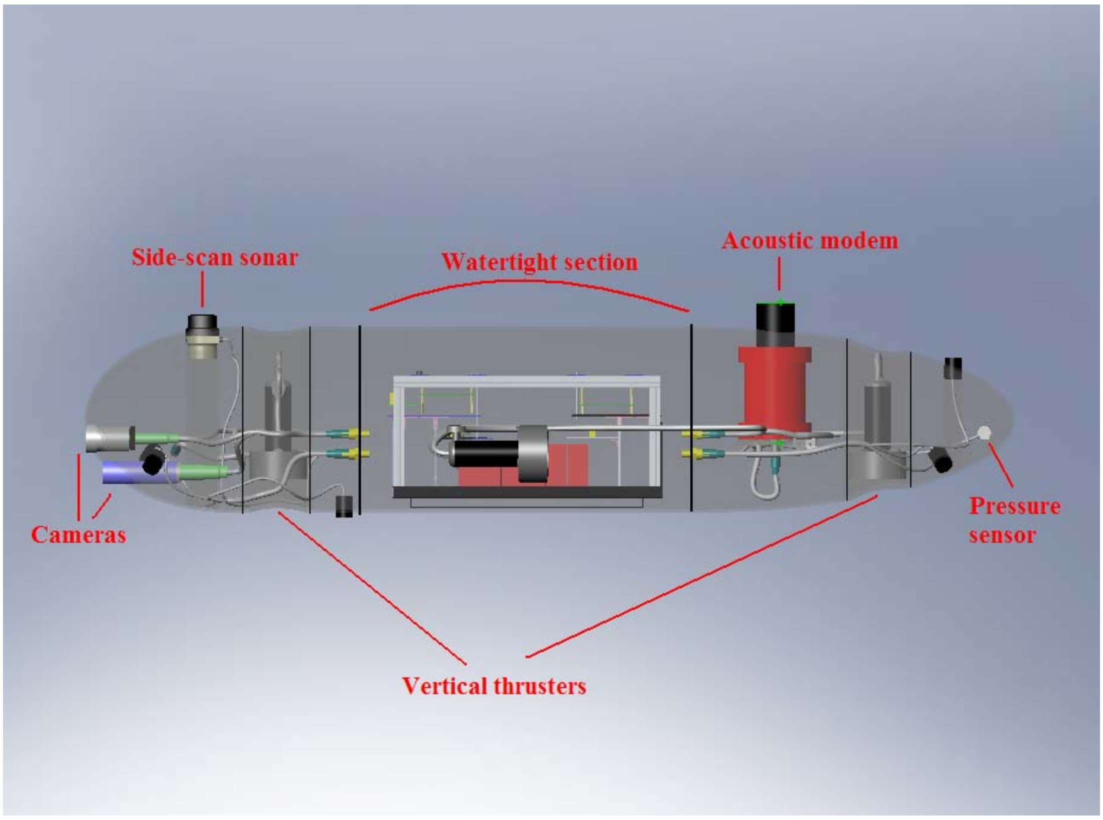

Figure 2.21 Internal arrangement of devices

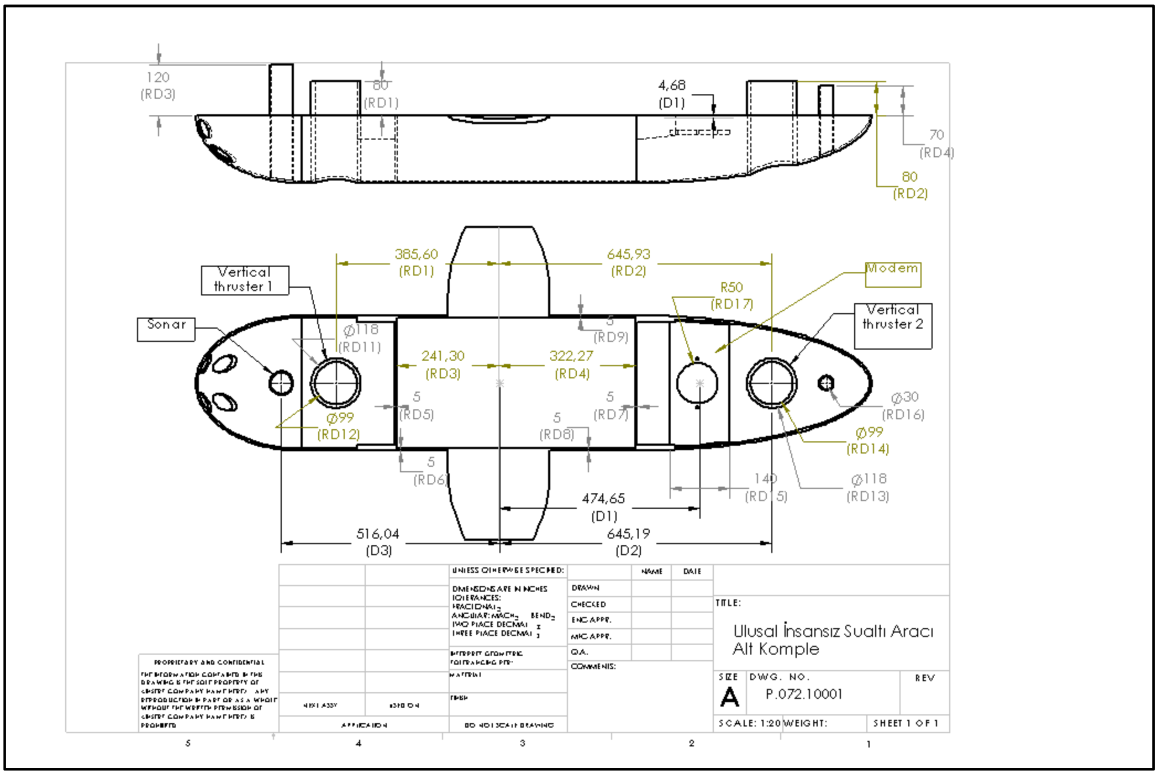

Figure 2.22 Technical drawing of the lower body part

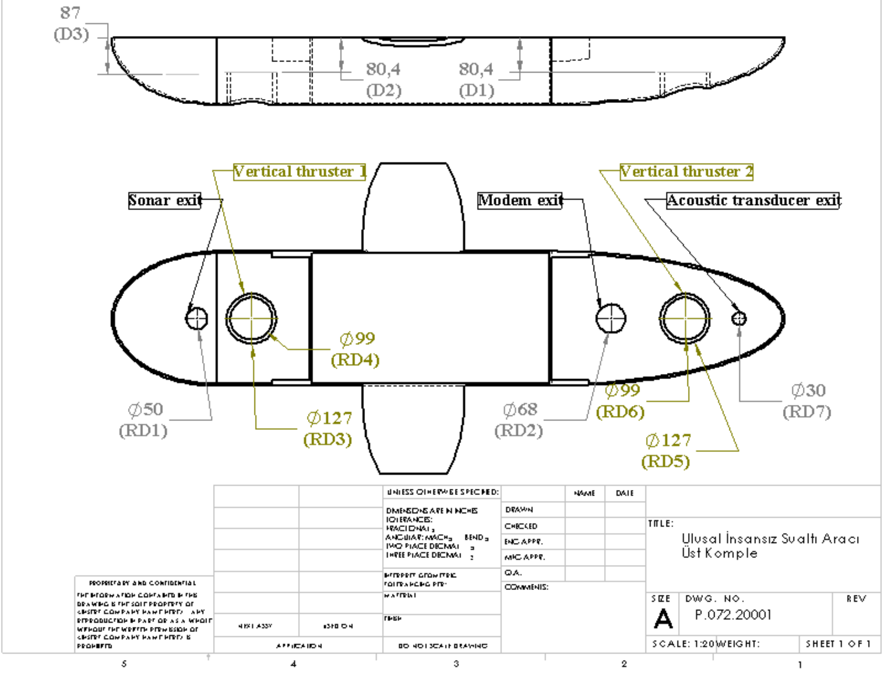

Figure 2.23 Technical drawing of the upper body part

While locating components inside the hull, a minimum separation of 5 cm is given between devices. The design proposal resulted in a body with a length of 1.6 m and a diameter of 0.32 m. *L/D* ratio becomes 5. In fact, this value is slightly lower than the optimum *L/D* ratio. Gertler states that *L/D* = 6.5 gives the minimum total drag for streamlined bodies [17]. Increasing the length of the vehicle could be done; however, it would increase the weight of the vehicle further. Nevertheless, as it is seen in Figure 2.2, assigning slightly lower or higher values to *L/D* do not increase the total drag significantly.

Gertler's studies show that prismatic coefficient value affects the resistance significantly [17]. He shows that a prismatic coefficient of about 0.61 is optimum for a range of *L/D* ratios between 5 and 7. A prismatic coefficient of 0.61 reduces the internal space available for devices significantly. A solutiof for this deficiency is employing a cylindrical middle section as it was given before [18]. Employing a cylindrical mid body with a length 0.495 times the length of the vehicle provides a prismatic coefficient of 0.84 with approximately the same resistance value which would be experienced with a prismatic coefficient of 0.682 with no paralel mid body. For this purpose a paralel mid body with a length of 0.79 meters is used which corresponds to a mid body ratio of 0.49 (close to 0.495). The dimensions of the front and rear ellipsoid sections are specified such that the prismatic coefficient of 0.84. The resulting volume of the body is 0.107 m^3 which gives a prismatic coefficient of 0.832 which is close to the intended value of 0.84. Therefore, one can argue that the resistance is minimized for the *L/D* ratio of 5.

2.6 Material Selection

Determining the hull shape and its dimensions is an important step in the design. After choosing the shape, material of the hull should be determined. It should be noted that the material selection is significant because it affects various design parameters like weight, heat removal capabilities, manufacturing cost and time. Moreover, design capabilities are affected. For instance an internal design approach which would be viable with a composite body may not be feasible with aluminum.

When the literature is searched, it is seen that various materials have been used for the manufacturing of underwater vehicles. The most common materials being used are aluminum, fiberglass composites and carbon fiber composites. A chart that is adopted from auvac.org exemplifies this situation; hull material alternatives and their suitability at different depths are demonstrated [19]. The chart can be seen in Figure 2.24.

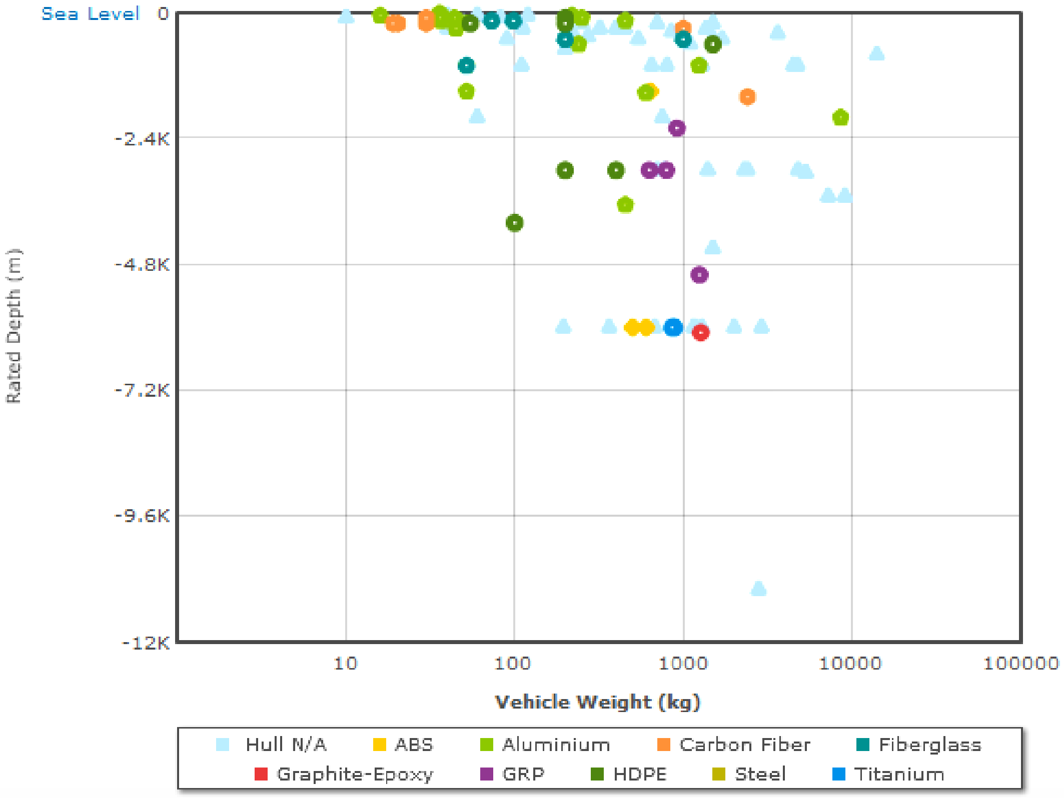

Figure 2.24 Hull materials chart [19]

Besides these common materials, there are other material alternatives as well. Titanium, steel, High-density polyethylene (HDPE) and graphite-epoxy are some of them. Each of these alternatives has distinctive properties. Titanium and graphite-epoxy offer high strength at relatively low densities; therefore, they are convenient for operations at high ocean depths. However, their costs are relatively high and this inhibits them from being common at simpler vehicles.

Amongst the common materials (aluminum, fiberglass composites and carbon fiber composites), there is a higher preference of using aluminum over composites as the hull material. Nevertheless, before making conclusions about the material selection, it is beneficial to give some brief information about composite materials and compare them with traditional materials.

2.6.1 Composite Materials

Composites are artificial materials that are formed by bringing two or more materials with different properties together. Materials form a rigid bond; however, they are separate at macroscopic level. The resulting material is usually anisotropic with different strength values at different directions. The strength is comparable to traditional metals alloys with significantly less weight. In other words, they have higher strength-to-weight ratios. This distinctive property makes composite materials attractive for weight critical applications like aerospace designs.

Composite materials are composed of two constituent materials. These are the reinforcing fibers and homogeneous matrix component. Fibers are strong and stiff elongated materials whose purpose is carrying the load on the material. On the other hand, they are not usable separately; therefore, they are impregnated in a matrix material. The matrix material, sometimes referred to as the resin, holds fibers together in a pre-determined orientation. They transmit and distribute the load to the fibers and also protect those fibers from environmental effects and damages. There are various types of fibers and matrix materials. The selection of the material determines the properties of the resulting composite.

2.6.1.1 Fibers

In composites technology, numerous materials have been used as reinforcing fibers. The most common fiber materials are carbon, graphite, glass, aramid, boron, aluminum, silicon carbide, quartz and polyethylene [21]. Carbon and graphite fibers provide great strength and stiffness to weight ratios. However, they are relatively expensive which limits their usage to cases where weight, not cost, is the priority. Moreover, carbon fibers are electrically conductive and may cause problems in that aspect. Aramid is also an advanced fiber material. Aramid fibers have high tensile strength and stiffness accompanied by high toughness. Especially, this high toughness and vibration damping characteristics make them valuable for armors and protection tools. Moreover, they have high thermal and chemical stabilities. Their high cost, however, make them inefficient for simpler applications. Glass fibers have been the most common ones being used in composites technology. Glass fiber composites have good strength properties with corrosion and moisture resistance. They are not electrically conductive which may be an advantage in some cases. They are not as advanced as carbon or aramid fibers in terms of tensile modulus and they are heavier; however, their lower cost makes them still attractive especially for simple applications.

2.6.1.2 Resins

Various resins with different chemical properties are used as matrix materials in composites. The most well-known examples are epoxy and polyester are the most common resin materials. Epoxies are used commonly due to their high strength, modulus, adhesion capability, corrosion resistance and ease of processing. They are, however, brittle. Polyester resins are inexpensive resins which are used for low-cost application. Moreover, they possess higher toughness compared to epoxies.

2.6.1.3 Production Methods

Method of combining the fiber and the matrix is a process which determines the quality of the final product. There are many ways of production and some of the common ones are hand lay-up, spray-up, filament winding and resin transfer molding.

In hand lay-up method, first of all the mold is prepared like every other method. Fibers are laid on the mold manually and the resin is applied with a brush. As new layers are laid, rollers can be used to compress these layers and release the entrapped air. Hand lay-up is a manual process; therefore, it requires expertise and it cannot be automated. It is not suitable for mass production. In spray-up process resin is applied with a nozzle so it can be automated.

Filament winding is the production technique where continuous fiber which is wetted by resin is wound around a male mandrel. The winding head moves over the mandrel and the speed of this head determines the winding angle and the fiber orientation. Mandrel can be modified to leave grooves or holes on the body. Filament winding is an expansive but efficient method particularly for axisymmetric bodies like rockets. On the other hand, the product has continuous filaments. Due to that, operations such as drilling and cutting are not advised because continuous filaments are cut and the strength is reduced. Therefore, it is best to predict necessary modifications before the production. An illustration about filament winding is seen in Figure 2.25.

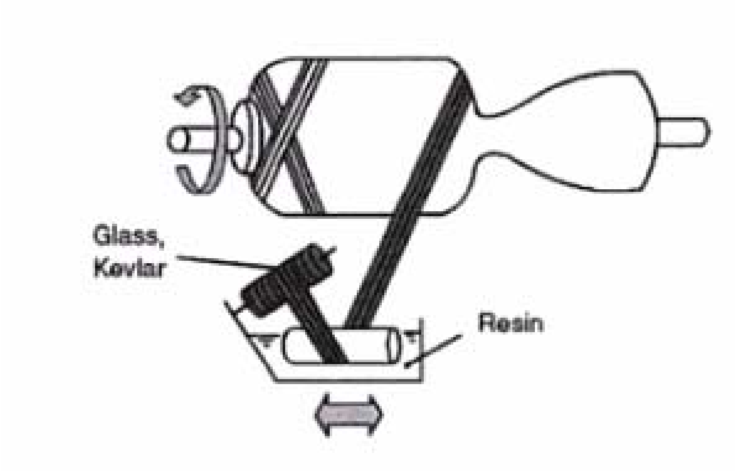

Figure 2.25 Filament winding illustration [22]

Resin transfer molding (RTM) is a production method where fibers are laid between two molds and resin is applied to compressed fibers with pressure. Since the pressure can be controlled, the desired resin ratios can be obtained with low void content [23]. Since there are two molds, the surface quality is good. However, tooling is heavy and expensive. Illustration of this method is seen in Figure 2.26.

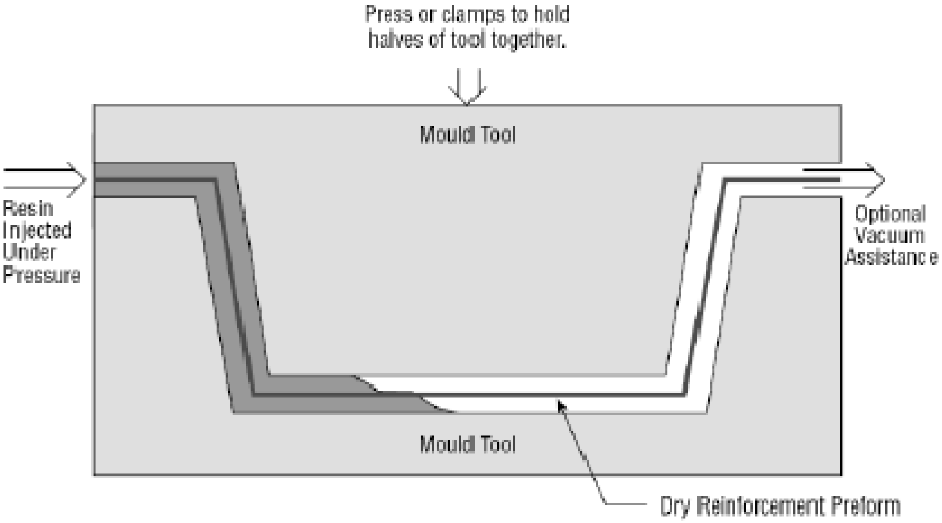

Figure 2.26 Schematic view of Resin Transfer Molding process [23]

RTM method has several varieties. One variety is the vacuum assisted RTM (VARTM). Different than the traditional RTM process, one mold is used and the fibers are laid on this mold. Later on a plastic bag is covered on the mold and vacuum is applied. This vacuum compresses the fibers and decreases void content. Later on resin flows into these fibers due to the vacuum. Its advantage is that only one mold is used; therefore, it is easier to perform compared to RTM. However, it is still a complicated process and needs detailed study. Schematics can be seen in Figure 2.27 [23].

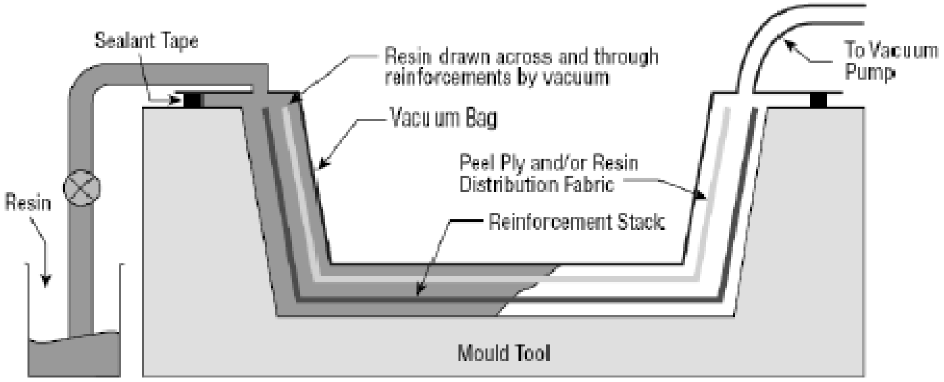

Figure 2.27 Schematics of Vacuum Assisted RTM [23]

Vacuum bagging is a method which can be assumed to be a hybrid of the conventional hand lay-up process and the RTM. In this method, a mold is prepared first. Fiber reinforcement which is usually in the form of fabric is laid on the mold manually and resin is applied. The number of layers to be laid is important because the thickness of the final product is determined by that. After the laying-up process, a plastic sealing bag covers the laminate and vacuum is applied. This vacuum causes the plastic bag compress the laminate. This compression reduces the void content of the composite and enhances the wetting of the fibers. Moreover, excess resin is forced out into the bleeder which increases the resin ratio. Vacuum bagging produces better results compared to hand lay-up. Moreover, it is simpler and cheaper than the RTM method. On the other hand, highly-skilled labor is still required and the surface quality at the plastic bag side is not satisfactory. A schematic representation of this method is seen in Figure 2.28 [23].

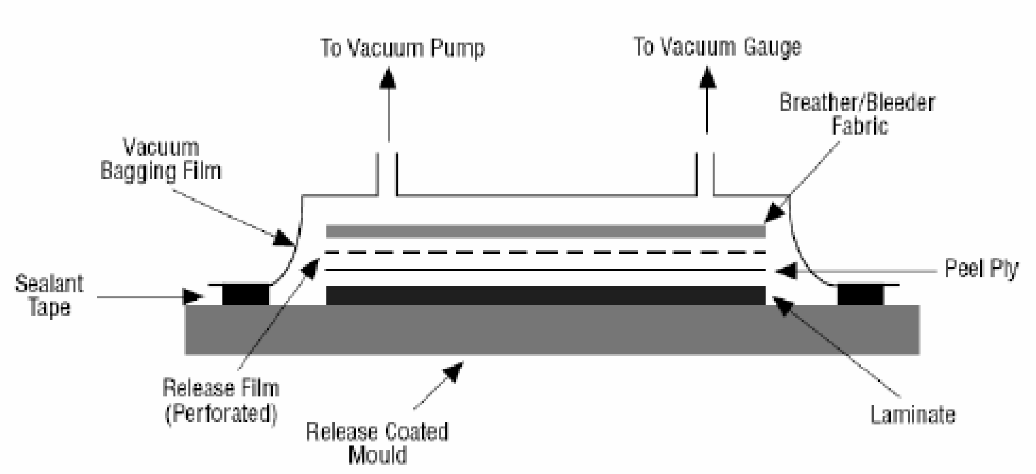

Figure 2.28 Schematic representation of Vacuum Bagging [23]

It should be noted that these processes are for the lay-up and application of the resin. After these, temperature should be applied to the laminate for the resin to cure.

2.6.1.4 Composite Materials and Metal Alloys

Composite materials have distinctive features that make them valuable for certain cases. Their most eminent advantage is the high mechanical properties at low weight. Due to this property, they are significant for aerospace applications where the weight is an important issue. Utilizing composite materials reduces the total weight of the system considerably. Moreover, they can be designed to be anisotropic. For situations where the loading is always in a certain direction, using composites can be very helpful because it can be designed such that it will possess higher strength in the critical direction. Composite materials, particularly aramid resin types, possess high values of damping and vibration reduction compared to metal alloys; hence, they are used for armors. Composite materials are produced by lying fiber reinforcement on a mold. As a result, it gives the designer the flexibility in design options and they are relatively easy to fabricate. Composites are excellent in terms corrosion resistance which means a lot for an underwater vehicle which will be subject to the sea water. On the other hand, composite materials have various disadvantages which inhibit them from being more commonly used. The most important issue is the cost. For operations where financial issues are more critical than weight criteria, using composites materials is not feasible. It is hard to rely on universal mechanical properties data because properties of composites may change for different specimens. Their long-term durability is also questioned. Composites have temperature limitations; hence, they may not be applicable to high-temperature problems.

A comparison of hull materials is seen in [24] and given in Figure 2.29. It is seen that composites provide excellent strength with low weight. Moreover, their low magnetic susceptibility makes them attractive for vehicles that aim to avoid detection.

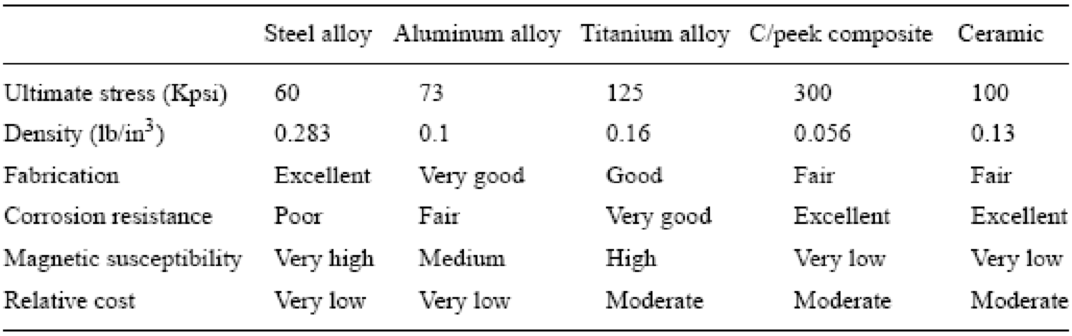

	Steel alloy	Aluminum alloy	Titanium alloy	C/peek composite	Ceramic
Ultimate stress (Kpsi)	60	73	125	300	100
Density (lb/in^3)	0.283	0.1	0.16	0.056	0.13
Fabrication	Excellent	Very good	Good	Fair	Fair
Corrosion resistance	Poor	Fair	Very good	Excellent	Excellent
Magnetic susceptibility	Very high	Medium	High	Very low	Very low
Relative cost	Very low	Very low	Moderate	Moderate	Moderate

Figure 2.29 Hull materials comparison [24]

In this project, the vehicle was produced from composite materials due to many reasons. First of all their ease of fabrication provides more freedom to the designer. Underwater vehicles have to be neutrally buoyant; therefore, weight is an important variable in the design. Composite materials provide the best strength-to-weight ratios. Corrosion resistance is advantageous for a vehicle which will operate underwater. Finally, the technical support given by the manufacturing firm, Barış Elektrik Endüstrisi Inc. has been important for the material selection. Glass-epoxy composite is utilized. Carbon was found unnecessary because diving depths are not so high (100 m). Moreover, carbons electrical conductance may cause problems with the electronic equipments. For the production method vacuum bagging is chosen. It is a relatively simple and low cost method; nonetheless, it provides high resin ratio with low void content.

CHAPTER 3

HEAT TRANSFER ANALYSES

As it was mentioned before, the hull has a watertight section which houses electronic card and batteries. These devices dissipate heat during their peformance. For ULİSAR this heat dissipation rate is 55 W (50 W from cards and 5 W from batteries). Even though the vehicle will operate underwater, over-heating may still occur inside the pressure hull. The reason is that glass-epoxy composites have low thermal conductance. When it is recalled that the pressure hull has thick walls, it can be deduced that the resistance to heat rejection from the body will increase. As the heat rejection rate decreases, the temperature in the pressure hull increases and it may affect the operation electronic cards negatively. The maximum allowable temperature in the pressure hull is 55 ˚C for ULİSAR. The pressure hull can be seen in Figure 3.1.

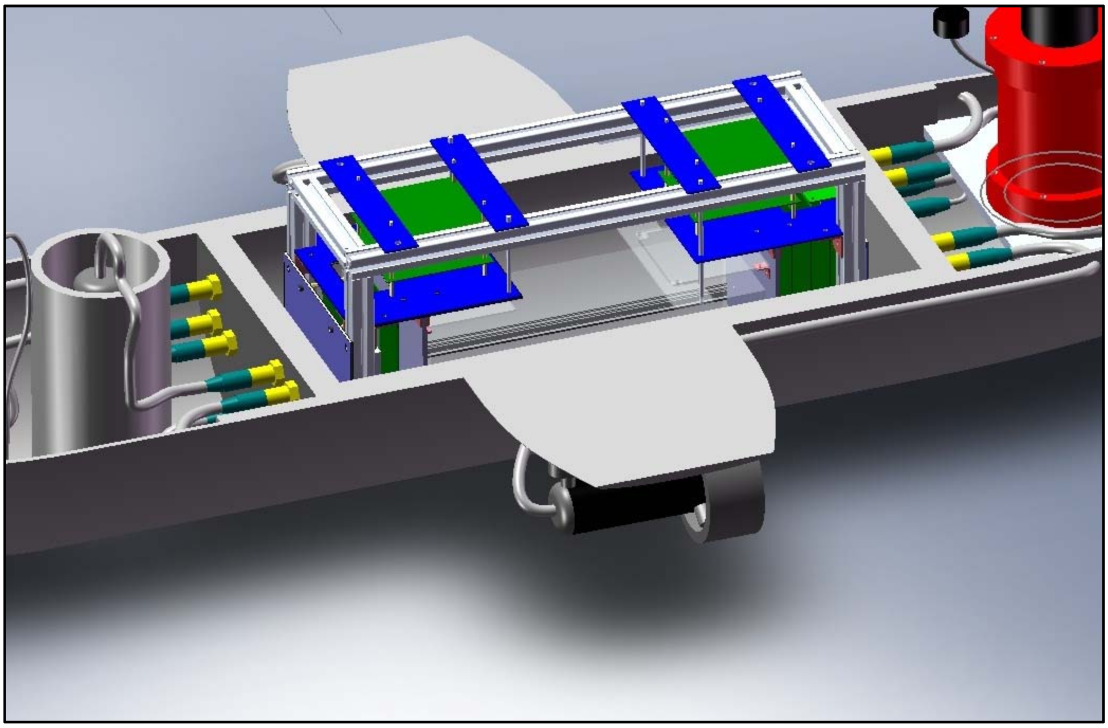

Figure 3.1 Pressure hull

3.1 The Software

For heat transfer analyses FLUENT 6.3.26 and Gambit 2.3.16 software are used. Gambit is used in the pre-processing step. Gambit is a program that can import geometry data from computer aided design (CAD) softwares. Edge meshes, surface meshes, boundary layer meshes and volume meshes can be generated on the flow domain. Both unstructured and structured meshes are available in Gambit.

FLUENT 6.3.26 is used for solution and post-processing. It can import structured and unstructured meshes from different programs including Gambit. It has several physical models to model flow, turbulence, heat transfer and reactions for a wide range of applications. Both steady and unsteady analyses can be performed. Boundary conditions for the problem are defined in Fluent and results are also seen after the solution. Contours of various flow parameters can be plotted. In this case, temperature distribution in the pressure hull is the most critical result.

3.2 Analyses

Unsteady solver of FLUENT is used in this case. Steady solver gives results for the steady-state solution and these results can be misleading. The maximum temperature obtained may be too high; however, reaching that temperature may take more than the operation time of the vehicle. Consequently, analyses were performed for 2 hours which is the expected operation time of the vehicle. 3D unsteady heat transfer analyses are very difficult to perform with the computational resources available. Therefore, 2D analyses were done. Two cases were solved.

3.2.1 Analysis for the First Case

For the first case, the front view cross-section of the pressure hull is modeled as seen in Figures 3.2, 3.3 and 3.4.

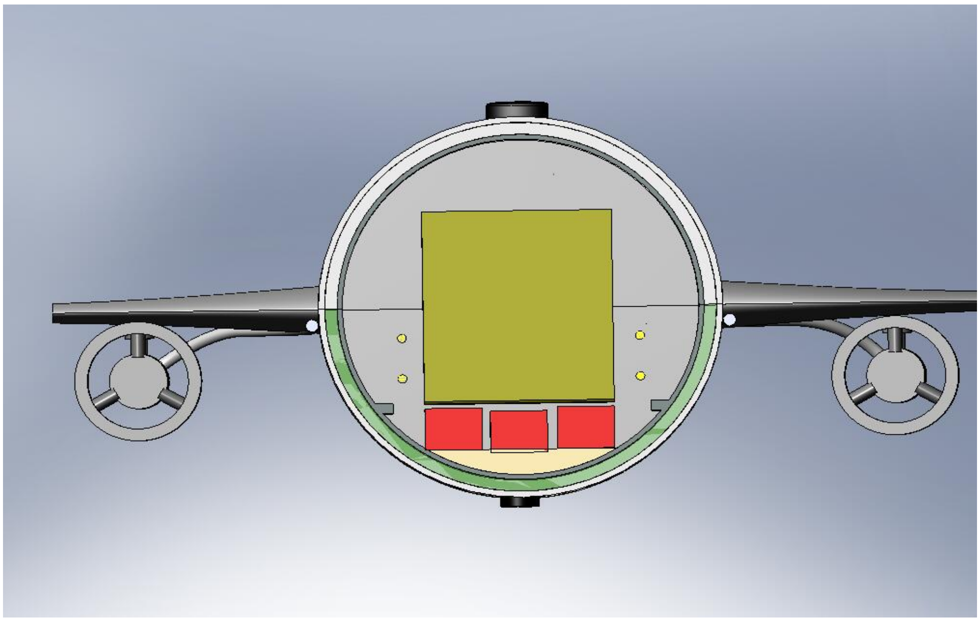

Figure 3.2 Front view cross-section

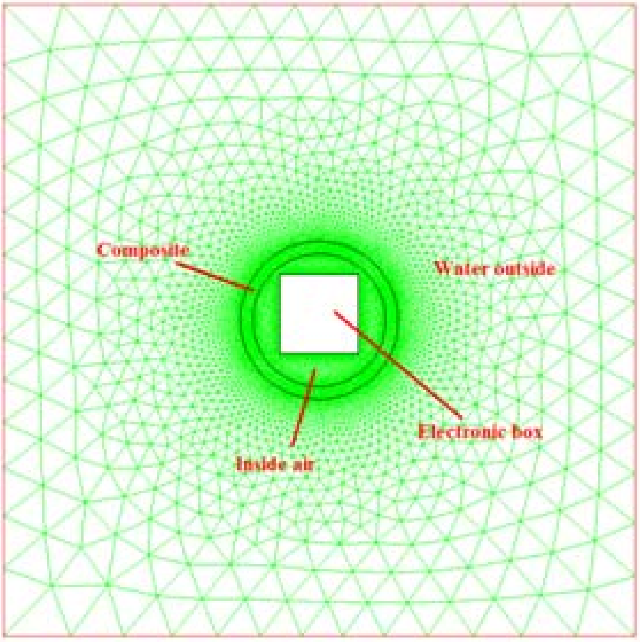

Figure 3.3 Computational model - 1

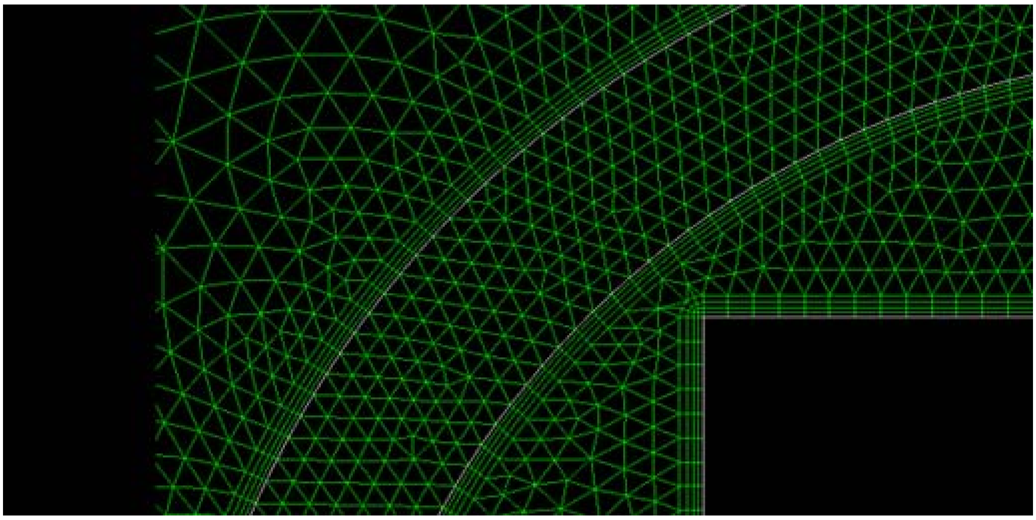

Figure 3.4 Details of the computational model - 1

2D, pressure based, unsteady solver was employed. Green-Gauss node based gradient option was enabled and laminar flow was solved. Air is defined to be compressible with the ideal gas formulation to be able to solve for natural convection inside the pressure hull. Water was defined to be incompressible. In order to be on the safe side, the vehicle was assumed to be stationary. It is obvious that the heat transfer rate will increase if the vehicle moves due to forced convection. Only the electronic box is modeled and a heat dissipation of 55 W was defined at the walls of the box. Initial temperature of the whole system is given 27 ˚C.

The temperature distribution in the pressure hull by the end of 2 hours (7200 s) can be seen in Figure 3.5. It is seen that the maximum temperature occurs on the box and has a value of 43 ˚C which is lower than the allowable temperature (55 ˚C).

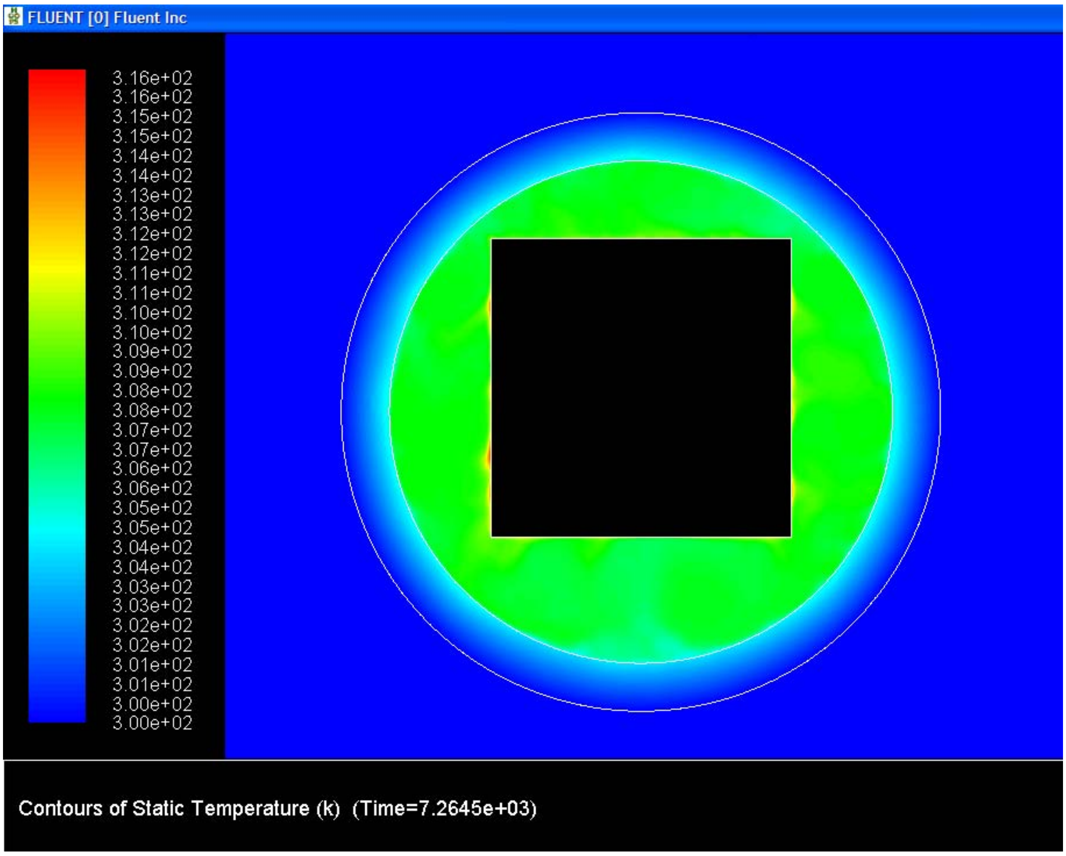

Figure 3.5 Temperature distribution inside the pressure hull

3.2.2 Analysis for the Second Case

An alternative analysis was performed later on. This time the cross section of the right side view is taken as seen in Figure 3.6. This time batteries are also added to the model. Moreover, the water that is entrapped in the flooded section is present; hence, heat rejection is expected to be predicted more accurately.

Solution parameters are the same as the previous case. This time the initial temperature of the water is 20 ˚C and the body is 30 ˚C. The temperature at an arbitrary time is seen in Figure 3.7. It is seen that the most critical points are on the box as expected.

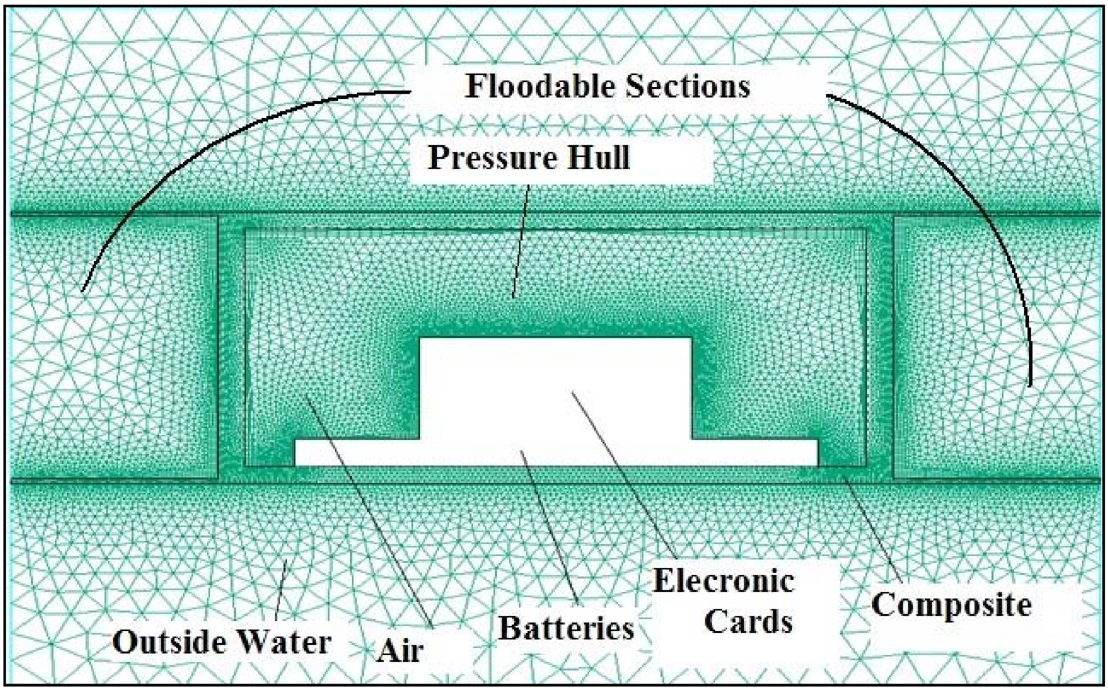

Figure 3.6 Details of the computational model – 2

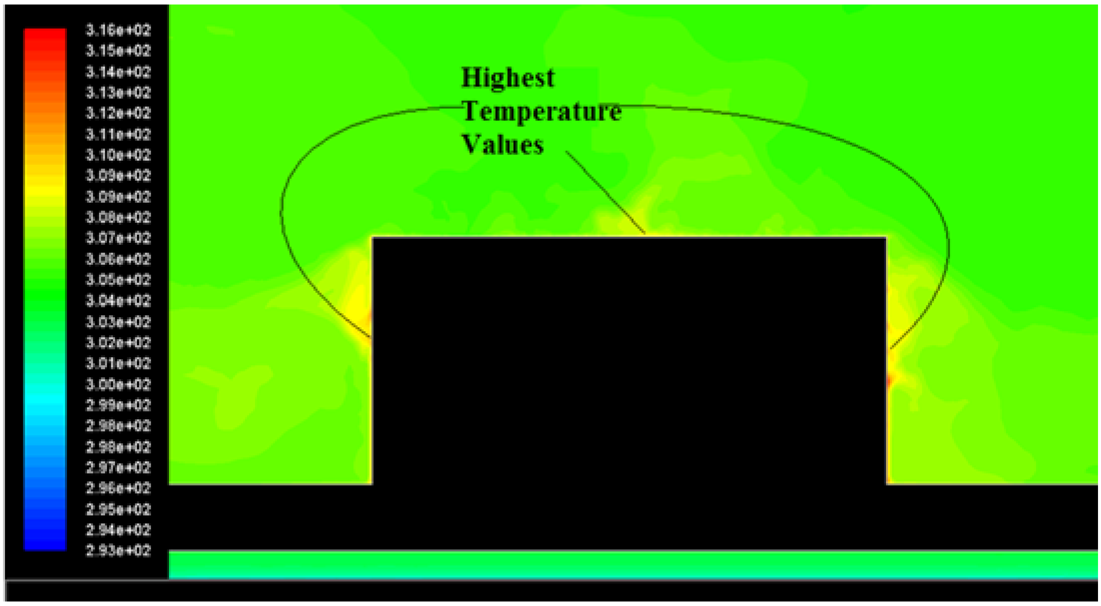

Figure 3.7 Critical temperature locations

The change of the maximum temperature in the pressure hull vs time is given in Figure 3.8. The graph has some oscillations; however, it is seen from the trend that the maximum temperature drops and converges to a steady value of about 37 ˚C. This value is again below the critical limit. It should be noted that the maximum temperature was higher (43 ˚C) in the previous case. This can be attributed to the cooling effect of floodable section. A free-flooding hull is advantageous in terms of heat rejection.

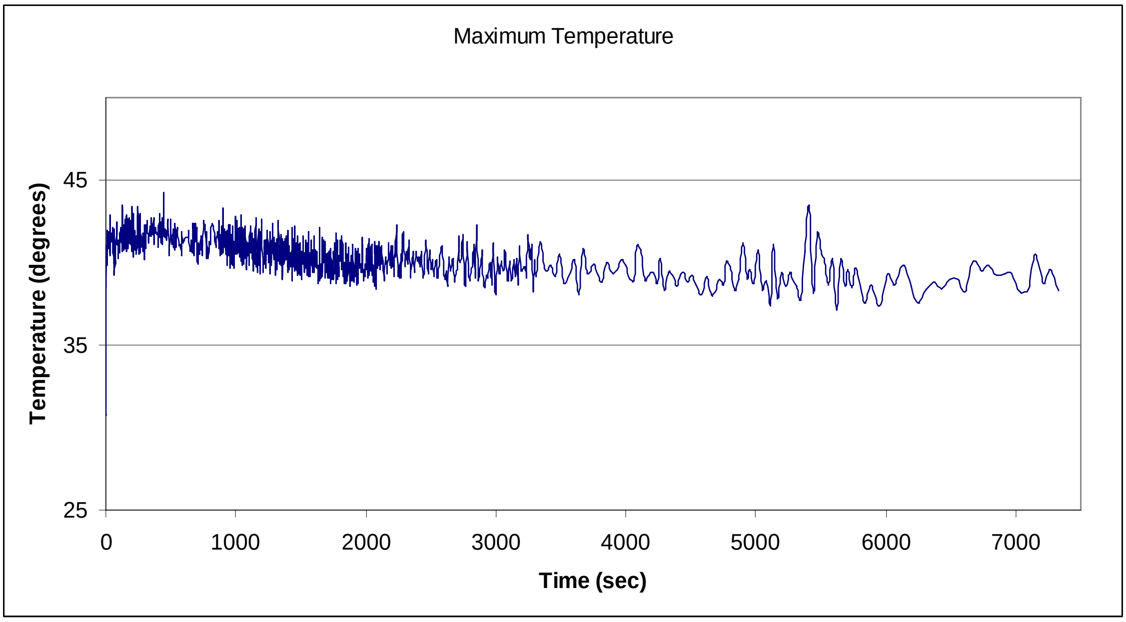

Figure 3.8 Maximum temperature vs time

These heat transfer analyses should be considered as preliminary analyses. Their results are not reliable because the analyses are two dimensional. Moreover, the electronic cards are modeled as a single box to simplify the model. The sandwich structure and resulting contact resistances are not included. Consequently, these analyses only give an idea on the temperature distribution.

3.2.3 Heat Transfer Test

To have a better understanding of the temperature distribution, a heating test is performed by Barış Elektrik Endüstrisi A.Ş. A composite hull which resembles the pressure hull of the vehicle is used. A 50 W lamp is placed and the body was immersed in water for 2 hours. The initial temperature of the body is 25 ˚C and water is at 18 ˚C. Temperature sensors are placed at different locations inside the hull and temperature is recorded. Figure 3.9 shows the experimental setup and Figure 3.10 illustrates the positions of the sensors.

Figure 3.9 Experimental setup

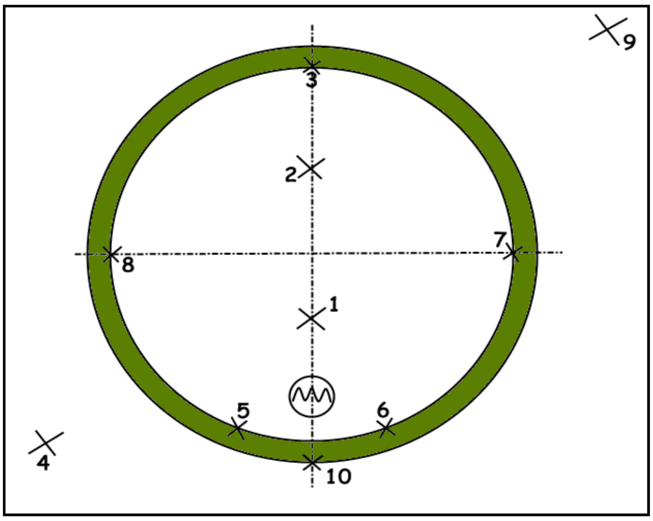

Figure 3.10 Temperature sensor positions

The temperature vs time graph is seen in Figure 3.11. Point 6 is the most critical one and its temperature converges to an approximate value of 35 ˚C.

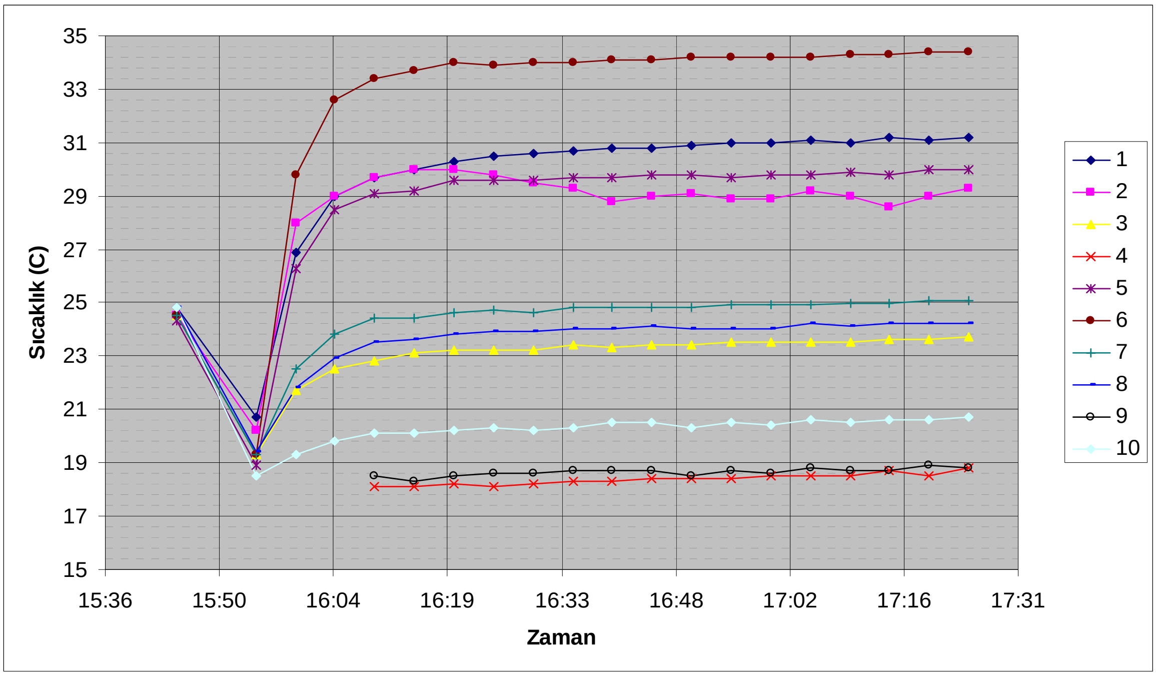

Figure 3.11 Temperature vs time inside the hull

Experimental results converge to a value of 35 ˚C and second analysis converges to 37 ˚C. When considering the fact that initial temperature of the hull was 30 ˚C for the analysis and 25 ˚C for the experiment, it is possible to deduce that experimental and simulation results match well. Therefore, we can conclude that the results of the second simulation are satisfactory even though they are very simple and preliminary calculations. Moreover, it is not expected to have over-heating at this point. Certainly, the actual results will be received when the vehicle is tested in real conditions.

CHAPTER 4

VALIDATION STUDIES

Determining the hull shape and its dimensions along with the thruster configuration is an important issue in vehicle design. However, before accepting the design proposal certain analyses are necessary. In our case the most critical requirement is about surging (forward) speed. Therefore; drag calculations should be performed to make sure that the offered design satisfies the speed criterion (2 m/s). For these analyses, Computational Fluid Dynamics (CFD) method is used and the commercial CFD solver software FLUENT 6.3.26 is employed. Before presenting the results of the analyses, it is helpful to give brief information on CFD and its applications in marine science.

4.1 Introduction to CFD

Computational fluid dynamics is a method used for determining fluid and flow properties like pressure, density, temperature and velocity vectors for different flow cases. These properties can be used for calculating important data like drag force, heat transfer rate, pressure distribution, acoustics, etc. In other words CFD enables the designer to predict the performance of a virtual system during the design. It is obvious that this is advantageous for the designer since the virtual system can be tested and modified if necessary until finding the optimum one. As a result, the chances of obtaining a successful design at the end increases, number of experiments required to find the optimum design decreases which in turn reduces the cost and duration of the design process.

In marine applications like an unmanned underwater vehicle design project, CFD can be used for many purposes. The most common usage is determining the drag force on the body in a specified scenario. This drag data is critical in choosing the propulsion system for achieving the speed requirement. For systems where speed criterion is strict or energy source is limited, the importance of performance prediction increases. As solver capabilities and computational resources have improved in recent years, CFD found new areas of application in marine science. One example is the propeller-hull interaction. The performance of a propeller strongly depends on the inlet flow quality of the propeller. Therefore, it is beneficial to make CFD analyses to predict the propeller performance. Maneuverability of the vehicle is another topic to investigate using CFD. It should be noted that unlike aerospace applications, experimental data for marine applications is scarce. Furthermore, it is harder to conduct experiments since experimental facilities like water tunnels are not common. These intensify the need for CFD simulations even more.

Speaking in general terms, a CFD simulation is the simultaneous solution of a set of governing equations of fluid flow in a discretized flow domain to obtain the distribution of various flow parameters. A CFD simulation process consists of three steps: namely, pre-processing, solution and post-processing. In pre-processing the geometry and the flow domain around it are generated. Later on the domain is divided into numerous elements and the computational mesh is formed. Boundary conditions and material properties are defined at this step. In the solution step governing equations of fluid flow are solved for each cell in the mesh to obtain the distribution of fluid and flow parameters. Post-processing is the last step where relevant flow data can be seen and results can be assessed.

In the following parts of the chapter, detailed information about the governing equations and turbulence models which are used in the software FLUENT are presented.

4.1.1 Governing Equations of Fluid Flow

Governing equations of fluid flow originate from conservation laws of physics; namely, conservation of mass, conservation of momentum in three dimensions and conservation of energy. Mathematically, one can derive governing equations for these laws. For a three dimensional, unsteady, viscous, compressible fluid flow following equations are given as [25]:

Continuity equation:

$$\frac{\partial \rho}{\partial t} + \nabla \cdot (\rho \boldsymbol{U}) = 0 \tag{4.1}$$

Momentum equation in the x-direction:

$$\frac{\partial (\rho u)}{\partial t} + \nabla \cdot (\rho u \boldsymbol{U}) = -\frac{\partial p}{\partial x} + \frac{\partial \tau_{xx}}{\partial x} + \frac{\partial \tau_{yx}}{\partial y} + \frac{\partial \tau_{zx}}{\partial z} + \rho f_x \tag{4.2}$$

Momentum equation in the y-direction:

$$\frac{\partial (\rho v)}{\partial t} + \nabla \cdot (\rho v \boldsymbol{U}) = -\frac{\partial p}{\partial y} + \frac{\partial \tau_{xy}}{\partial x} + \frac{\partial \tau_{yy}}{\partial y} + \frac{\partial \tau_{zy}}{\partial z} + \rho f_y \tag{4.3}$$

Momentum equation in the z-direction:

$$\frac{\partial (\rho w)}{\partial t} + \nabla \cdot (\rho w \boldsymbol{U}) = -\frac{\partial p}{\partial z} + \frac{\partial \tau_{xz}}{\partial x} + \frac{\partial \tau_{yz}}{\partial y} + \frac{\partial \tau_{zz}}{\partial z} + \rho f_z \tag{4.4}$$

It should be noted that $\boldsymbol{U}$ refers to the velocity vector which is composed of velocities in x, y and z directions.

In marine CFD applications, energy equation is usually neglected since system is isothermal and flow is incompressible. For Newtonian flows where density and viscosity are constant and body forces are not present, equations become:

Continuity equation:

$$\frac{\partial u}{\partial x}+\frac{\partial v}{\partial y}+\frac{\partial w}{\partial z}=0 \tag{4.5}$$

Momentum equation in the *x*-direction:

$$\rho\left(\frac{\partial u}{\partial t}+u\frac{\partial u}{\partial x}+v\frac{\partial u}{\partial y}+w\frac{\partial u}{\partial z}\right)=-\frac{\partial p}{\partial x}+\mu\nabla^2 u \tag{4.6}$$

Momentum equation in the *y*-direction:

$$\rho\left(\frac{\partial v}{\partial t}+u\frac{\partial v}{\partial x}+v\frac{\partial v}{\partial y}+w\frac{\partial v}{\partial z}\right)=-\frac{\partial p}{\partial y}+\mu\nabla^2 v \tag{4.7}$$

Momentum equation in the *z*-direction:

$$\rho\left(\frac{\partial w}{\partial t}+u\frac{\partial w}{\partial x}+v\frac{\partial w}{\partial y}+w\frac{\partial w}{\partial z}\right)=-\frac{\partial p}{\partial z}+\mu\nabla^2 w \tag{4.8}$$

Equations (4.5) to (4.8) include four flow variables, p, u, v and w and there are four equations. Therefore, one can create a mesh and solve these equations simultaneously for all cells and find the value of p, u, v and w for each cell. This is true for the laminar, incompressible, three dimensional flow. However, in reality these variables are subject to instabilities and laminar flow usually leads to turbulent flow where flow turbulence modeling is necessary for solution.

4.1.2 Introduction to Turbulence Modeling

Turbulence is one of the most important and complex topics in CFD. In this part of the thesis only brief information about it will be given. Basically, turbulent flow is a three dimensional, highly irregular and time dependent mode of flow.

Turbulent flows have a swirling character with local vortices. These vortices are called turbulent eddies and their time and length scales vary significantly. These eddies are responsible for the enhanced mixing of transportation quantities in the flow domain. It is no longer possible to define steady quantities for pressure and velocities. Instead, these quantities have unsteady characters.

It should be noted that these energy carrying eddies have varying length and time scales. For turbulent flow simulations, one should consider the effect of these eddies, regardless of their scale, to calculate flow variables accurately. The effort to calculate the effect of turbulence on flow variables is called turbulence modeling. The complexity of the turbulence model depends on the scale of eddies that are taken into account while modeling. Turbulence models can be divided into three categories depending on their complexity: Direct Numerical Simulation (DNS), Large Eddy Simulation (LES) and Reynolds Averaged Navier-Stokes (RANS) method.

Direct Numerical Simulation (DNS) is the most complex simulation approach. In this method all of the scales of turbulence in the flow are solved no matter how small those scales are. In fact no modeling is made; instead, all the scales of turbulence are solved directly. DNS enables the researcher to get data of the fluid even at very small scales. On the other hand, solving the Navier-Stokes equations at such small scales requires extremely fine meshing and the total number of cells in the mesh increases to huge numbers. It is even worse for high Reynolds number flows where the length scale of the smallest eddies are even smaller. Even for low-Reynolds number flows it is not possible to solve complex problems with the computational resources available today.

Even though DNS makes extremely accurate predictions, most of the practical cases in CFD do not require such fine detail at small scales. Therefore; engineers tend to use simpler models which can still provide accurate results with reasonable computational time. One such approach is the Large Eddy Simulation (LES). As its name implies, LES considers only large scales of eddies. Large eddies are solved directly while small eddies are filtered and their effects are modeled. This requires the solution of Navier-Stokes equations with an additional stress term for small scales. Filtering small scales of turbulence makes LES require less computational resources compared to DNS and still give accurate results. The instantaneous flow characteristics are still captured. On the other hand, computational requirements are still high for LES which makes it unsuitable for most of the practical applications.

As it was mentioned, LES and DNS offer excellent solutions for flow simulation; however, the computational resources of today make them unsuitable for majority of practical cases. One approach to overcome this difficulty is Reynolds Averaging. In this approach, it is assumed that flow variables have mean and fluctuating components. When mean and fluctuating variables are used in the three dimensional unsteady Navier-Stokes equations, a new set of equations called Reynolds-Averaged Navier-Stokes (RANS) equations are obtained. RANS equations solve for only mean values of the flow variables. Due to fluctuating quantities, additional terms appear in RANS equations. These terms represent the unsteady effect of turbulence and they act as an additional viscosity term in the equation. Therefore these terms are named as “turbulent stresses” or “Reynolds stresses”.

Modifying Navier-Stokes equations for obtaining RANS equations has two effects. First of all there is a great loss of information. Only mean variables are solved and the effect of eddies are modeled. This enables a steady solution of equations with less number of elements. Hence, computational requirements and solution time are much lower compared to LES and DNS. On the other hand, RANS methods provide only time-averaged results while LES and DNS give instantaneous flow variables. The second effect is that additional terms are added to Navier-Stokes equations. As a result, the set of equations are not closed anymore and additional equations are necessary for solution. Turbulence modeling is, in fact, performed for defining Reynolds stress components in terms of known variables of flow and additional equations are obtained.

RANS models give acceptable results with reasonable computational time and resources; therefore, they are widely used for practical applications. In this thesis, emphasis will be on RANS models and these models will be used for underwater vehicle simulations.

4.1.3 Reynolds Averaging

Reynolds averaging is decomposing flow variables into its mean and fluctuating components. For instance x-velocity can be decomposed as

$$u = u(x) + u'(x,t) \tag{4.9}$$

where $u(x)$ is the mean and $u'(x,t)$ is the fluctuating component of velocity. Similar forms of equations can be written for the velocity components in y and z directions. When these pressure and velocity definitions are used in Equations (4.6) to (4.8), momentum equations become:

Momentum equation in the x-direction:

$$\rho\left[\frac{\partial(u^2)}{\partial x}+\frac{\partial(uv)}{\partial y}+\frac{\partial(uw)}{\partial z}\right] = -\frac{\partial p}{\partial x}+\frac{\partial}{\partial x}\left[\mu\frac{\partial u}{\partial x}-\rho\overline{u'^2}\right] \\ +\frac{\partial}{\partial y}\left[\mu\frac{\partial u}{\partial y}-\rho\overline{u'v'}\right]+\frac{\partial}{\partial x}\left[\mu\frac{\partial u}{\partial x}-\rho\overline{u'w'}\right] \tag{4.10}$$

Similar equations can be written for y and z momentum equations. It is seen that additional variables like $\rho\overline{u'v'}$, $\rho\overline{u'w'}$ are created. These are known as Reynolds stresses and they should be modeled.

For modeling these Reynolds stresses, two common approaches are held. The first one is the Boussinesq approach and the second one is directly calculating these stresses through transport equations.

4.1.4 Boussinesq Approach

According to Boussinesq approach:

$$-\rho\overline{u'v'} = \mu_t\left(\frac{\partial u_i}{\partial x_j} + \frac{\partial u_j}{\partial x_i}\right) - \frac{2}{3}\left(\rho k + \mu_t\frac{\partial u_k}{\partial x_k}\right)\delta_{ij} \tag{4.11}$$

where k is the turbulence kinetic energy per unit mass and μ_t is the turbulent (eddy) viscosity. As it is seen in Equation (4.11), Reynolds stresses can be calculated for a cell if μ_t and k are known for those cells. Furthermore, μ_t is related to k with a simple equation by the turbulence model being used. Hence, for computing Reynolds stresses, one has to know the turbulence kinetic energy per unit mass. On the other hand, k is calculated by defining a dissipation term for it and solving those equations simultaneously over the whole domain. The relationship between turbulent viscosity and turbulence kinetic energy along with transport equations for k and its dissipation depends on the turbulence model being used. The success of the turbulence model is determined by these relations.

Spalart-Allmaras, k - ε and k - ω turbulence models use Boussinesq approach. Spalart-Allmaras is a one-equation model where only a single transport equation is solved for turbulent viscosity. k - ε and k - ω turbulence models are two equation models. In k-ε model, two additional equations are solved for k and turbulence kinetic energy dissipation rate, ε. In k - ω turbulence model, two additional equations are solved for k and turbulence kinetic energy specific dissipation rate, ω. These models are commonly used in CFD and also by the users of FLUENT. Their advantage is that they assume that μ_t is isotropic and this reduces computation costs significantly. On the other hand they may give inaccurate results when turbulence in the domain of interest has anisotropic character.

As an alternative to Boussinesq approach, one can solve six transport equations along with an equation for dissipation (usually ε) for Reynolds stress components. This means that five additional equations for 2D case and 7 additional equations for 3D case will be solved. It is obvious that the computation time will increase; however, the accuracy is much better compared to two equation models especially for complex flows where anisotropy is present in Reynolds stresses. Some examples of complex flows are given in FLUENT 6.3 User's Guide [26] as cyclone flows, highly swirling flows in combustors, rotating flow passages, and the stress-induced secondary flows in ducts. Models that use this approach are called Reynolds Stress Models (RSM). Conversely, it will not be feasible to use this model for simple flows since the improvement in the accuracy will not overcome the increased computation cost. Nevertheless, as computational resources are progressing, RSM models are gaining popularity.

4.1.5 Turbulence Models

CFD analyses in this thesis are performed by the FLUENT 6.3.26 software. In FLUENT various turbulence models with different capabilities and complexities are offered. These models are Spalart-Allmaras, k - ε, k - ω, RSM, Detached Eddy Simulation (DES) and LES.

It should be noted that none of these turbulence models are proven to be applicable for all cases. Each of them has advantages and disadvantages. The analyzer has to make a decision based on needs, computational resources and time.

Spalart-Allmaras model is a simple RANS model that adopts Boussinesq approach. This model solves only one transport equation for turbulent viscosity, μ_t. Computation time is lower compared to two-equation models. For wall-bounded flows in aerospace applications, the popularity of the model is increasing. On the other hand, it is a relatively new model and its efficiency for comlex flows is not verified yet [26].

RSM provides accurate results for complex flows; however, its feasibility is not justified for simple problems due to high computational cost. In this project, CFD simulations are performed for calculating the drag force on the streamlined hull shape. It is obvious that this problem is a simple external flow problem and the use of RSM is not critical. Similarly, LES and DES models have high computational costs which make them unsuitable for the analyses of the vehicle.

LES model is a much more complex model where instantaneous flow characteristics can be captured due to solving equations for large eddies in the flow. DES is a hybrid model between LES and RANS models.

Two-equation models solve a transport equation for k along with an additional equation for its dissipation. These models are the most popular ones for industrial applications because they provide accurate results with reasonable computational time. FLUENT offers k - ε and k - ω models with their variations as two-equation models. In this thesis these models are chosen for review since they meet project requirements best.

4.1.5.1 k - ε Turbulence Models

k - ε turbulence model in FLUENT has three variations: standard, RNG and realizable $k - \varepsilon$ models. Standard model is the earliest and simplest $k - \varepsilon$ model. It is a semi-empirical model since the dissipation term ε is obtained through empirical relations [26]. As an early model, it has several weaknesses. It has been noted to give inaccurate predictions for flow cases involving separation, swirling, re-circulation, re-attachment and mixing [25]. Due to these deficiencies this model is improved to obtain the variations of the $k - \varepsilon$ model.

RNG model is another variation of the k - ε model. The ε equation is modified and effect of swirl on turbulence is added. It is claimed that the model works for a wider class of flows and performs well for flows for rapidly strained flows and swirling flows.

Realizable $k - \varepsilon$ is the most common model being used. It is a relatively recent improvement on the standard model. Turbulent viscosity and turbulent dissipation rate equations are modified over the standard model. It has been claimed that the model gives superior results for flows involving rotation, boundary layers under strong adverse pressure gradients, separation, and recirculation.

4.1.5.2 k - ω Turbulence Models

FLUENT has two k - ω turbulence model variations. These are standard $k - \omega$ model and the Shear-Stress Transport (SST) model. These models solve transport equations for turbulence kinetic energy, k, and its specific dissipation rate, ω. The standard model is known to predict accurately for wall-bounded flows and free shear flows. One drawback of the model is its sensitivity to free stream effects.

To eliminate the inaccuracies due to free stream effects, a variation was developed. This model is called the SST $k - \omega$ model. In this model the standard $k - \varepsilon$ and standard $k - \omega$ models are combined. For the near-wall region SST $k - \omega$ is employed and for the free stream the less sensitive $k - \varepsilon$ is used. This modification makes SST a suitable model for a wide range of flows.

4.1.6 Near Wall Treatment

One of the key points in turbulence modeling is the near wall treatment. In the region close to wall there are different layers with varying characteristics due to the strong effect of the wall. A turbulence model may not be valid for all of these regions; therefore, while creating the mesh and choosing the turbulence model, one has to be careful about this region. The accuracy of the simulation depends strongly on the accurate modeling near the wall.

In the region closest to the wall, viscous effects are dominant. This effect causes a region with laminar characteristics. It is called the viscous sublayer or laminar sublayer. In this region molecular viscosity is dominant over the turbulent viscosity. Due to this fact many turbulence models are not valid in this region. In the outermost region of the boundary layer there is the fully-turbulent or log-law region where viscous effects are suppressed and the flow is entirely turbulent. Turbulence models perform well in this region. Between these two regions, there is a transition region named as the buffer layer or blending region where the effects of the wall and free stream are comparable. These layers can be seen in detail in Figure 4.1.

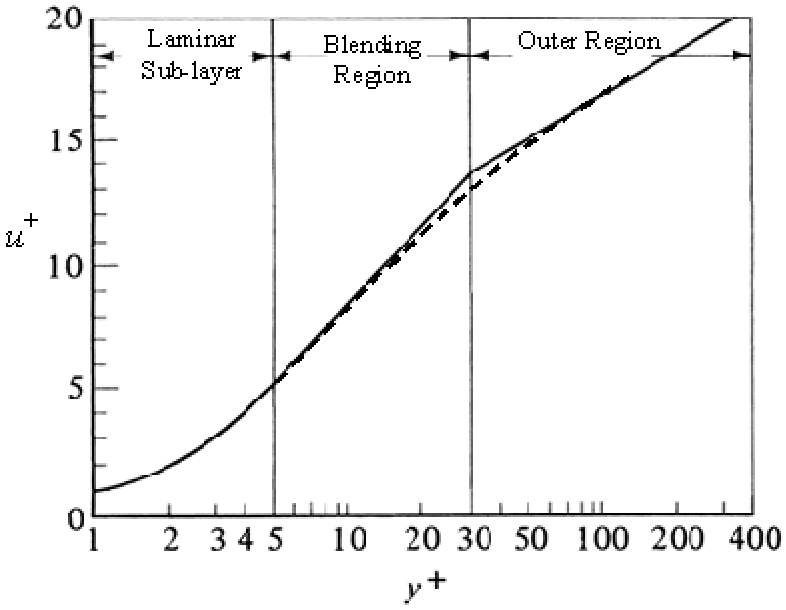

Figure 4.1 Near wall region

In Figure 4.1, u^+ is the non-dimensional velocity and y^+ is the non-dimensional distance of the cell to wall where

$$y^+ = \frac{\rho u_T y_p}{\mu} \tag{4.12}$$

$$u^{+} = \frac{u}{u_T} \tag{4.13}$$

$$u_T = \sqrt{\frac{\tau_w}{\rho}} \tag{4.14}$$

In Equations (4.12) to (4.13) u_T is the friction velocity, y_p is the distance from the cell to the wall and τ_w is the wall shear stress.

The most important issue in near wall treatment is deciding the level up to which the boundary layer needs to be resolved. As it was shown in Figure 4.1, it is seen that the boundary layer consists of three regions. If it is desired to resolve the boundary layer all the way up to the laminar sublayer, first cell adjacent to the wall should be placed in the that region. Alternatively, one can place the first cell in the fully turbulent outer region if the viscous sublayer is not aimed to be captured exactly. These two alternatives lead to two approaches: near wall modeling and utilization of wall functions. In the wall function approach, viscous sublayer and buffer layer regions which require fine mesh are not modeled. Instead of this semi-empirical functions are called wall functions are used to represent these regions. In the near wall modeling approach, the boundary layer all the way up to the viscous sublayer is solved.

Wall functions are useful especially for high-Reynolds number flows. Since there is no need to generate extremely fine meshes, this approach reduces mesh size and computation time. However, for low-Reynolds number flows the mesh size may increase too much in order to locate the first cell in the fully turbulent region and this may cause bad mesh quality. Near wall treatment requires a fine mesh near the wall; hence, computation time increases; however, better accuracy is achieved. This method is beneficial for low-Reynolds number flows where required mesh size is not very small.

In FLUENT the turbulence model SST, when transitional option is activated, is a low-Reynolds number model; in other words, it solves all the way up to the viscous sublayer. Therefore; one has to create a very fine mesh near the wall when using SST. On the other hand, $k-\varepsilon$ is a high-Reynolds number model so one has to begin with a coarse mesh so that the first element in the mesh falls into the fully-turbulent region. $k-\varepsilon$ model use two types of wall functions; namely, Standard Wall Functions (SWF) and Non-equilibrium Wall Functions (NWF). Moreover, $k-\varepsilon$ has an Enhanced Wall Treatment (EWT) option which can be activated if it is desired to solve the complete boundary layer with this model.

At this point it is necessary to define criteria to check whether the near wall mesh is fine enough or not. Wall y^*, y^+ and Re_y can be used for this purpose. y^+ and y^* represent dimensionless distance from the wall to the cell and can be given as

$$y^* = \frac{\rho C_\mu^{1/4} k_p^{1/2} y_p}{\mu} \tag{4.15}$$

$$Re_y = \frac{\rho y_{p\sqrt{k}}}{\mu_{lam}} \tag{4.16}$$

where C_μ (=0.09) is the modeling constant, k_p is the kinetic energy of that point at point P, y_p is the distance from the point to the wall, u_T is the friction velocity and μ_{lam} is the laminar viscosity.

When using the wall function approach, it is important to locate the first cell off the wall in an interval of $30 < y^* < 300$ because wall functions are valid in this region (log-law region). It is advised not to exceed values of 100 [26].

For enhanced wall treatment, fine mesh is required. A mesh with the first cell in the viscous sublayer at y^+ is 1 is the ideal. However, higher y^+ values are also acceptable until $y^+ < 4$ to 5 [26].

The aim while creating the boundary layer mesh should be making the mesh either fine or coarse so that the first element height does not fall in the interval $5 < y^+ < 30$.

Besides the first cell height, number of cells inside the boundary layer should also be checked. FLUENT User's Guide [26] suggests that there should be at least 10 cells until $Re_y < 200$. After the analyses it is useful to make plots of y^+ and y^* on the wall and contours of Re_y and check them to see whether the mesh is suitable for the given case.

4.2 Validation Studies

The brief introduction on turbulence models and near wall modeling approaches gives an idea on suitable modeling approach of the vehicle. The realizable $k - \varepsilon$ model with wall functions, realizable $k - \varepsilon$ model with enhanced wall treatment and SST $k - \omega$ models seem to be appropriate for the simulations of the vehicle. Usually, it is not a good idea to begin simulations with this superficial knowledge. Beforehand some validation simulations should be performed on bodies that have experimental results in the literature. These bodies should be chosen such that the geometry is as similar as possible to the intended vehicle design. Validation studies are useful in many aspects. It helps the user check his/her capabilities in flow modeling. The user can check the pros and cons of various models and validate their applicability to the problem. The effect of solution parameters on the results can be seen by changing them in a controlled manner. Due to these reasons, some validation studies were performed before beginning the actual analyses.

4.2.1 The Software

For validation studies and actual simulations of the vehicle FLUENT 6.3.26, Gambit 2.3.16 and Tgrid 4.0.16 software were used. Gambit and Tgrid were used in the pre-processing step. Gambit is a program that can import vertex data or geometry from computer aided design (CAD) software. Edge meshes, surface meshes, boundary layer meshes and volume meshes can be generated on the flow domain. Both unstructured and structured meshes are available in Gambit. Tgrid is also capable of these duties; however, the main advantage of Tgrid is its high performance on creating boundary layer meshes. In this thesis surface meshes are generated by Gambit and boundary layer meshes are generated by Tgrid. Later on volume meshes are generated with either Gambit or Tgrid depending on the problem.

FLUENT is used for solution and post-processing. It can import structured and unstructured meshes from different programs. It has several physical models to model flow, turbulence, heat transfer and reactions for a wide range of applications. In this thesis an external flow problem is investigated by FLUENT using the above mentioned turbulence models. Results were post-processed and required data like pressure distribution, velocity vectors and drag force are obtained.

4.2.2 Series 58 Studies

The first validation studies were performed on Series 58 models. Series 58 experiments were held by Morton Gertler in 1950 [17]. The purpose of these experiments was determining the resistance of several axisymmetric underwater bodies. Geometrical properties like prismatic coefficient, nose radius, tail radius, *L/D* ratio and location of maximum diameter on resistance was observed by systematic experiments. The ultimate aim was presenting a guideline and database for submarine design. In fact, this is one of the earliest attempts to create a database on resistance of streamlined bodies in deep submergence case. Therefore, these results gained popularity and have been cited many times.

Investigated bodies are derived from a sixth degree polynomial. The coefficients of the polynomial were changed to vary the shape of the body and the geometric coefficients. 24 models were developed and tested. All 24 models have a length of 9 feet (2.74 m). Models were held inside the towing tank with a pair of struts. The additional drag due to these struts was later on removed from the results. The test apparatus can be seen in Figure 4.2.

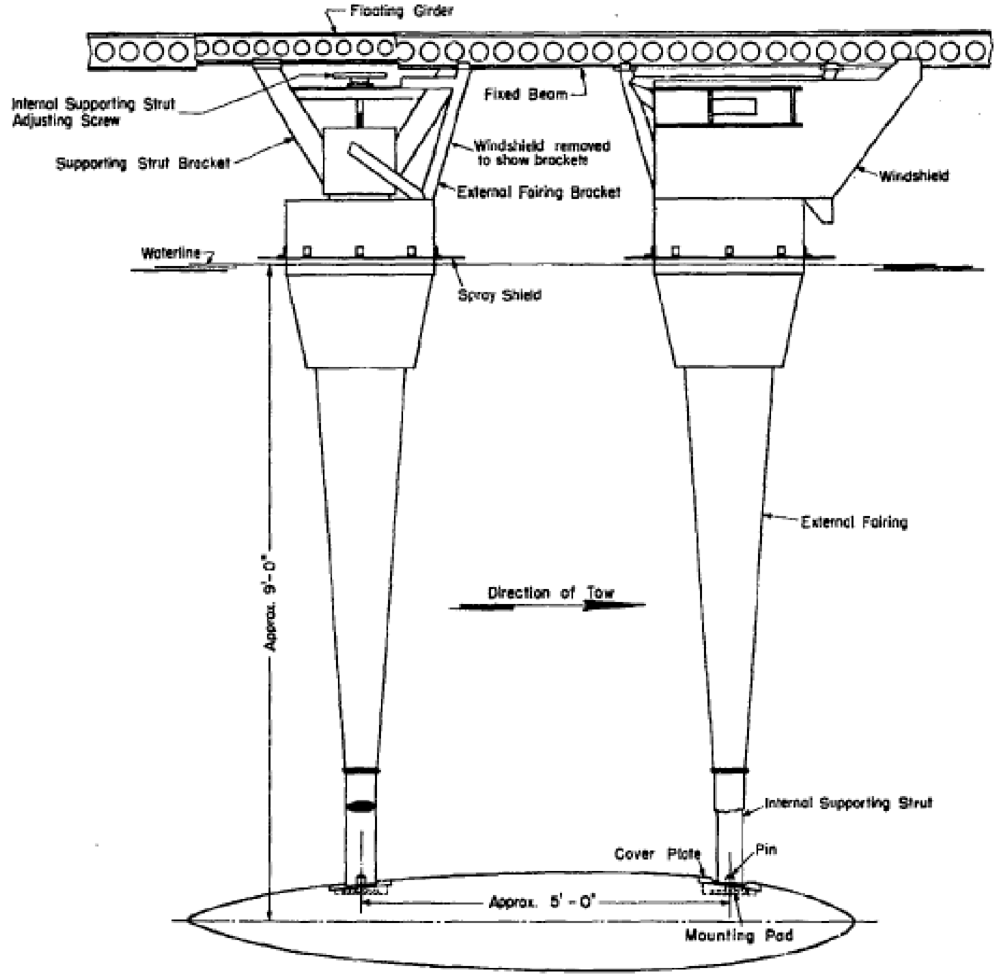

Figure 4.2 Test Apparatus for Series 58 Experiments [17]

Sand strips are placed near the leading edge of the model to stimulate the transition to turbulence. Tests were performed for both bare hull case and sand stripped case.

Experiments are performed for all of the bodies for a range of Reynolds numbers. Reynolds number usually changes from $2x10^6$ to a maximum of $2x10^7$ to $3x10^7$ based on body length. Total resistance coefficient, C_t is plotted against Reynolds number for all of the models. Gertler defines resistance coefficient as

$$C_t = \frac{R}{\frac{\rho}{2} S U^2} \tag{4.17}$$

where *R* is the resistance (total drag) on the body and *S* is the wetted surface area for the corresponding body.

In this validation study, three of these models are chosen. These models are Model 4159, Model 4158 and Model 4154.

4.2.2.1 Model 4159

The first analyzed body is Model 4159. The forward (surging) motion of the body is tested. It is assumed that the body is stationary and the fluid is flowing over the body. 2D axisymmetric solver of FLUENT is employed for simulations. Axisymmetric solver was preferred over the 3D solver because for such simple geometries with no secondary flows or angle of attack, axisymmetric solver is as accurate as the 3D solver with considerably less solution time. Solution time is important for this case because many solution parameters are changed in a controlled manner over a range of Reynolds numbers. Axisymmetric simulation is commonly used for these cases and it can be seen in the literature.

Initially 3 types of mesh are created for Model 4159. Mesh 1 is coarse along the body and coarse in the boundary layer. It is used for turbulence models that do not require a fine mesh in the boundary layer ($y^+ > 30$). Mesh 2 has the same number of grid points along the body; however, the mesh resolution is fine in the boundary layer to make it suitable for enhanced wall treatment. Finally, for some cases a third configuration, Mesh 3, is generated which is fine both along the body and in the boundary layer. Details of Mesh 1 are seen in Figures 4.3 and 4.4. Mesh 1 has 1264 quadrilateral boundary layer cells and 2740 triangular cells which results in a mesh with a total of 4004 cells.

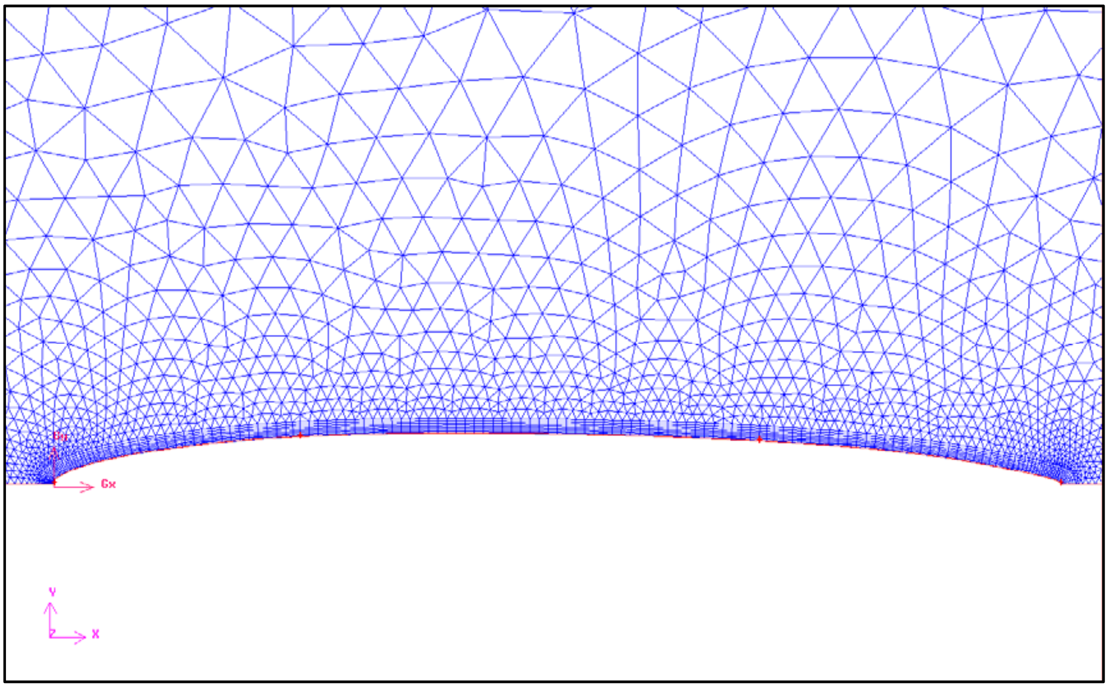

Figure 4.3 Mesh 1 for Model 4159 – boundary layer

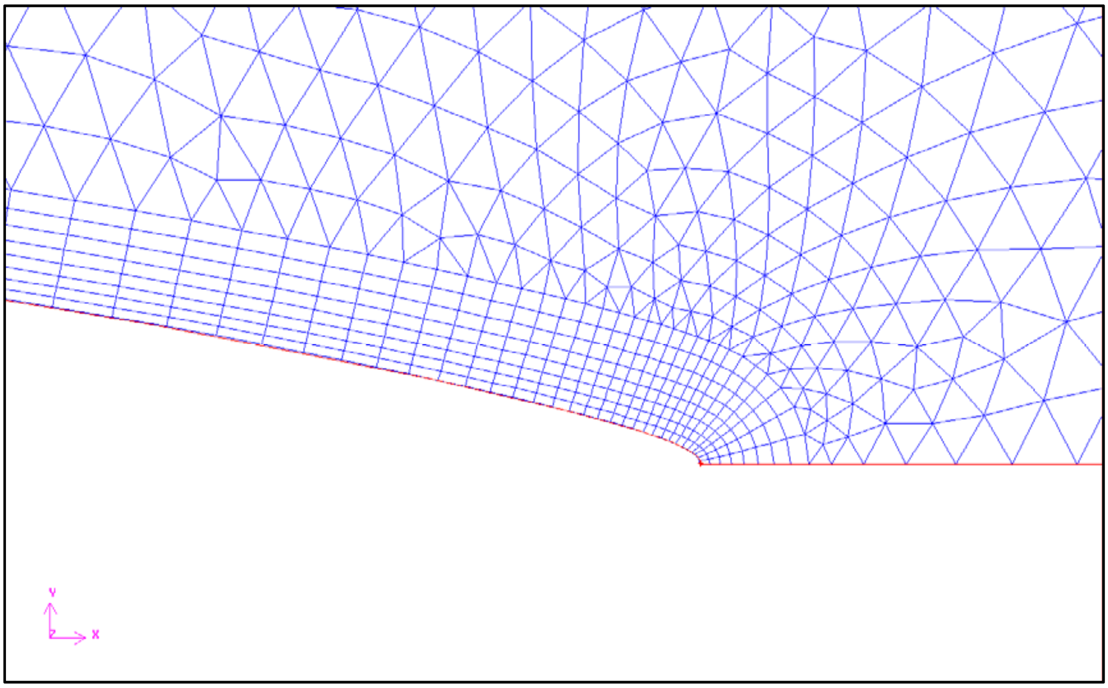

Figure 4.4 Mesh 1 for Model 4159 - trailing edge detail

The domain around the body is seen in Figure 4.5. If the model length is assumed to be *L* and the maximum diameter is *D*; the domain has a length of 4*L* with a length of

L ahead of the body and a length of 2*L* behind the body and the height of the domain is 11*D*. The domain has a total length of 11 m and a diameter of 1.5 m.

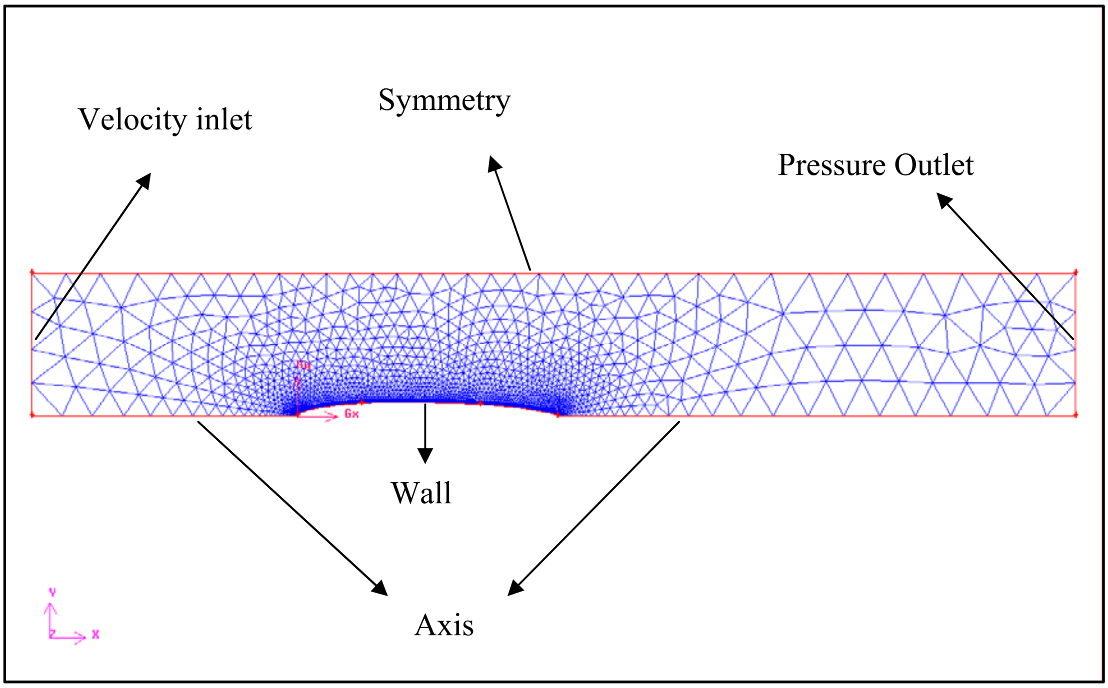

Figure 4.5 Mesh 1 for Model 4159 – flow domain and boundary conditions

Some of the solution parameters are the same for all of the analyses. For instance, Green-Gauss node based gradient option is turned on. Green-Gauss node based is preferred over Green-Gauss cell based because it performs better for unstructured meshes like the one that is used in these analyses (triangular elements). Cell based option is more accurate for structured meshes [26]. Besides that, second-order discretization schemes are used for pressure, momentum and turbulence quantities. Second-order solutions are known to be much more accurate than first-order schemes. In fact, first order schemes are usually used for the initial iterations of the analyses for faster convergence. They are later on switched to second-order.

Boundary conditions are the same for all analyses: Velocity inlet at the inlet, pressure outlet at the outlet, symmetry condition at the upper edge of the domain and axis at the lower edge. Finally, wall boundary condition is applied for the body. Velocity value at the inlet depends on the Reynolds number of the flow. On the other hand, turbulence quantity selection at the inlet is also critical. FLUENT offers four options for defining these quantities. Intensity and hydraulic diameter option is the most appropriate option for the present case. The hydraulic diameter is taken as the height of the inlet. Turbulence intensity, on the other hand, usually comes from the experimental data in these cases. Most of the modern wind tunnels provide the intensity value at the inlet of the tunnel. Unfortunately, for this towing tank experiment no such data is provided. Nevertheless, an approximate intensity value can be taken. Most of the simulations that are similar to this case use a turbulence intensity value of less than 1 % is used. For modern wind tunnels, this value may even drop below 0.1 %. Turbulence levels of some water tunnels in the literature can be given to demonstrate it. For instance, the water tunnel of Rolling Hills Research Corporation has a turbulence intensity level of less than 1 % [27]. In these analyses, turbulence intensity at the inlet is usually given a value less than or equal to 0.5 %. In some cases this value is modified.

Various cases are simulated for exploring the effect of turbulence mode and near wall modeling on solutions. These cases can be seen in Table 4.1.

Table 4.1 Simulation cases

MESH	CASE	Viscous	Viscous Model	Near-Wall Treatment
1,2,3	Case 1	laminar	-	-
1	Case 2	k - ε	Realizable	SWF
1	Case 3	k - ε	Realizable	NWF
2,3	Case 4	k - ε	Realizable	EWT
1	Case 5	k - ε	RNG	SWF
1	Case 6	k - ε	RNG	NWF
2,3	Case 7	k - ε	RNG	EWT
1	Case 8	k - ω	SST	Transitional flows option (disabled)
2,3	Case 9	k - ω	SST	Transitional flows option (enabled)

For Mesh 1, Case 2, Case 3, Case 5, Case 6 and Case 8 are solved; on the other hand for Mesh 2 and Mesh 3, Case 4, Case 7 and Case 9 are solved. Moreover, Mesh 1 and Mesh 2 are solved for laminar case. Details of this laminar solution is presented after turbulent analyses. The reason for using different cases for different meshes is that these meshes have different mesh densities and this affect the suitability of turbulence models for each. Mesh 1 is a coarse mesh and Cases 2, 3, 5, 6 and 8 use turbulence models which operate at coarse meshes. The intended wall y^+ value is 30 as the guideline suggests. This aim was satisfied for Re=2x10^6 as it can be seen in Figure 4.6. Similar results are achieved for other cases. However, as the Reynolds number is increased, the wall y^+ value gets very high values as seen in Figure 4.7 and exceeds 100 which is advised by the User's Guide as the upper limit. It should be noted that the transitional flow option is a low-Reynolds number correction to the turbulent viscosity. If this option is disabled like in Case 8, a coarse mesh should be used; however, if this option is enabled like in Case 9, a fine mesh should be used [26].

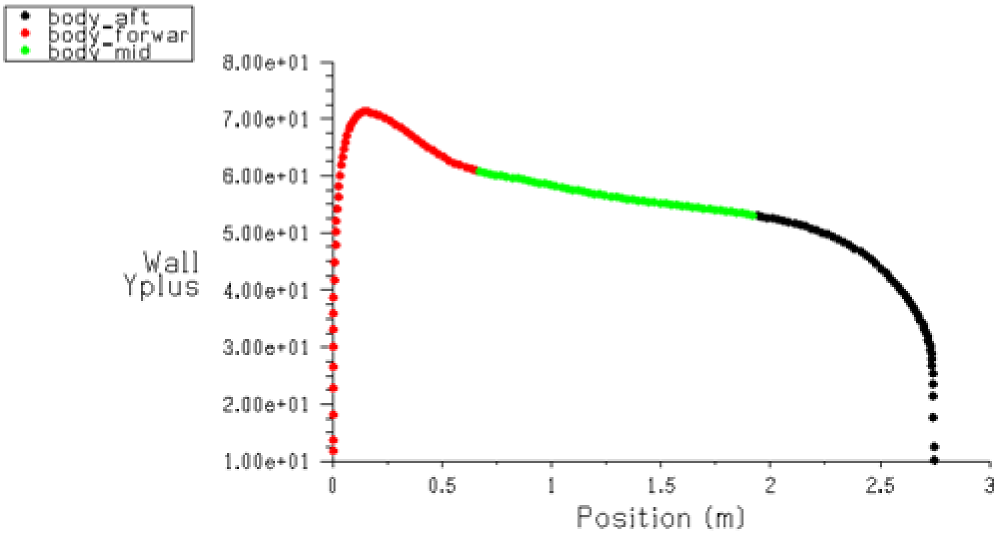

Figure 4.6 Wall y^+ for Mesh 1 Case 2 at *Re*=2x10^6

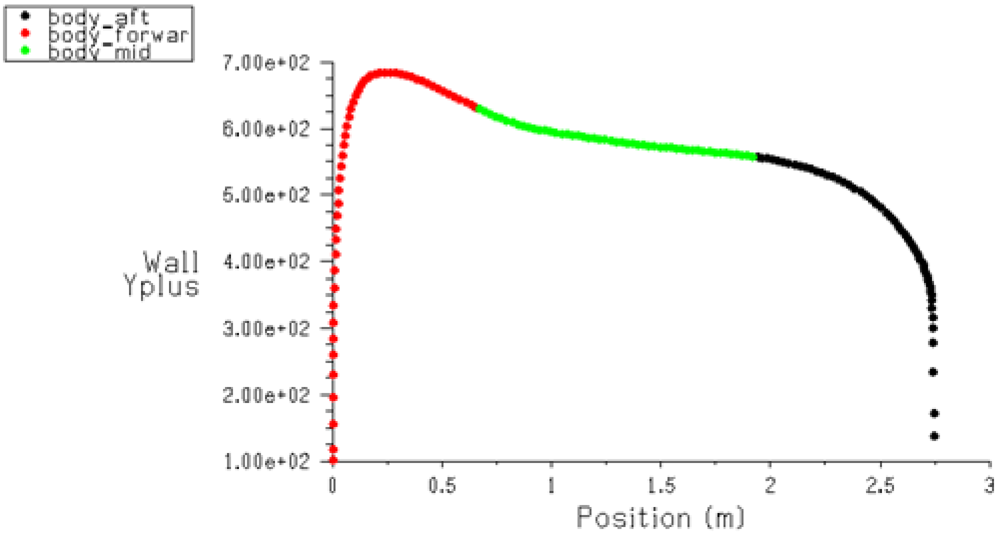

Figure 4.7 Wall y^+ for Mesh 1 Case 2 at *Re*=2.5x10^7

In Figure 4.8 a comparison of these cases with the experimental data for resistance coefficient can be seen.

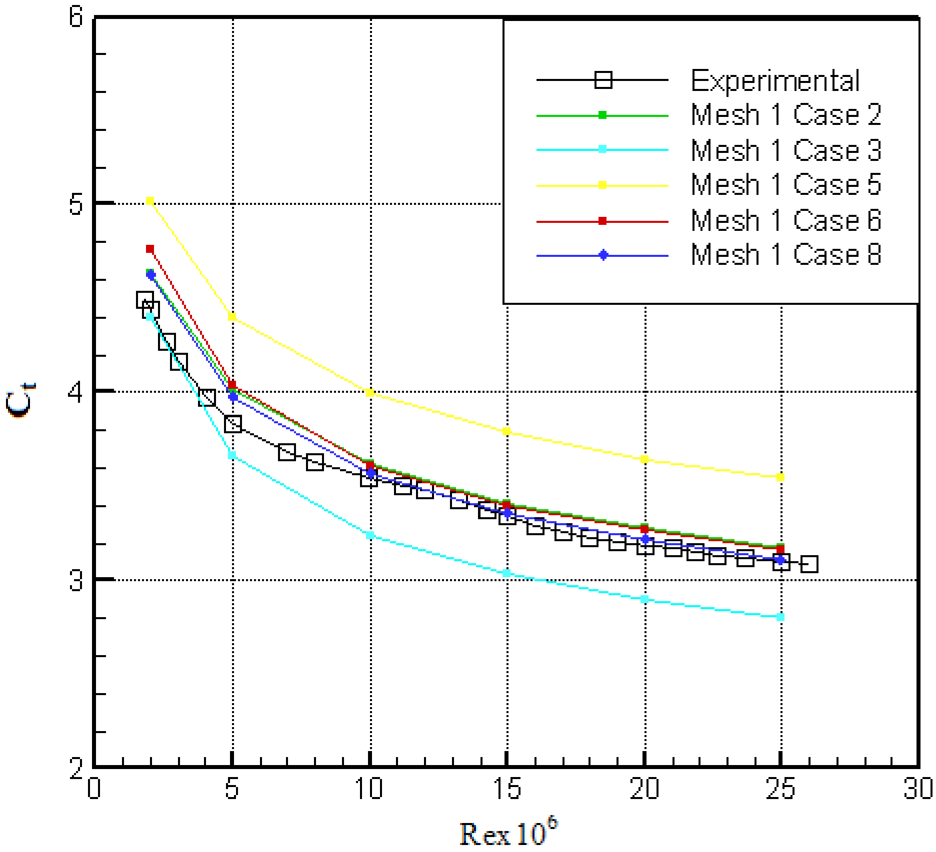

Figure 4.8 Comparison of Mesh 1 results – total resistance coefficient

As it is seen, RNG model with SWF's fails to match the resistance coefficient at all Reynolds numbers. The $k - \varepsilon$ model with NWF's is accurate for low-Reynolds numbers and loses accuracy at higher speeds. The $k - \varepsilon$ model with SWF's, RNG with NWF's and SST gives inaccurate results for low-Reynolds numbers but matches the experimental data at higher *Re* numbers.

As it was mentioned before, at high *Re* numbers wall y^+ values get values above 100. To check whether it is affecting the results or not, mesh is adapted so that wall y^+ value is between $30 < y^+ < 100$. For Case 2, Case 3 and Case 6 results are almost identical. Comparison of case 3 and its adapted version is seen in Figure 4.9. Moreover, in Figure 4.10 mesh generated for Re=2 x10^7 after adapting the grid is shown.

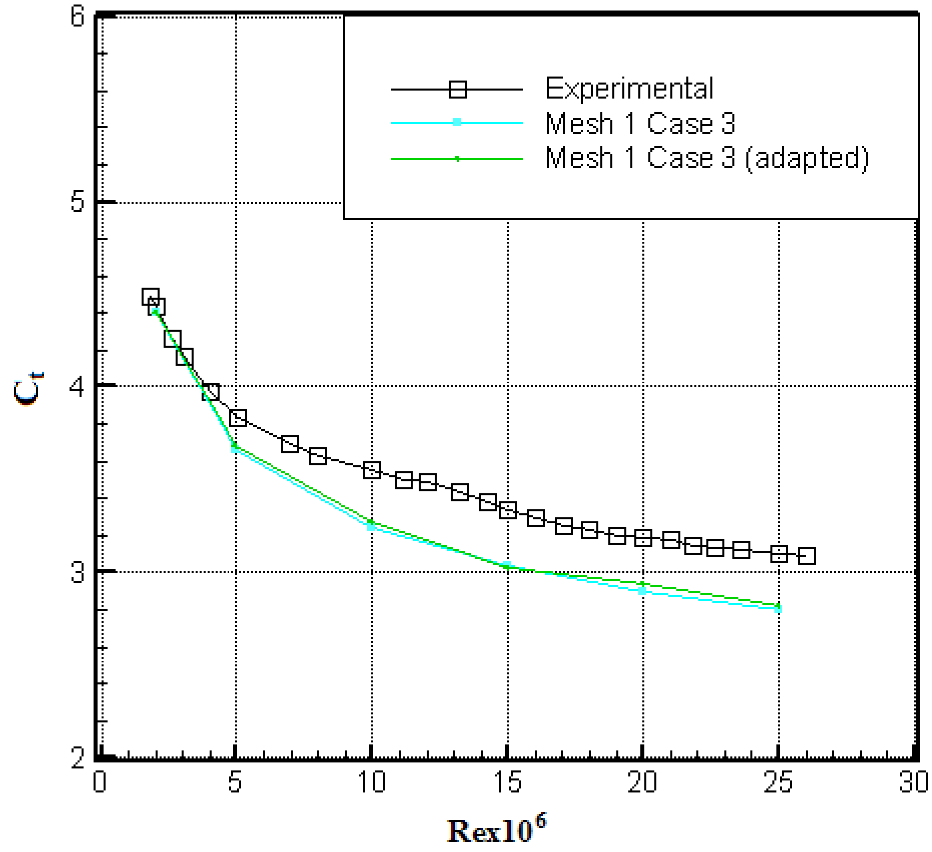

Figure 4.9 Adaptation results for Mesh 1 Case 3

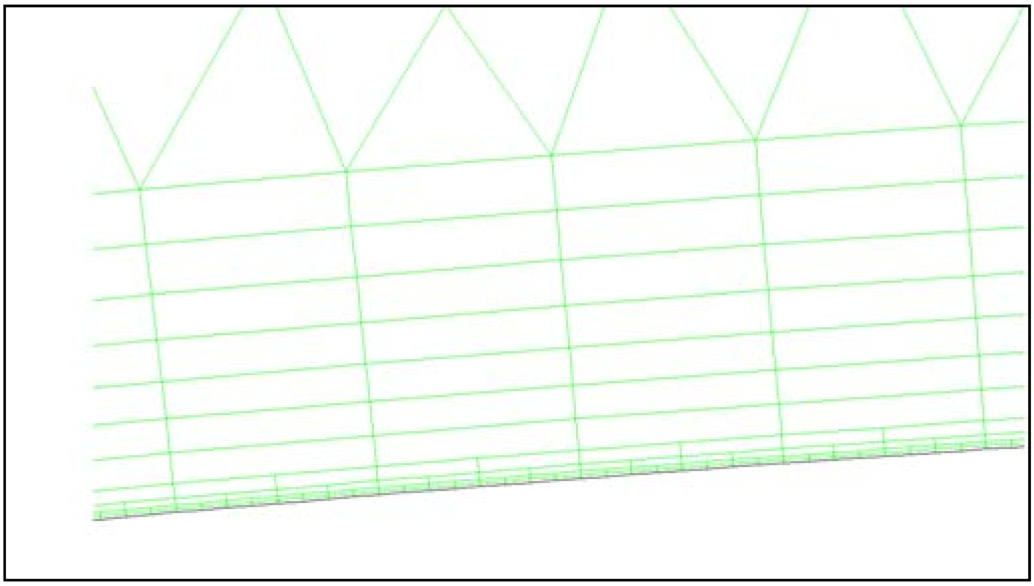

Figure 4.10 Modified Mesh 1 after y^+ adaption

For Case 5 results are improved but still not satisfactory as seen in Figure 4.11.

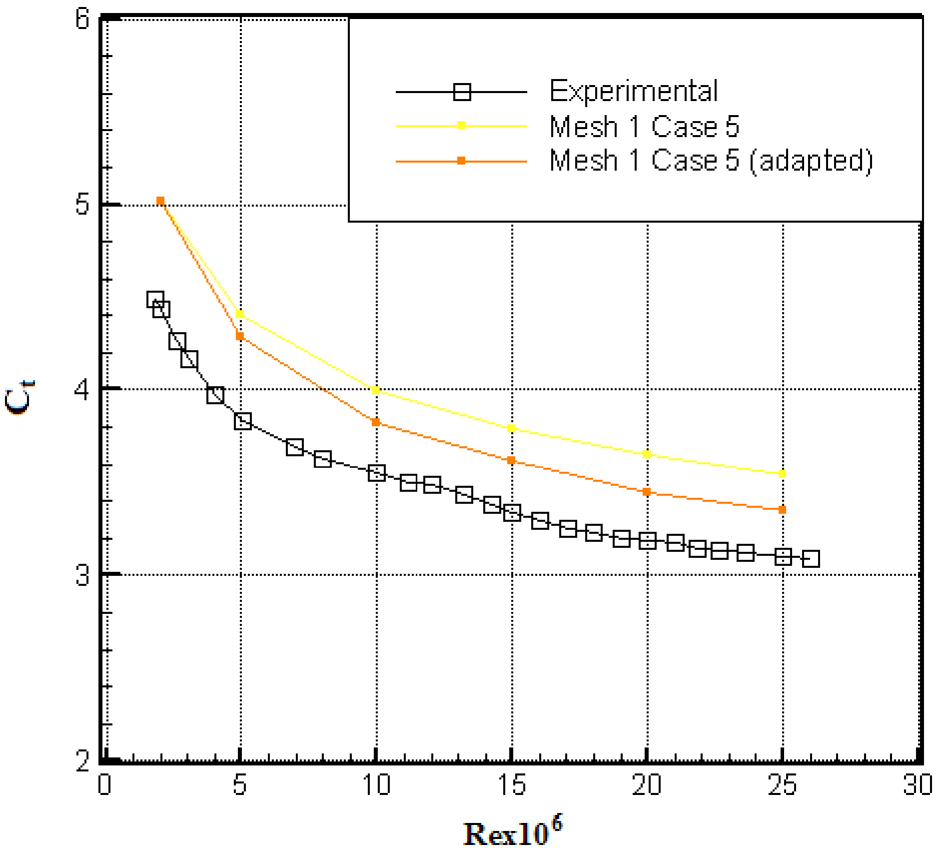

Figure 4.11 Adaptation results for Mesh 1 Case 5

An attempt is taken to check whether the turbulence intensity level has negative effects on the solution. For Case 3, higher and lower turbulence intensity levels are assigned at the inlet. For the high turbulence case, intensity is taken as 1% and for the low turbulence case; it is taken as 0.1 %. Results are seen in Figure 4.12. Low turbulence case is accurate for Re numbers up to 1x10^7 and high turbulence case is accurate for higher Re numbers. These results show the importance of the inlet turbulence intensity level on the accuracy of solutions. To sum up, for the coarse mesh Case 2, Case 6 and Case 8 are successful.

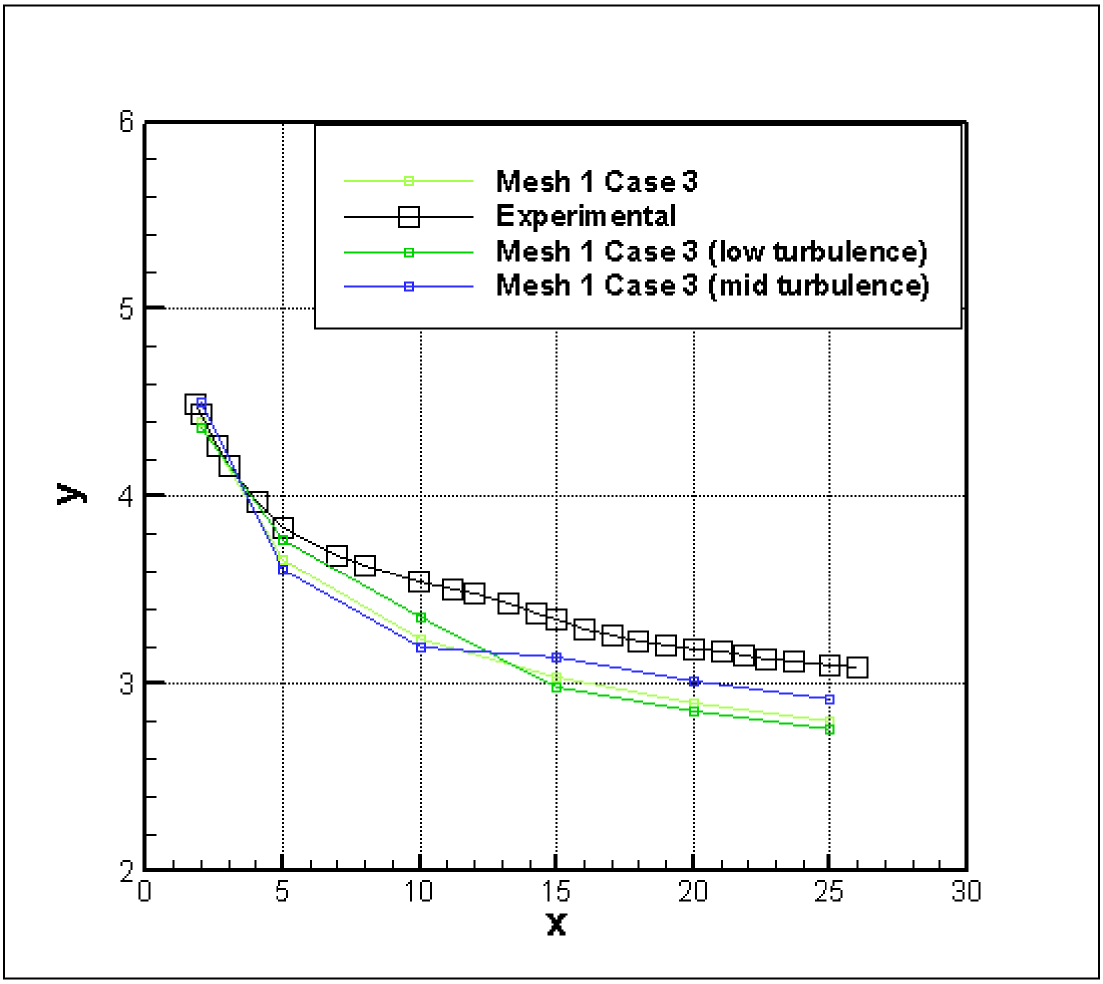

Figure 4.12 Effect of turbulence intensity on total resistance coefficient

After Mesh 1 simulations, a finer mesh, Mesh 2, is used. This mesh has the same number of grid points along the body; however, the mesh is more tightly clustered in the boundary layer. The purpose is achieving a fine mesh with wall $y^+ < 5$. Details of Mesh 2 are seen in Figures 4.13 to 4.15. Mesh 2 has 3160 quadrilateral boundary layer cells and 3434 triangular cells which results in a mesh with a total of 6594 cells. The same domain with Mesh 1 is used. For Re=2x10^6 y^+ is around acceptable limits; however, at higher Re numbers y^+ exceeds the limiting value of 5. Due to this fact, adaptation is applied to get the required mesh quality.

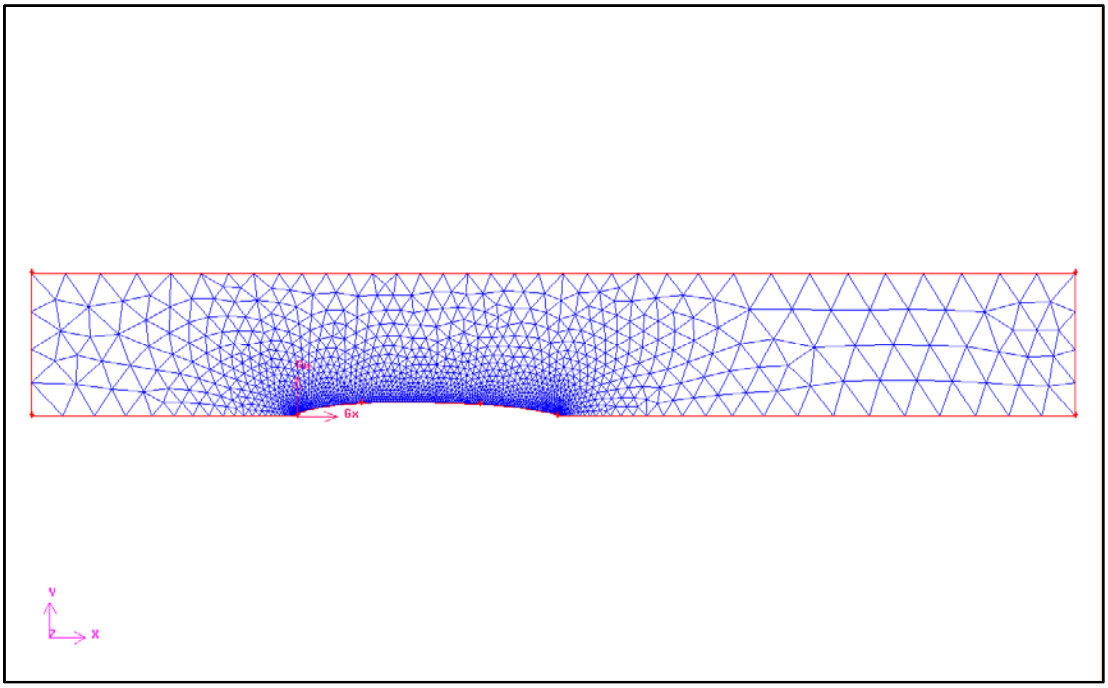

Figure 4.13 Mesh 2 for Model 4159 – flow domain

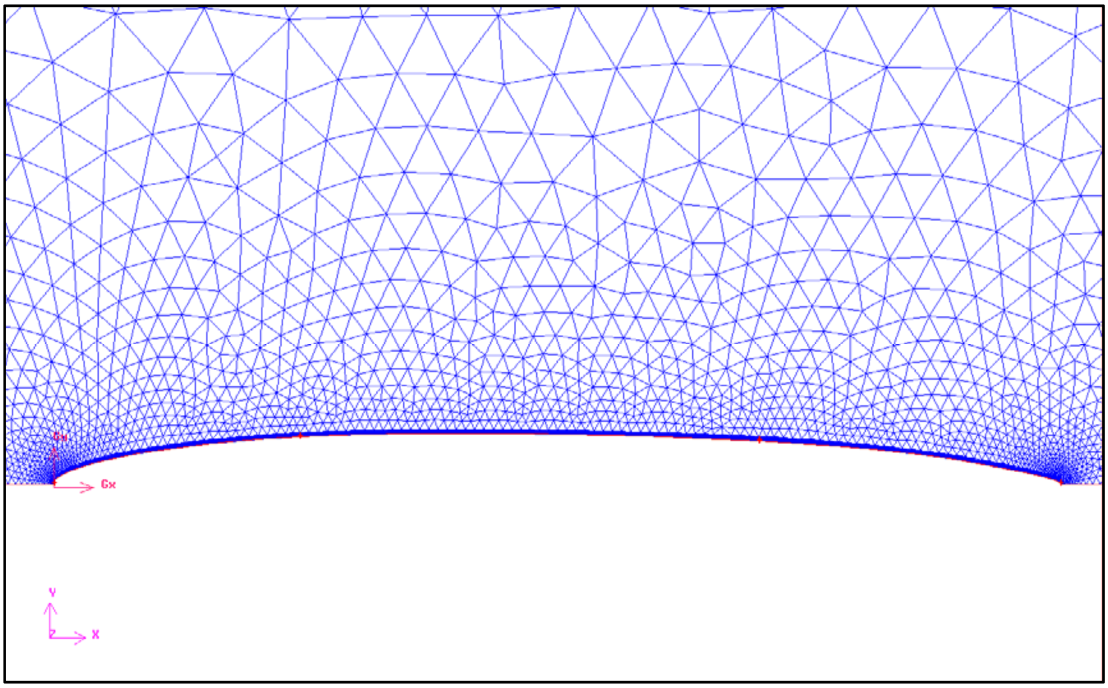

Figure 4.14 Mesh 2 for Model 4159 – boundary layer

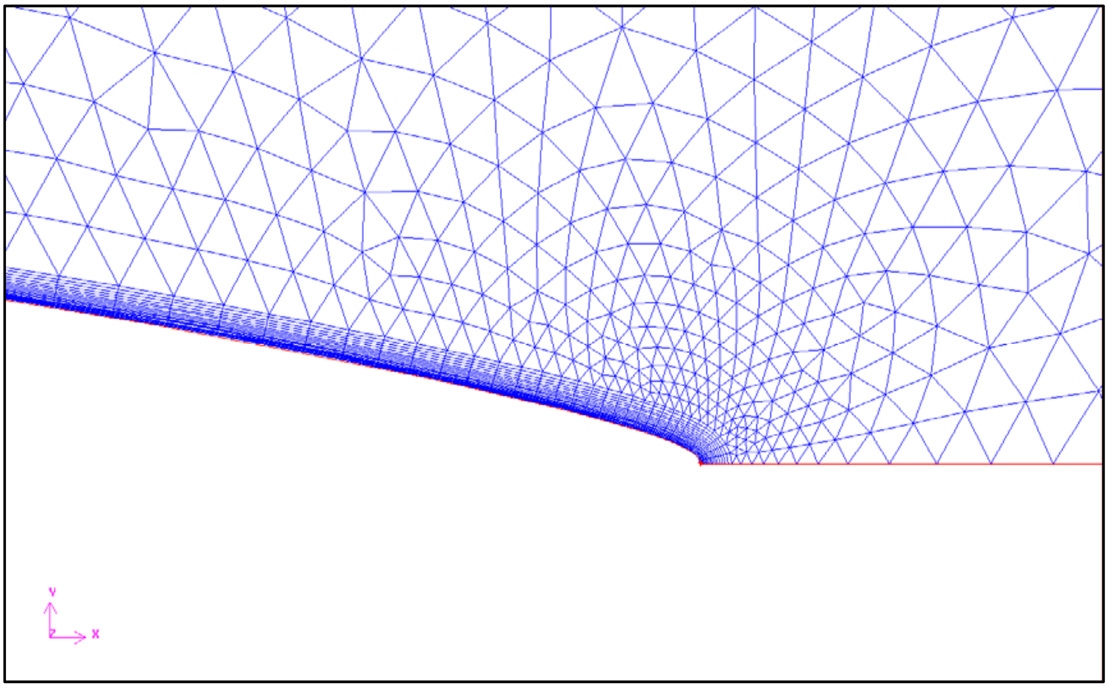

Figure 4.15 Mesh 2 for Model 4159 – trailing edge

Mesh 2 is aimed to be a fine mesh to solve for Cases 4, 7 and 9 which require a mesh with wall y^+ lower than 5. This dependency is especially critical for Cases 4 and 7 because these cases use EWT approach. Results of these cases without adaptation are seen in Figure 4.16. It is seen that all cases give inaccurate results. The most probable reason for this is the unsatisfactory mesh resolution especially at high *Re* numbers.

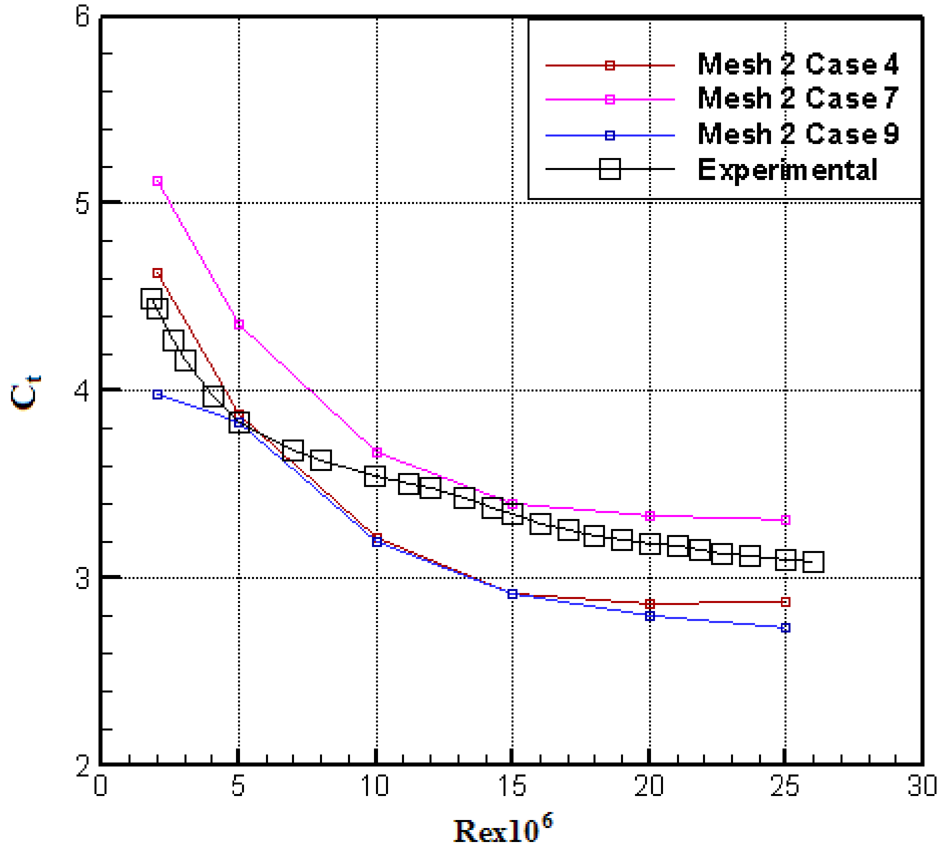

Figure 4.16 Comparison of Mesh 2 results – total resistance coefficient

To overcome the poor mesh quality at the wall, adaptation is done. Cases 4, 7 and 9 are adapted for $y^+ = 5$ and $y^+ = 1$. The results are presented in Figures 4.17 to 4.19.

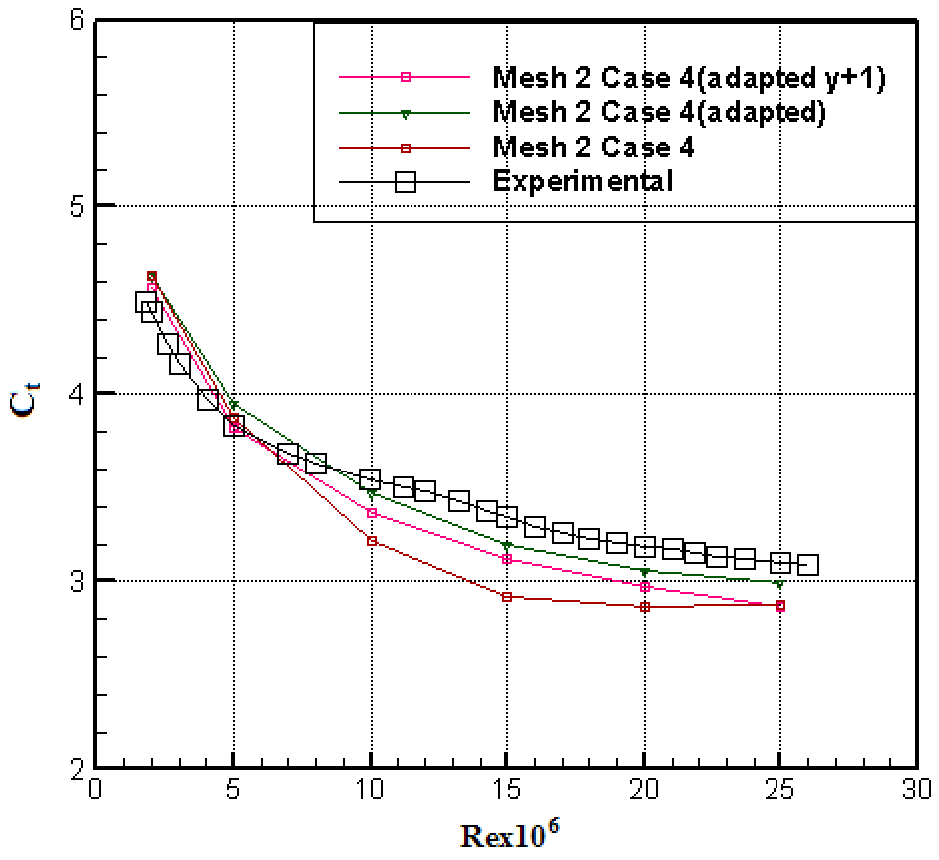

Figure 4.17 Adaptation for Case 4 with Mesh 2 – total resistance coefficient

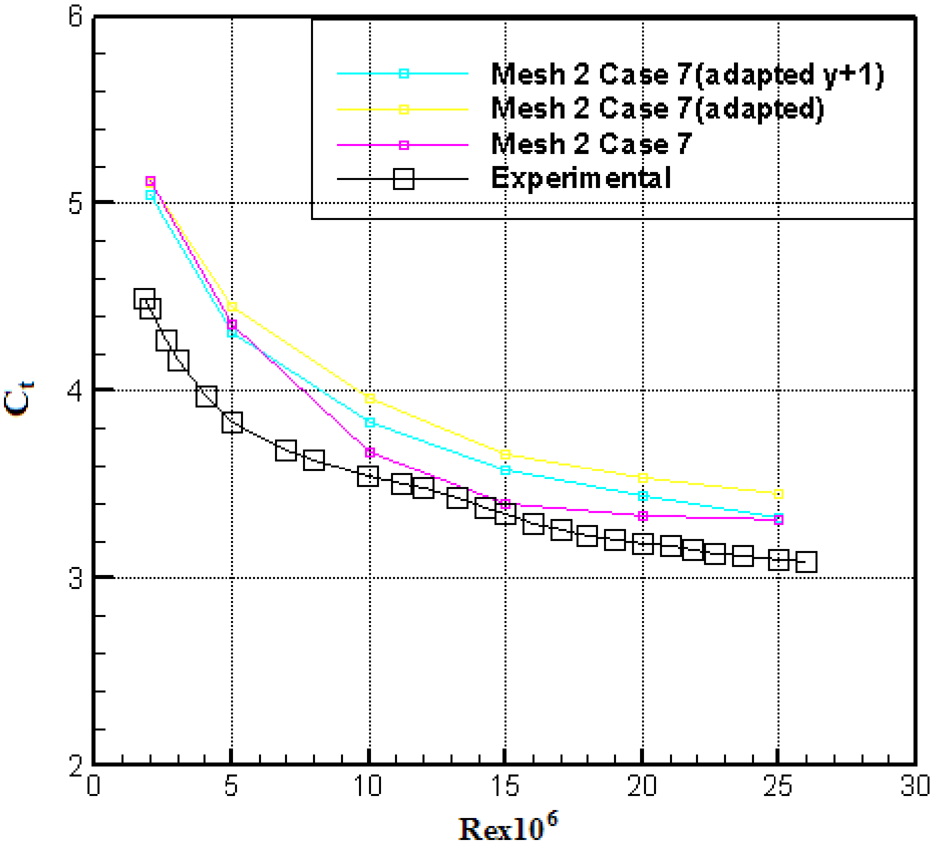

Figure 4.18 Adaptation for Case 7 with Mesh 2 – total resistance coefficient

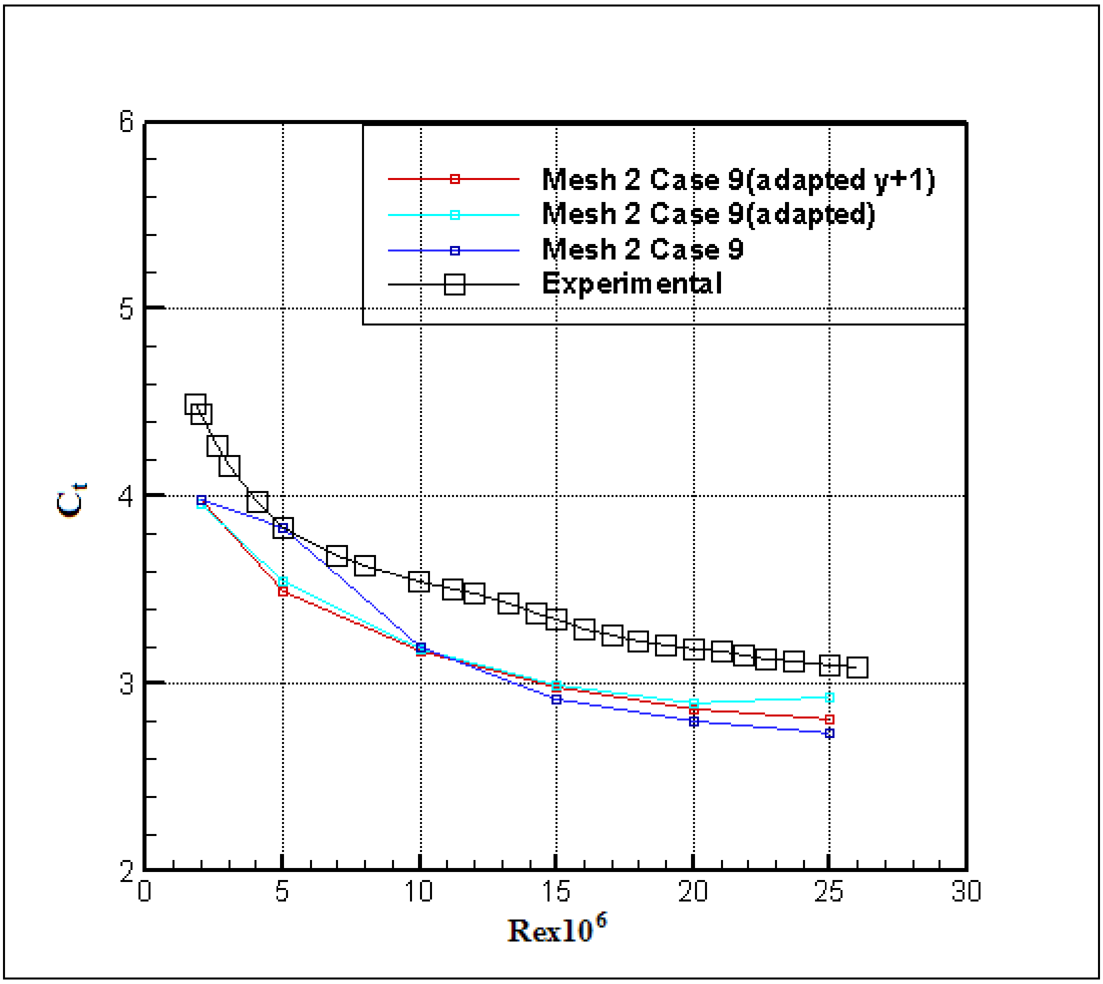

Figure 4.19 Adaptation for Case 9 Mesh 2 – total resistance coefficient

For case 4, adaptation is helpful. In Figure 4.17, Case 4 with Mesh 2 (adapted) refers to the case where adaptation is made for $y^+ = 5$. It is seen that $y^+ = 5$ adaptation improved the results of case 4 significantly. Interestingly, $y^+ = 1$ adaptation predicted worst. Conversely, for Cases 7 and 9, adaptation results are poor as seen in Figures 4.18 and 4.19, respectively. To sum up, for the fine mesh (Mesh 2), Case 4 which is adapted to $y^+ = 5$ provides the best prediction.

After the analyses on Mesh 1 and Mesh 2, a final attempt is done with Mesh 3. This mesh has the same density in the boundary layer as Mesh 2; however, the mesh density is increased along the body. Mesh details are seen in Figures 4.20 to 4.22. Mesh 3 has 12760 quadrilateral boundary layer cells and 18002 triangular cells which results in a mesh with a total of 30762 cells. The same domain with Mesh 1 and Mesh 2 is used.

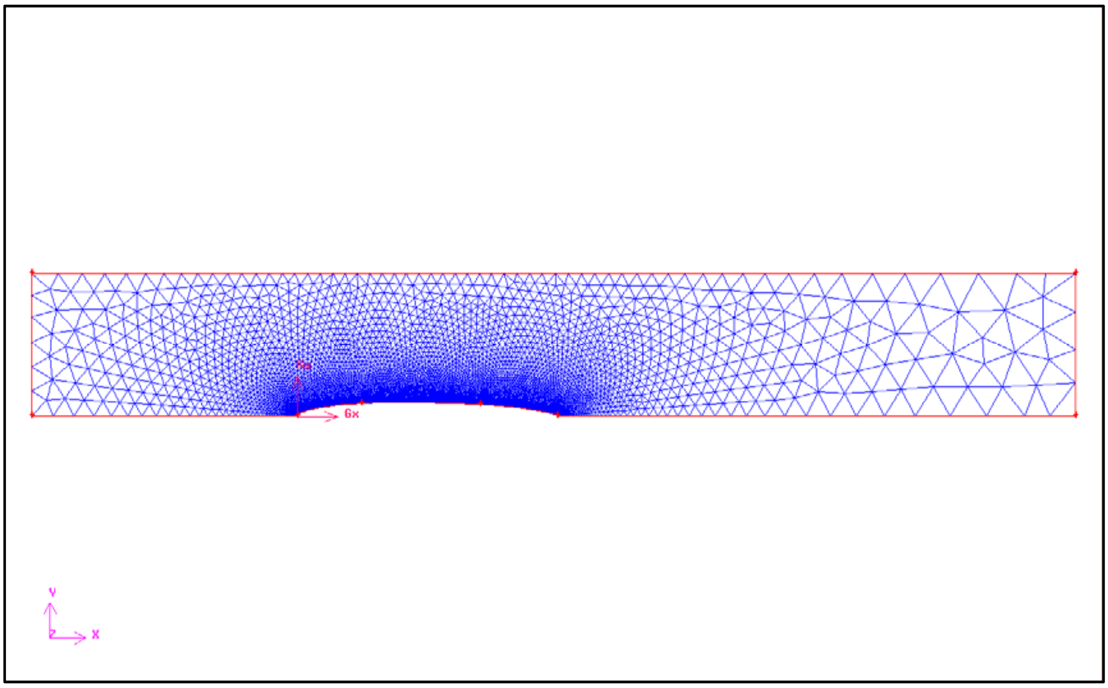

Figure 4.20 Mesh 3 for Model 4159 – flow domain

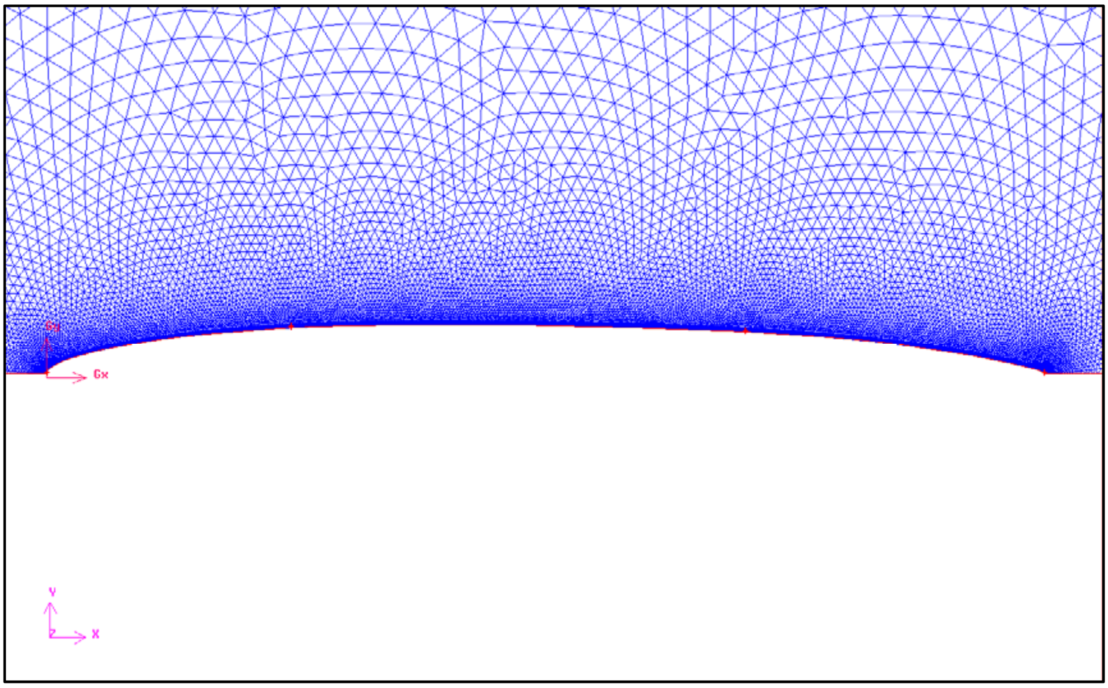

Figure 4.21 Mesh 3 for Model 4159 – boundary layer

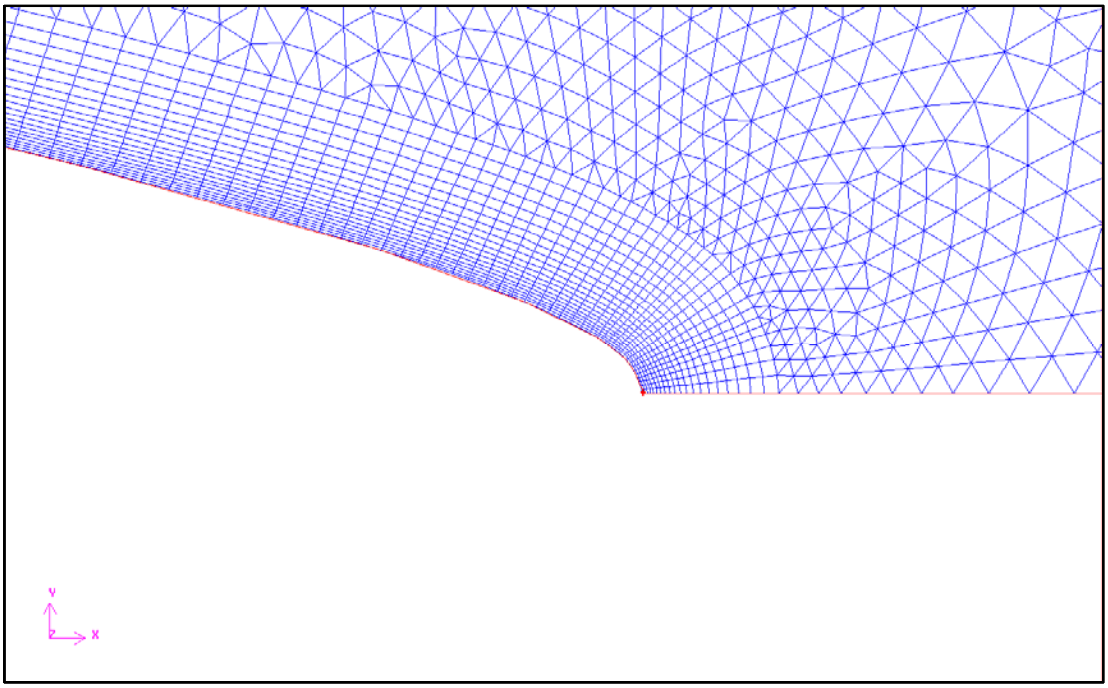

Figure 4.22 Mesh 3 for Model 4159 – trailing edge

Since Mesh 3 is a low-Reynolds number mesh Case 4, Case 7 and Case 9 are simulated. As seen in Figure 4.23, none of the cases is accurate. When adaptation is applied, results improved, especially for Case 4, as seen in Figure 4.24.

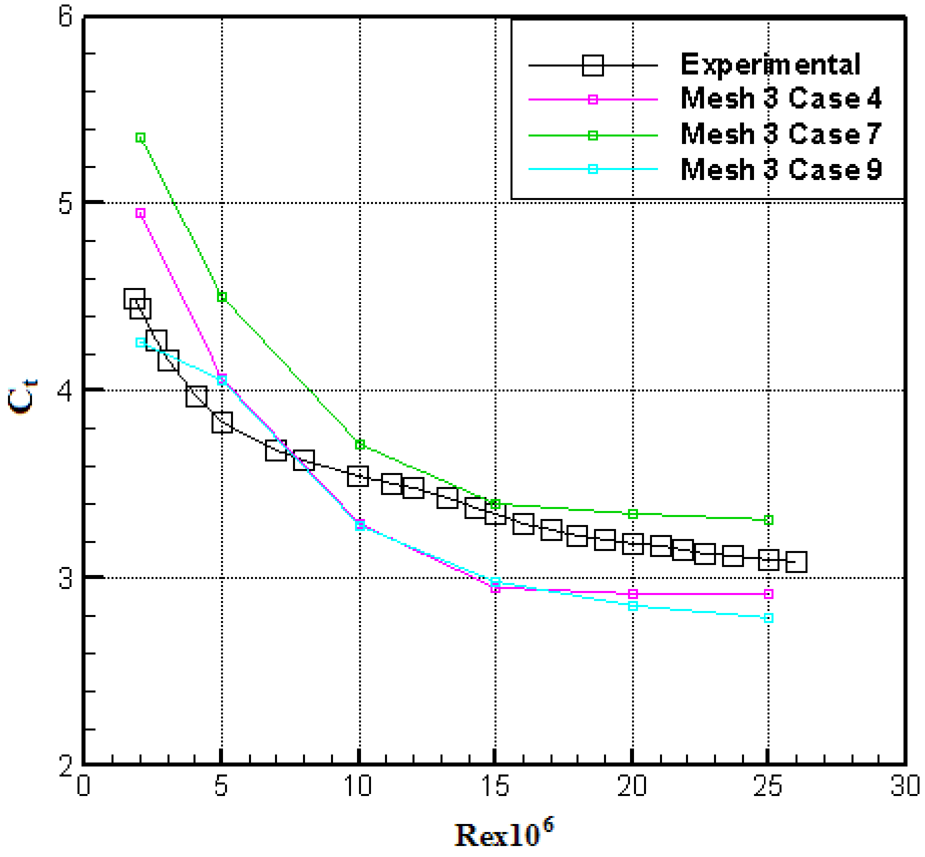

Figure 4.23 Comparison of Mesh 3 results – total resistance coefficient

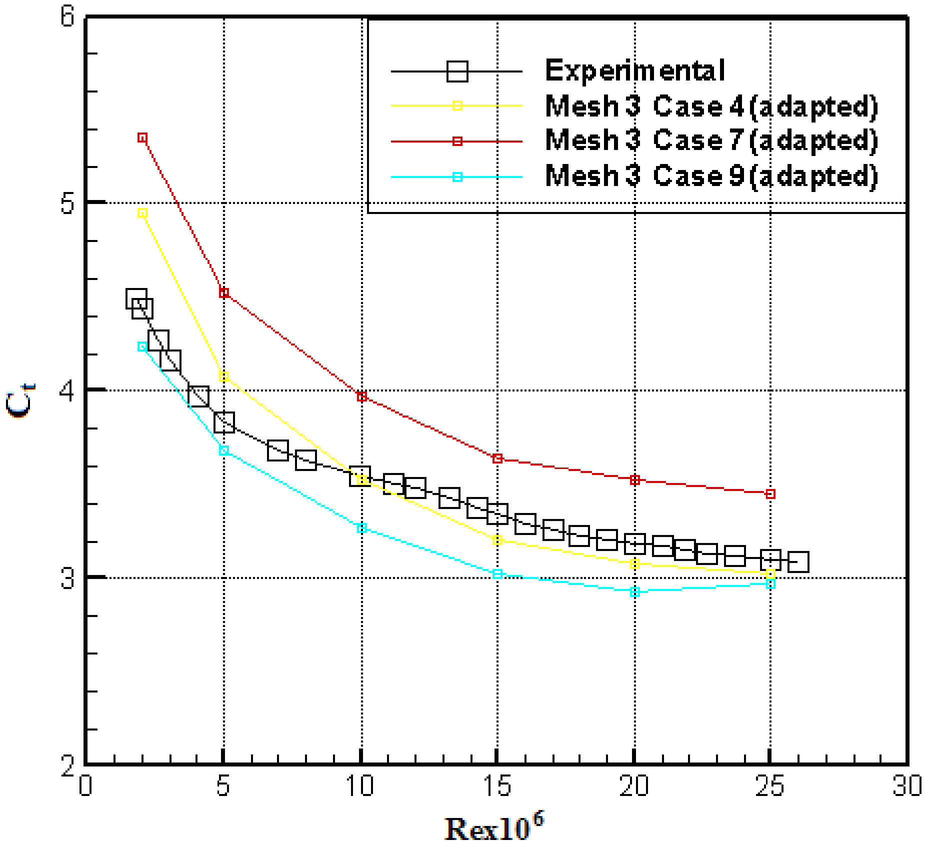

Figure 4.24 Adaptation results for Mesh 3 – total resistance coefficient

After these simulations, several conclusions are made. First of all, adaptation is not always successful. Even though results are improved for some situations, such as Mesh 2 - Case 4 and Mesh 3 - Case 4, poor results are received as well. Due to erroneous results of adaptation, a new approach is tested for Model 4159. This time the mesh is generated for each Reynolds number separately so that wall y^+ is about 1-2 for each case without any need for adaptation. For instance, for Case 4 at Re=2x10^7, the y^+ plot over the body is seen in Figure 4.25.

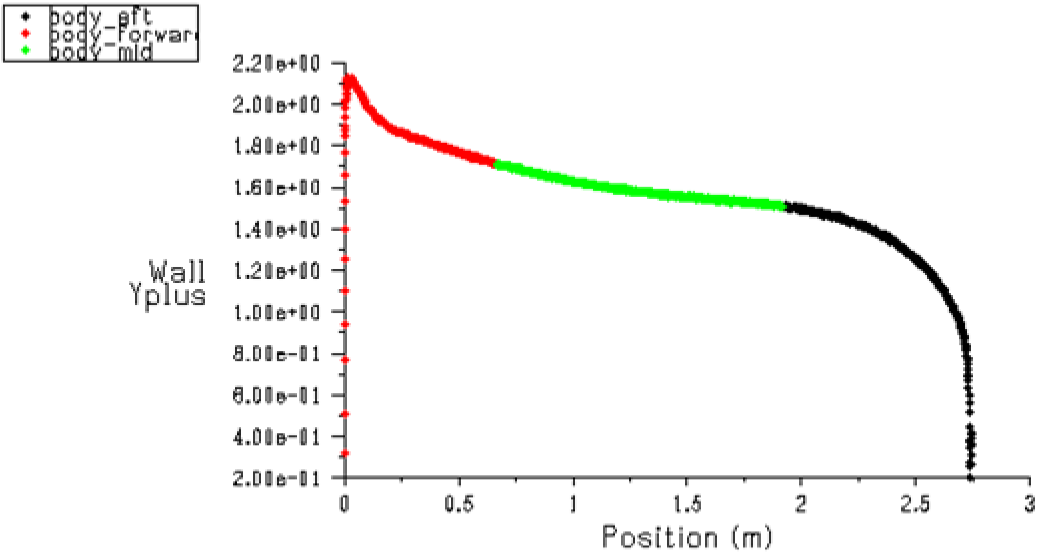

Figure 4.25 Wall y^+ plot for Case 4 at *Re*=2x10^7

This approach was applied for Case 4, Case 7 and Case 9. Results are seen in Figure 4.26. It is seen that Case 4 gives accurate results at all Reynolds numbers while other cases fail to match the experimental data.

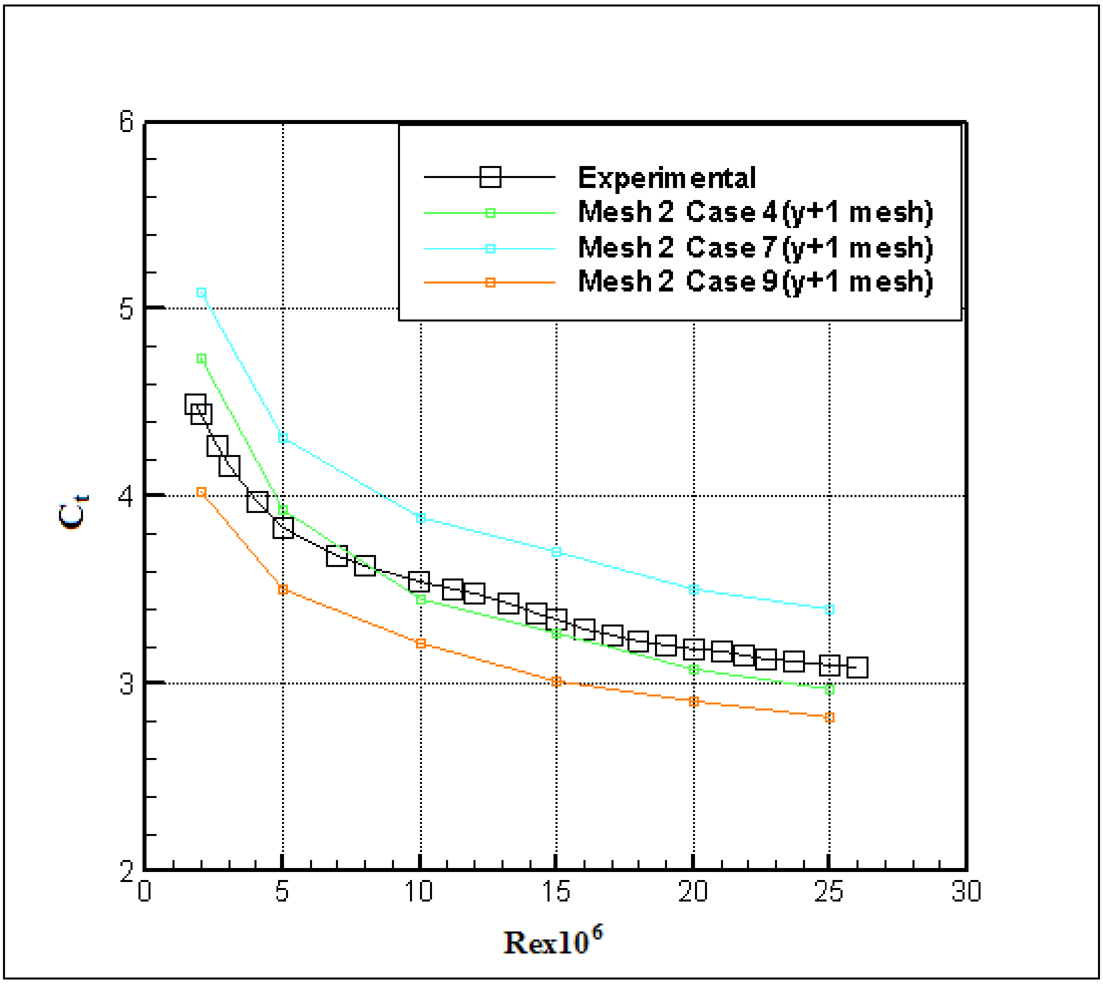

Figure 4.26 Comparison of total resistance coefficient for y^+ meshes

Up to now it is seen that Case 4 (realizable *k* - *ε*, EWT) gives consistently good results provided that the mesh resolution is fine enough at the wall. Other than Case 4; Case 6 (RNG *k* - *ε*, NWF), Case 2 (realizable *k* - *ε*, SWF) and Case 8 (SST, transitional option disabled) give good results for Mesh 1 (coarse mesh). Conversely, for fine meshes (Mesh 2 and Mesh 3), RNG and SST predict inaccurately. At this point, it seems that realizable *k* - *ε* model with enhanced wall treatment (Case 4) is the most appropriate choice for the simulation of the unmanned underwater vehicle. At first glance the fine mesh requirement of Case 4 may seem to be a drawback due to high computation time. However, it should be noted that marine applications usually have relatively lower Reynolds number values; hence, the mesh requirement does not increase to very high values. Using a fine mesh near the wall has another advantage. As it will be given in the following chapter, there are several small appendages protruding out of the body. When these protrusions are included in the model, it is inevitable to use fine mesh. If a coarse mesh is used, the flow around the appendage will most probably be ignored. It is important to note that in some cases drag due to appendages may have a considerable contribution on the total drag of the vehicle.

As it was mentioned before, Case 1 which is the laminar case is solved for Mesh 1 and Mesh 2 of Model 4159. Steady laminar analyses usually have problems with convergence; hence, analyses are solved unsteady with a time step of 0.01 s. Results are seen in Figure 4.27. It is seen that laminar solutions predicted the flow case inaccurately.

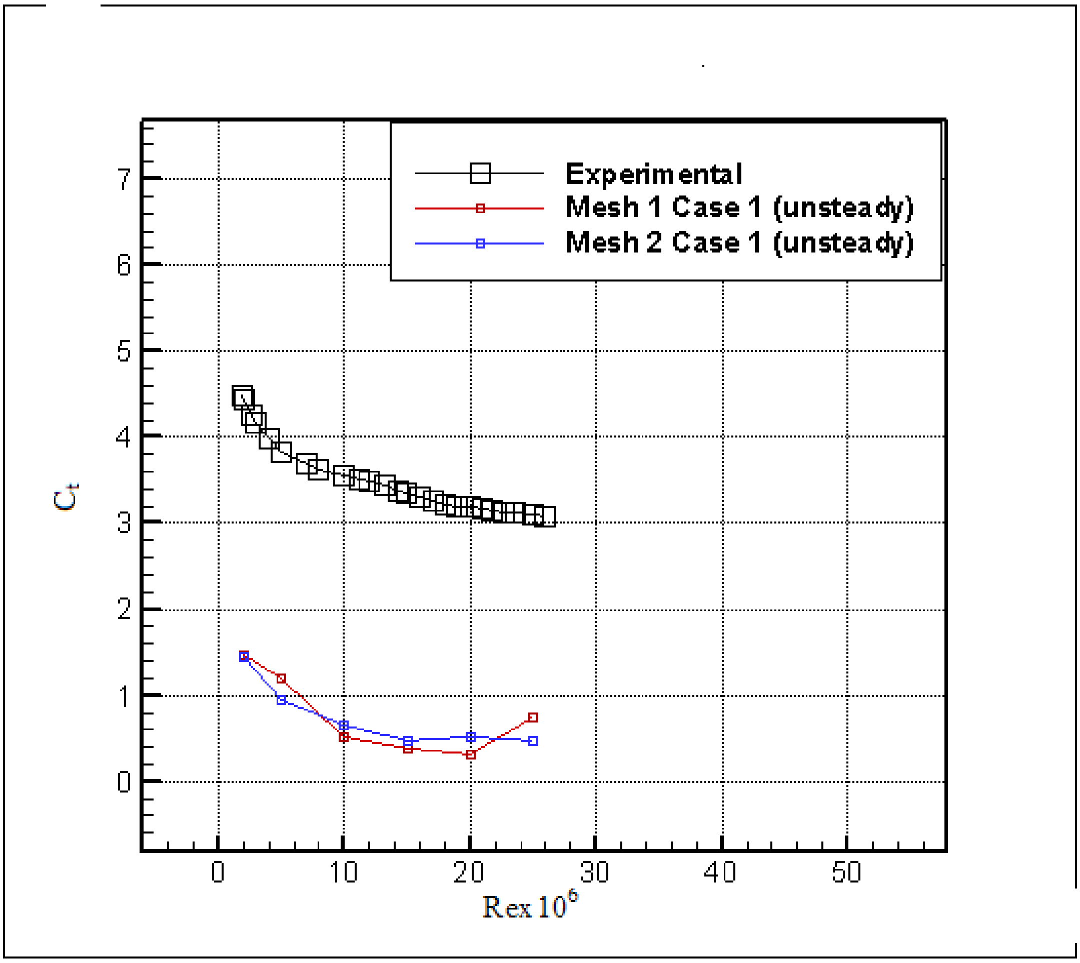

Figure 4.27 Laminar solution of Model 4159 Meshes 1 and 2

To demonstrate the accuracy of Case 4, additional comparisons were made. This time Models 4158 and 4154 were analyzed.

4.2.2.2 Model 4158

Model 4158 is one of the 24 models tested by Gertler [17]. Solution parameters similar to Model 4159 are used. Analyses are performed based on the concept explained in the previous part. A new mesh is generated for each Reynolds number so that the y^+ is around 1 without any adaptation. Cases 4, 7 and 9 are used. Results are seen in Figure 4.28. None of the models predicted the total resistance correctly. Nevertheless, amongst these cases, Case 4 still provides the most accurate answer.

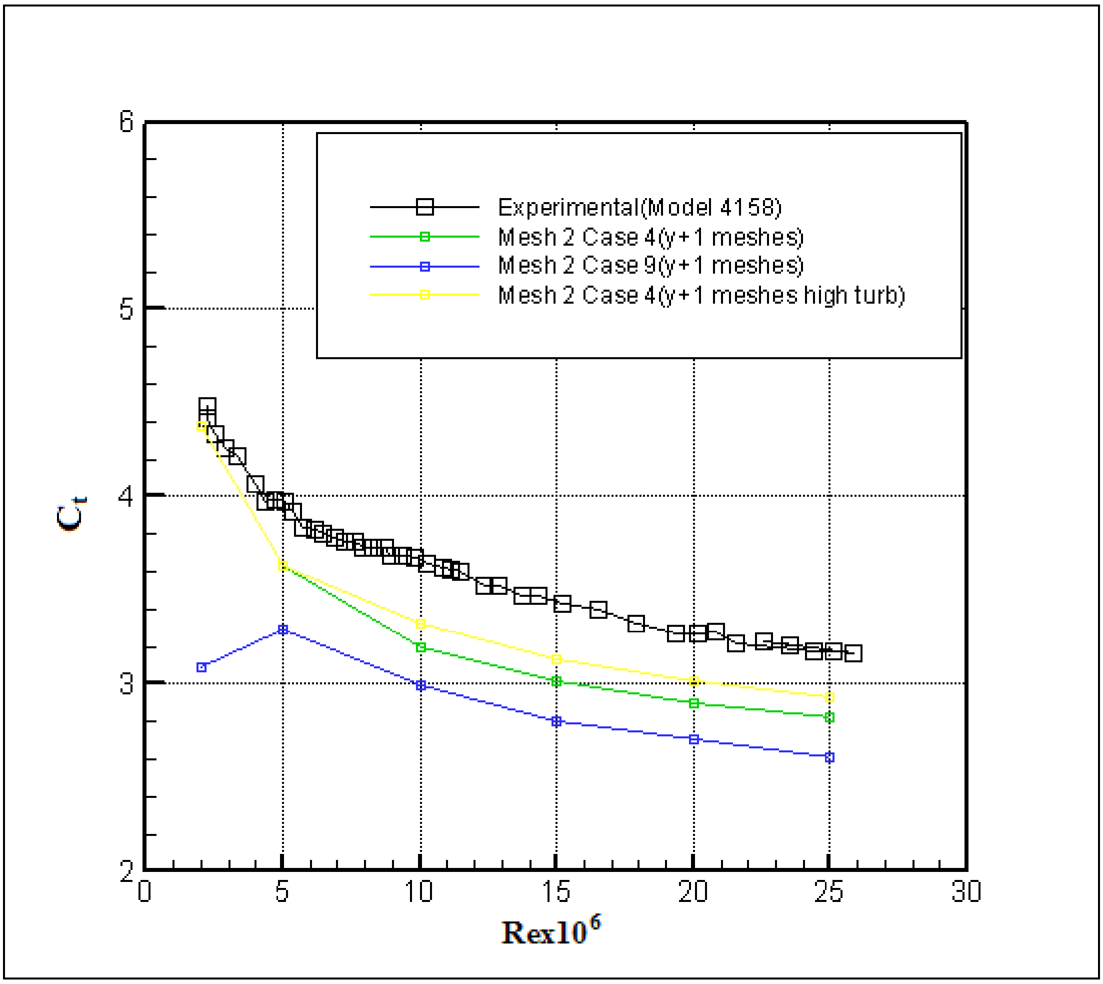

Figure 4.28 Total resistance comparison for Model 4158

Gertler's experiments were performed for resistance only. No pressure distribution or other data were provided. There are, however, some computational studies done with the Series-58. One such study was performed by Gorski [28]. Gorski used Models 4159, 4158 and 4155 in his studies. A finite-volume based code which solves incompressible Navier-Stokes equations for axisymmetric cases was used for simulations. The algebraic eddy viscosity model of Baldwin-Lomax is used for turbulence modeling. Resistance coefficient results of Gorski match well with experimental data. Gorski also provided surface pressure coefficient, $C_{p,}$ distribution of Models 4159 and 4158. Surface pressıre coefficient is defined as

$$C_P = \frac{P - P_{ref}}{\frac{1}{2}\rho U^2} \quad (4.18)$$

where P_{ref} is the reference pressure which is usually taken as the operating pressure FLUENT.

C_P data of Model 4158 are used for comparison with results that are obtained in this study. In Figures 4.29 and 4.30, these comparisons can be seen for Model 4158 with $Re=2\text{x}10^6$ and $Re=2.5\text{x}10^7$, respectively. It is seen that computed surface pressure coefficient distribution of Gorski is very similar to those obtained here especially at the leading and trailing edges.

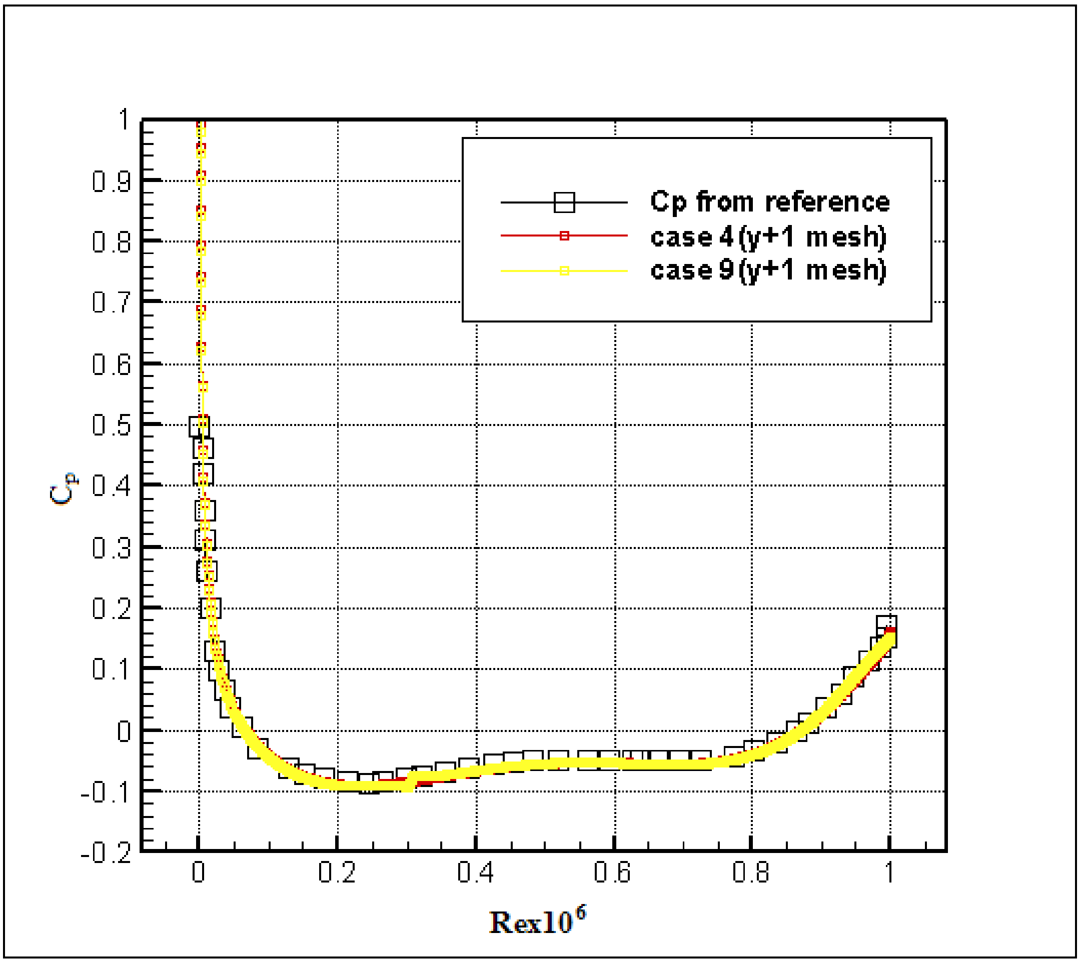

Figure 4.29 Presure coefficient comparison at $Re=2\text{x}10^6$

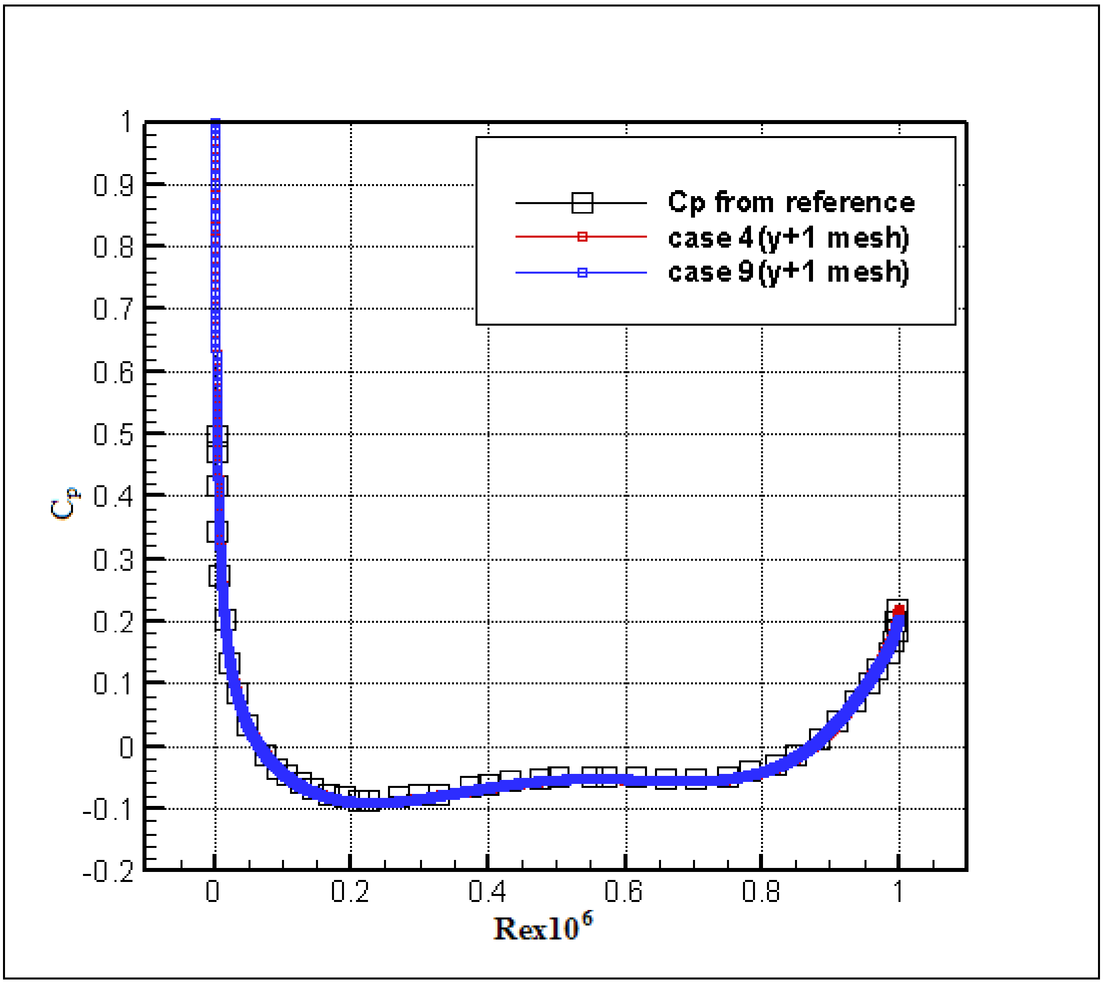

Figure 4.30 Presure coefficient comparison at *Re*=2.5x10^7

4.2.2.3 Model 4154

Model 4154 is the last model which is simulated for validation purposes. It is similar to Model 4159 and Model 4158; however, this model is relatively thicker with an *L/D* ratio of 4. Similar studies to Model 4158 were performed. Meshes with wall y^+ = 1 are generated for each Reynolds number. Cases 4, 7 and 9 were tested again. Results are seen in Figure 4.31.

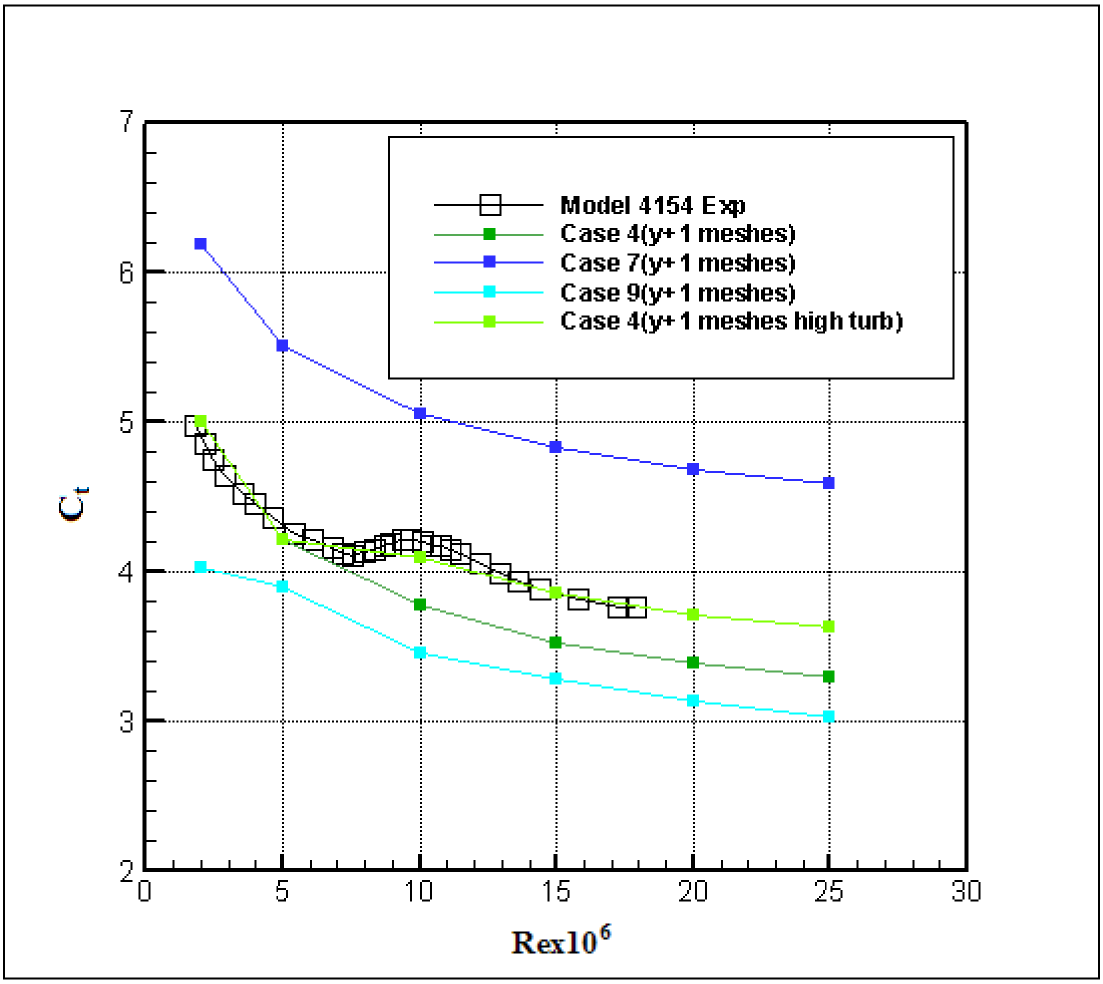

Figure 4.31 Total resistance comparison for Model 4154

It is seen from Figure 4.31 that only Case 4 predicts resistance correctly at low Reynolds numbers. However, Case 4 fails to predict correctly for higher *Re* numbers while maintaining a parallel trend with the experimental data. Due to that, for Reynolds numbers higher than or equal to $1x10^7$, turbulence intensity was increased to 1 % from 0.5 %. After this modification, Case 4 predicted almost the same resistance for high Reynolds numbers.

These additional studies also demonstrate the suitability of realizable $k - \varepsilon$ model with EWT for the unmanned underwater vehicle simulations. It is obvious that turbulence intensity changes resistance results significantly. Studies performed here serve as guidelines for determining turbulence quantities while simulating the vehicle.

CHAPTER 5

DRAG CALCULATIONS

CFD simulations given in this study are performed to determine the drag forces exerted on the vehicle. The most critical criterion is the surging (forward) speed. The vehicle is required to have a surging speed of 2 m/s. Therefore, emphasis is put on drag calculations in forward motion. Later on, heaving (vertical) motion of the vehicle is simulated as well.

In the previous chapter, it was shown that realizable k - ε model with EWT gives accurate results provided that the mesh is fine enough near the wall. This approach is adopted in this part of the study.

5.1 Hull Geometry

As it was stated in Chapter 2, a cylindrical hull shape with wing-like appendages is proposed. Two wing-like appendages on the sides of the hull are used for attaching the forward thrusters. There are two vertical tunnels throughout the hull inside which vertical thrusters are placed.

Apart from determining the hull shape in principle, one has to specify the dimensions of it. Dimensions are also determined in Chapter 2 during the internal design process. The hull is a streamlined body with a cylindrical mid-body and ellipsoid ends at the fore and aft. The aft ellipsoid is elongated to ensure a smooth flow over the body. During simulations, three configurations were used. These configurations are bare hull, hull with wings and full-appended hull.

5.1.1 Bare Hull

Bare hull configuration consists of only the axisymmetric hull. No appendages are included in the model. Details of this model are seen in Figures 5.1 and 5.2. This configuration is used for preliminary analyses. Moreover, it is beneficial for stressing the effects of appendages.

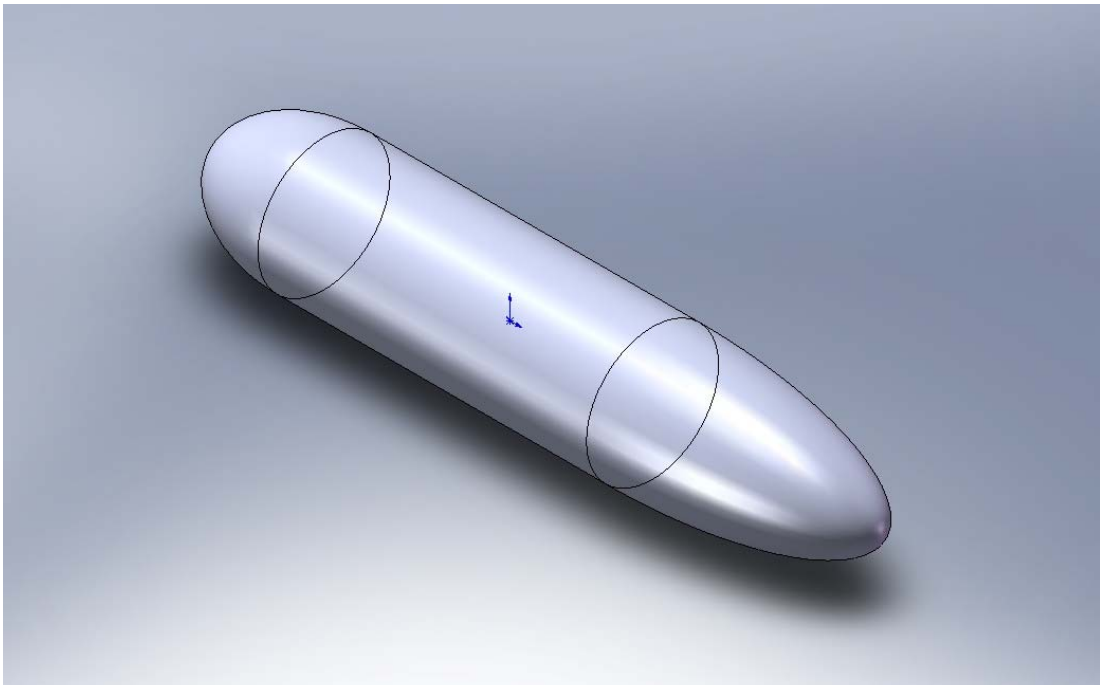

Figure 5.1 Bare hull of the vehicle

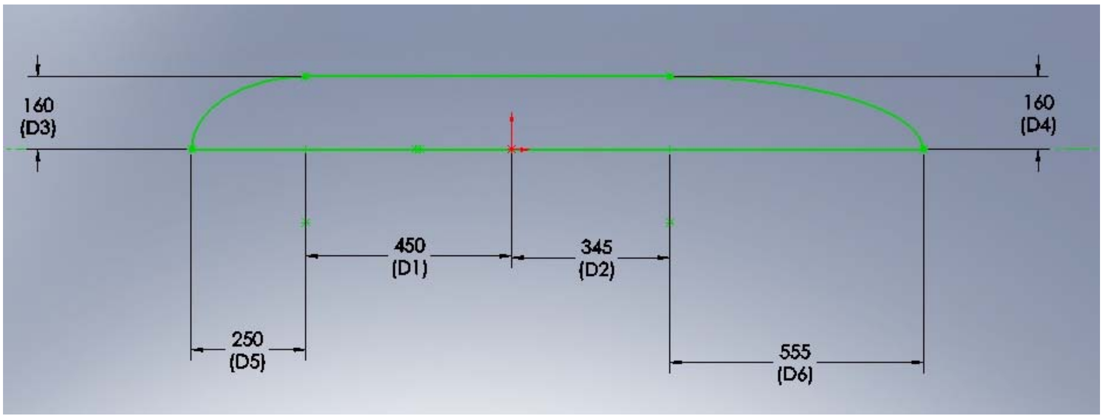

Figure 5.2 Dimensions of the bare hull

5.1.2 Hull with Wings

In this configuration side wings are added to the model as seen in Figure 5.3. The contribution of these wings on drag is seen by simulating this configuration.

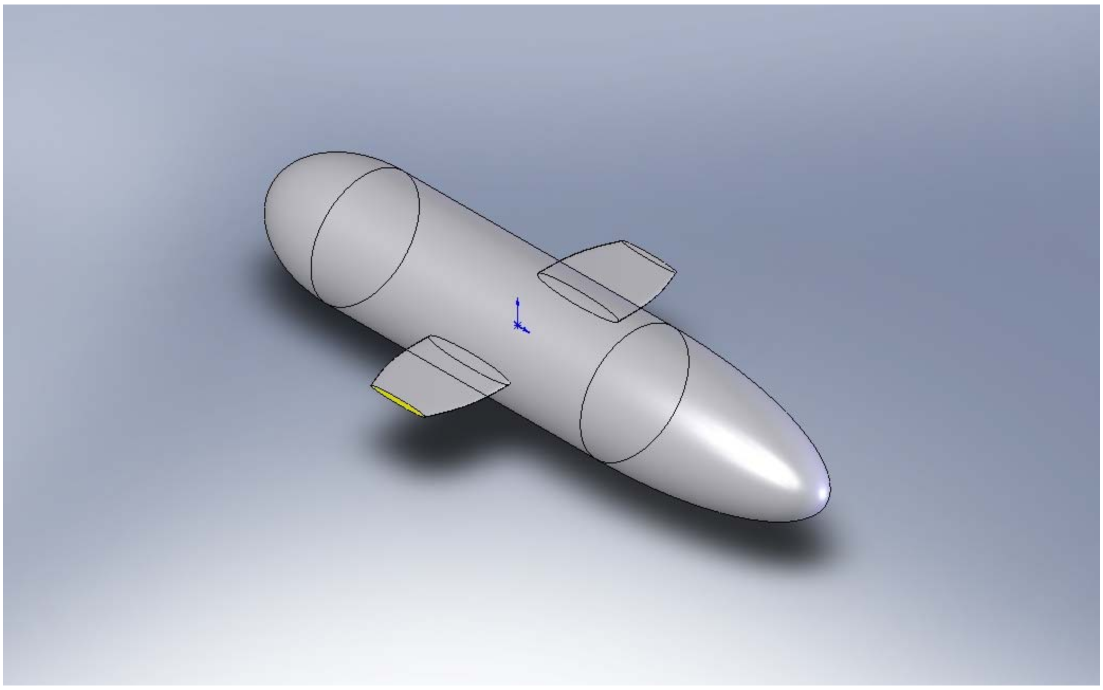

Figure 5.3 Hull with wings

5.1.3 Fully Appended Hull

This is the most complex model. Apart from the wings; cameras, lights, sonar, acoustic modem and vertical tunnels are added to the model. This configuration was beneficial for understanding the extra drag due to appendages thoroughly. Model can be seen in Figure 5.4.

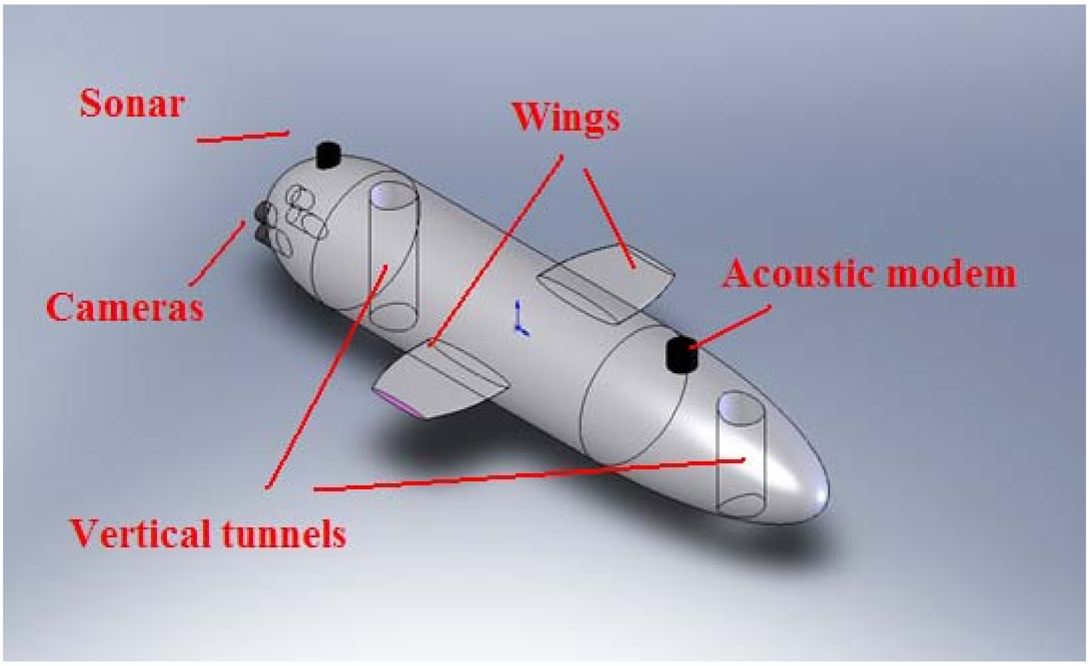

Figure 5.4 Fully Appended Hull

5.2 Solution

Solution of these configurations is similar to the validation studies performed before. Surface meshes are created at the surface in Gambit and 3D boundary layer was created in Tgrid. For volume meshes, tetrahedral elements were used. Length of the domain is chosen to be five times the length of the body with 3 times the length of the body left behind the trailing edge.

Green-Gauss node based gradient option was turned on and realizable $k - \varepsilon$ turbulence model with enhanced wall treatments was used. Turbulence intensity was specified as 0.5 % at the inlet. The most important difference between the validation studies is that this time 3D solver is utilized whereas 2D axisymmetric solver was used for validations.

At this point one may question whether the flow over the vehicle is turbulent or not. It is known that laminar flow is very unstable and it is likely to be turbulent due to disturbances. For the case of an underwater vehicle, there are many disturbances. Appendages on the body, propeller-hull interaction and surface roughness are some examples. Therefore, one can infer that flow will be mostly turbulent in real conditions. Nevertheless, it is wise to check critical Reynolds numbers.

Two modes of motion are simulated in this thesis study: forward motion and vertical motion. For forward motion, the vehicle may be treated as a streamlined body and characteristic length is taken as body length (1.6 m). Reynolds number in this case becomes:

$$Re = \frac{998.2\left(\frac{kg}{m^3}\right)x2\left(\frac{m}{s}\right)x1.6\ (m)}{0.001003\ (\frac{kg}{ms})} \cong 3.18x10^6 \tag{5.1}$$

which is higher than the critical Reynolds number $5x10^5$ for a flat plate. Even though the flat plate is not a true representative of the streamlined body, still it is logical to expect turbulent flow over the vehicle. It is obvious that the Reynolds number of the vehicle is higher; hence, turbulent flow assumption is reasonable.

For the vertical motion, the vehicle may be treated as a cylinder in cross-flow; hence, bluff body motion is present. For this case characteristic length can be taken as the diameter of the vehicle (0.32 m). There is no criterion for vertical speed. A vertical speed of 0.5 m/s can be assumed as a reasonable value. In this case, Reynolds number becomes:

$$Re = \frac{998.2\left(\frac{kg}{m^3}\right)x0.5\left(\frac{m}{s}\right)x0.32\ (m)}{0.001003\ (\frac{kg}{ms})} \cong 159234 \tag{5.2}$$

For $Re > 2x10^5$, transition to turbulence occurs in the front part of the body. This value is close to the Re number of the body. When the effects of irregularities on the body are considered, it can be inferred that assuming turbulent flow is a reasonable choice.

5.2.1 Forward Motion

Forward motion is the most critical case because it determines the thrust and power requirements of the vehicle. Forward motion is analyzed for all three configurations.

5.2.1.1 Forward Motion with Bare Hull Configuration

The purpose of this simulation is to determine the drag for the single bare hull. The flow domain and the mesh on the model are seen in Figures 5.5 and 5.6, respectively.

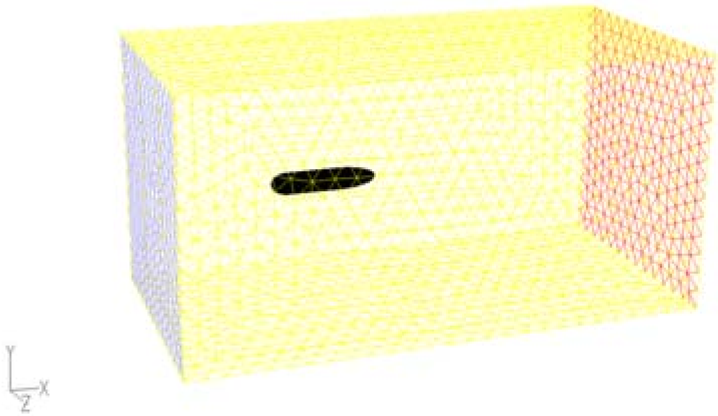

Figure 5.5 Flow domain for bare hull configuration in forward motion

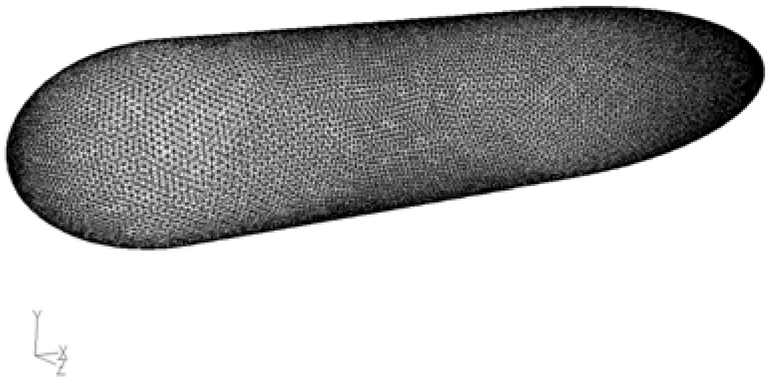

Figure 5.6 Surface mesh for bare hull configuration in forward motion

It should be noted that the aim is to obtain a fine mesh on the surface so that the wall y^+ value is around 1 throughout the surface. While making the initial guess for the first cell height, experience from the validations studies and preliminary 2D studies are used. The wall y^+ contours on the body, as seen in Figure 5.7 show that the mesh is fine enough for enhanced wall treatment. Moreover, for EWT it is suggested to put at least 10 elements in the boundary layer until Re_y > 200. This condition is also satisfied. Pressure contours on the body can be seen in Figure 5.8.

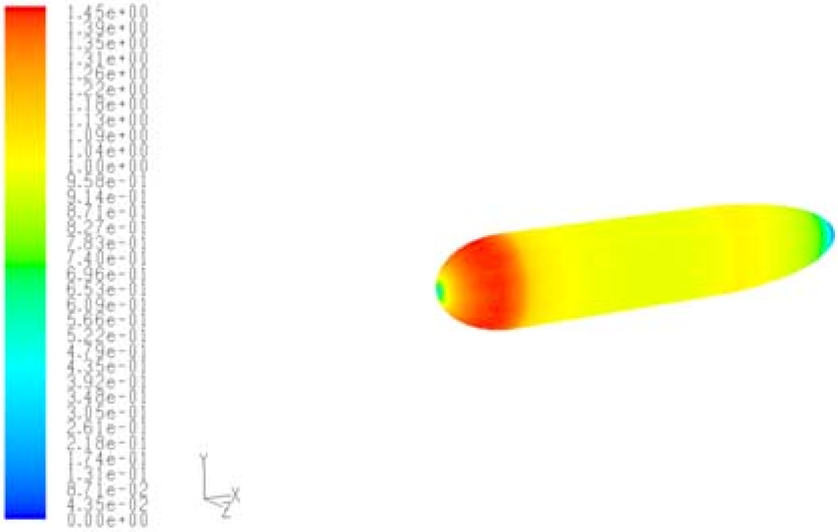

Figure 5.7 Wall y^+ contours for bare hull configuration in forward motion

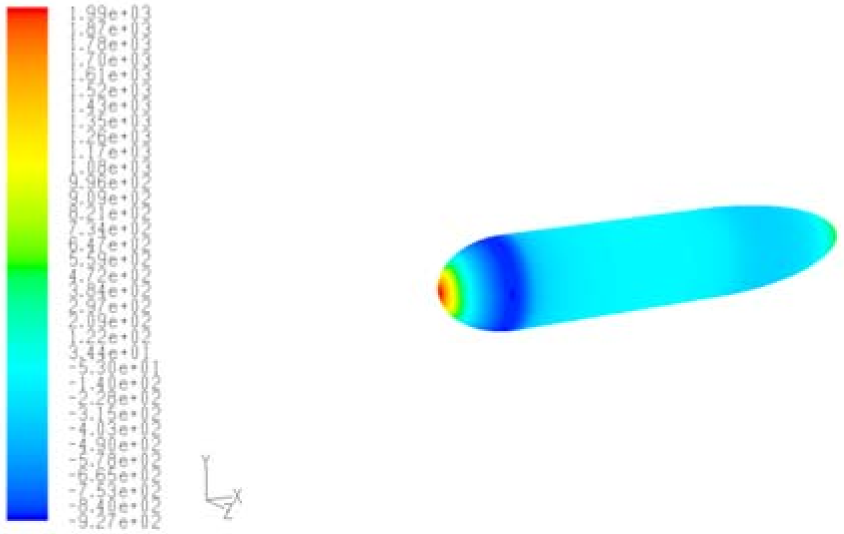

Figure 5.8 Pressure contours for bare hull configuration in forward motion

The total resistance force on the body is seen in Table 5.1.

Table 5.1 Drag components on bare hull for forward motion

	Friction drag (N)	Pressure drag (N)	Total drag (N)
Bare hull (total)	3.19	10.83	14.02

5.2.1.2 Forward Motion for Hull with Wings Configuration

This time the effect of the wing appendages is also seen. The same domain with the bare hull configuration is used. Mesh details can be seen in Figures 5.9 and 5.10. *y+* values are again satisfactory and can be seen in Figure 5.11. Pressure distribution is seen in Figure 5.12.

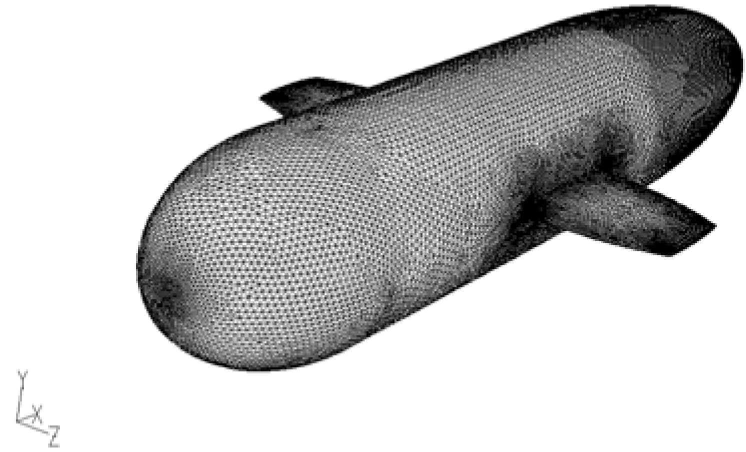

Figure 5.9 Surface mesh for hull-wings configuration in forward motion

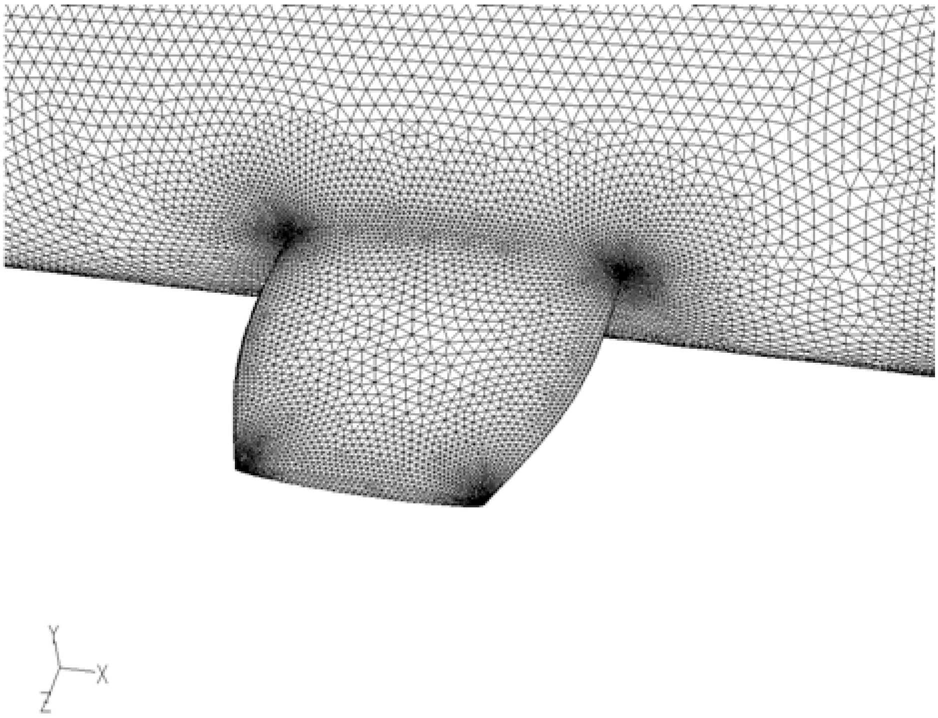

Figure 5.10 Mesh details for hull-wings configuration in forward motion

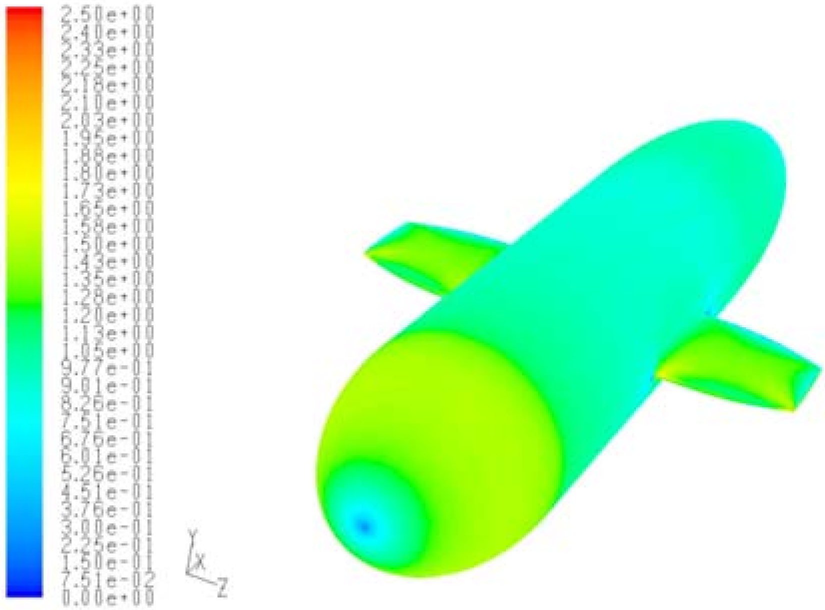

Figure 5.11 Wall y^+ contours for hull-wings configuration in forward motion

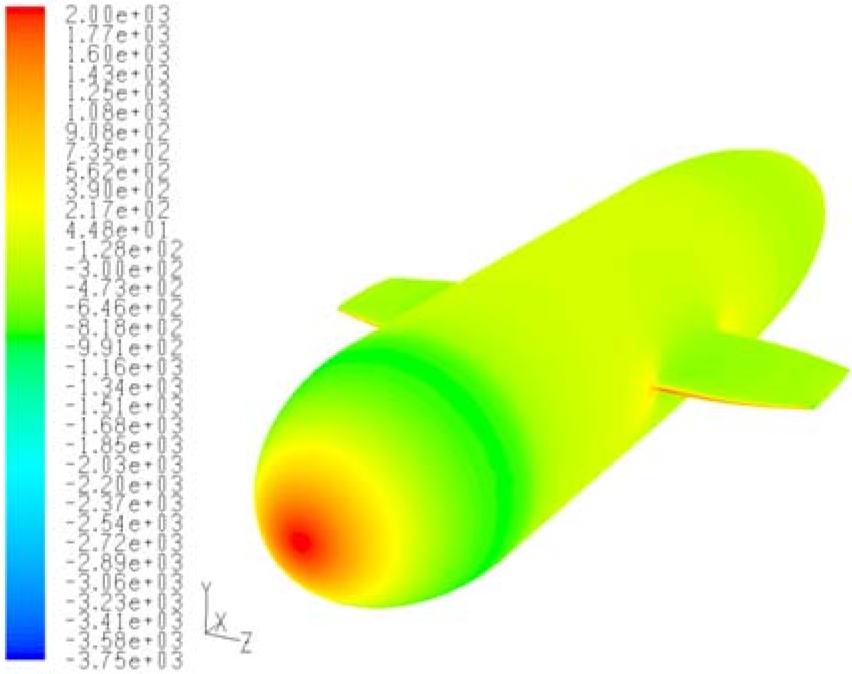

Figure 5.12 Pressure contours for bare hull configuration in forward motion

The total resistance force on the body is seen in Table 3.3.

Table 5.2 Drag components for forward motion for hull-wings configuration

	Friction drag (N)	Pressure drag (N)	Total drag (N)
Hull	9.85	3.32	13.18
Wings	2.26	1.41	3.66
Total	12.11	4.73	16.84

Friction drag is a surface property; therefore, it is expected to have higher friction drag for hull which has a larger surface area. On the other hand, even though these wings are thin, they still produce comparable amount of pressure drag (about 30% percent).

5.2.1.3 Forward Motion for Fully Appended Hull Configuration

In this configuration, almost all of the appendages are included in the model: sonar, modem, tunnels, cameras and wings. The increase in the complexity of the model results in a large number of grid points and eventually longer computation time. Moreover, the complexity makes it difficult to generate boundary layer mesh at the surface. Fortunately, Tgrid provides easy and efficient means of boundary layer and volume mesh generation.

The domain, boundary conditions and solution parameters are chosen the same for the previous two models. The surface mesh can be seen in Figures 5.13 to 5.15.

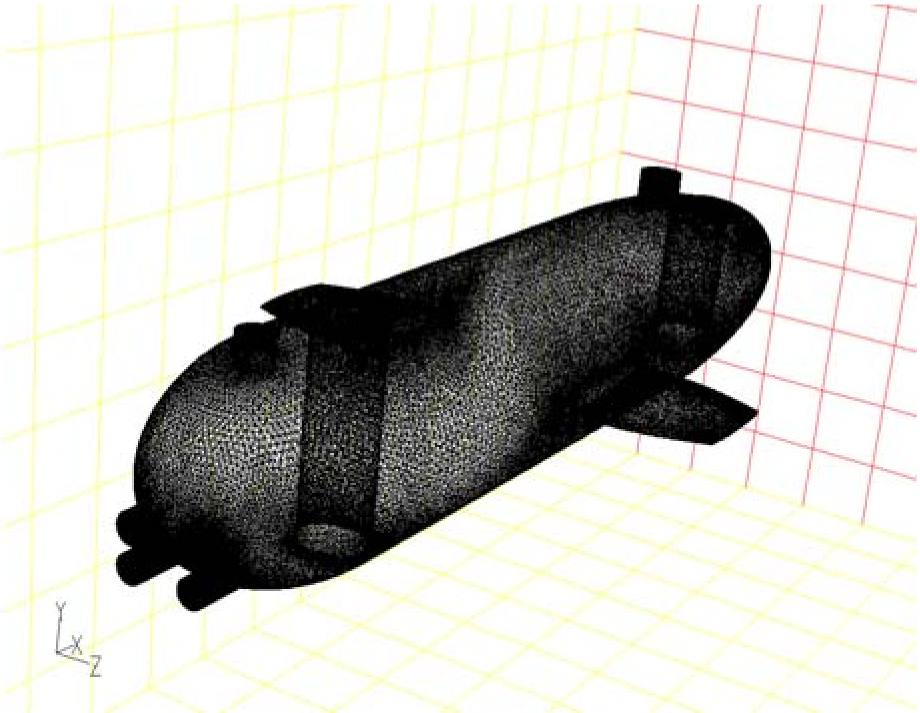

Figure 5.13 Mesh for fully appended configuration in forward motion – 1

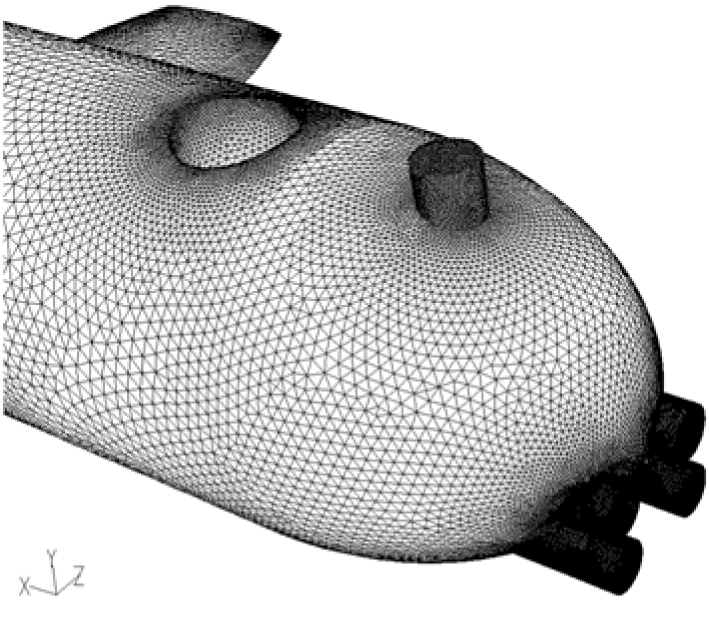

Figure 5.14 Mesh for fully appended configuration in forward motion – 2

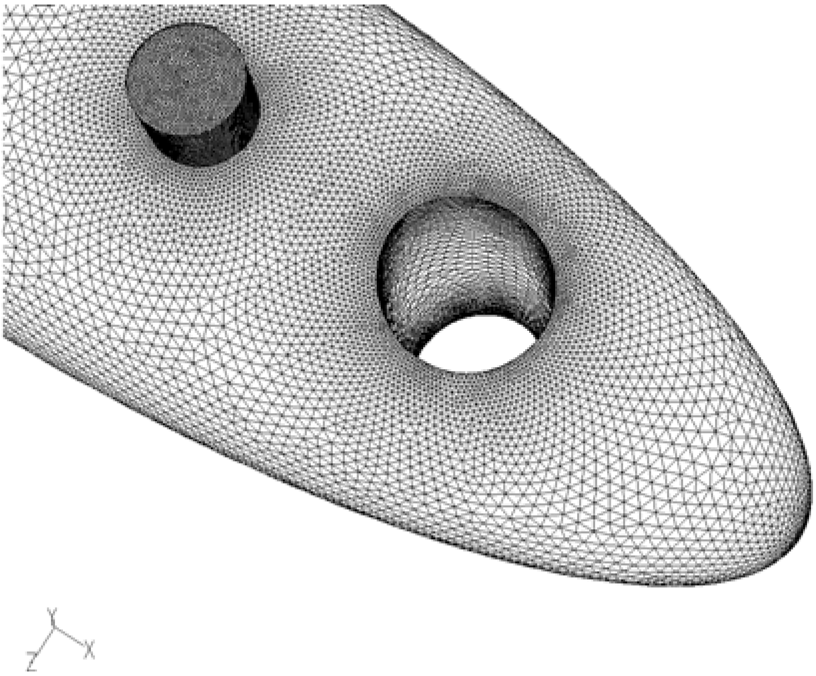

Figure 5.15 Mesh for fully appended configuration in forward motion – 3

The contours of wall y^+ on the body are seen in Figure 5.16. Only for a few accelerating regions around appendages, the y^+ value exceeds 2. Other than that, wall y^+ is mostly around a value of 1 which makes the mesh suitable for enhanced wall treatment.

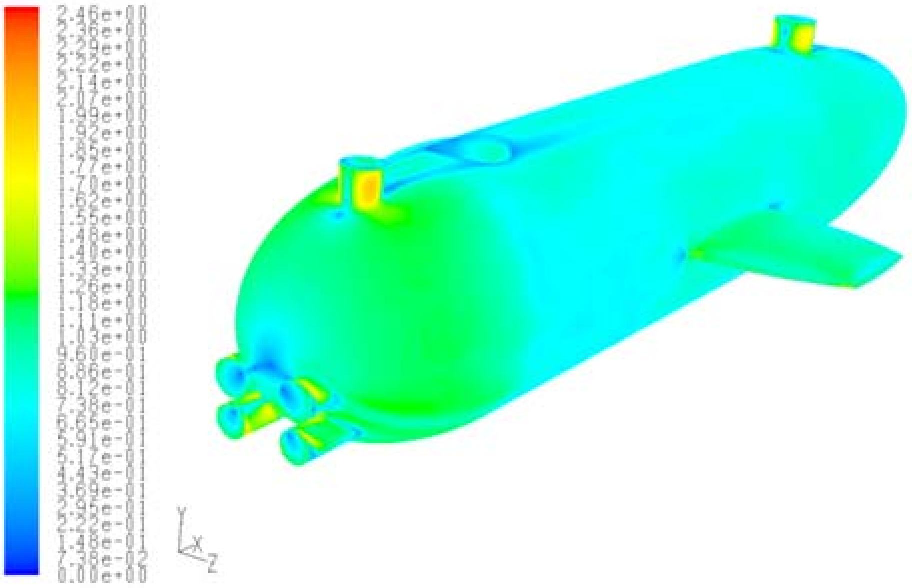

Figure 5.16 Wall y^+ contours for fully appended configuration

In Figures 5.17 and 5.18, static pressure contours are seen.

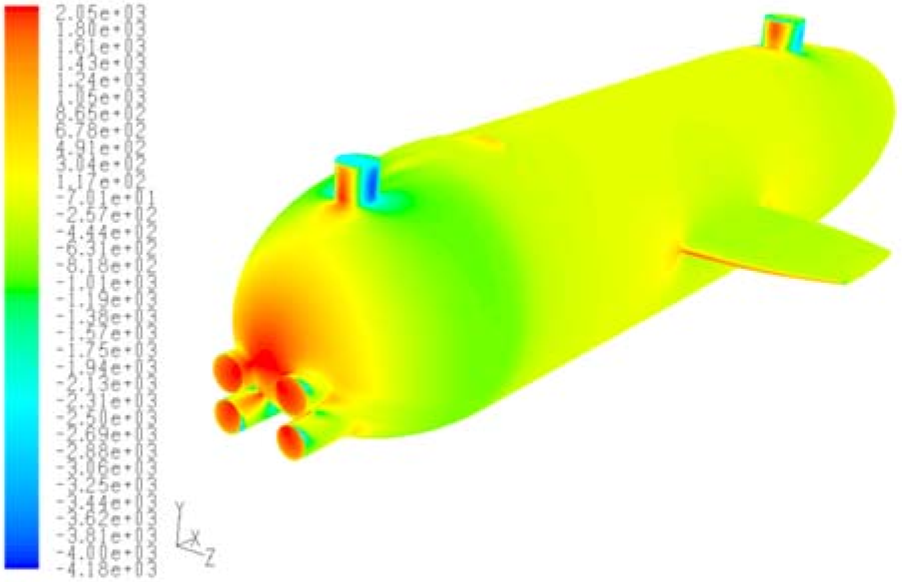

Figure 5.17 Pressure contours for fully appended configuration - 1

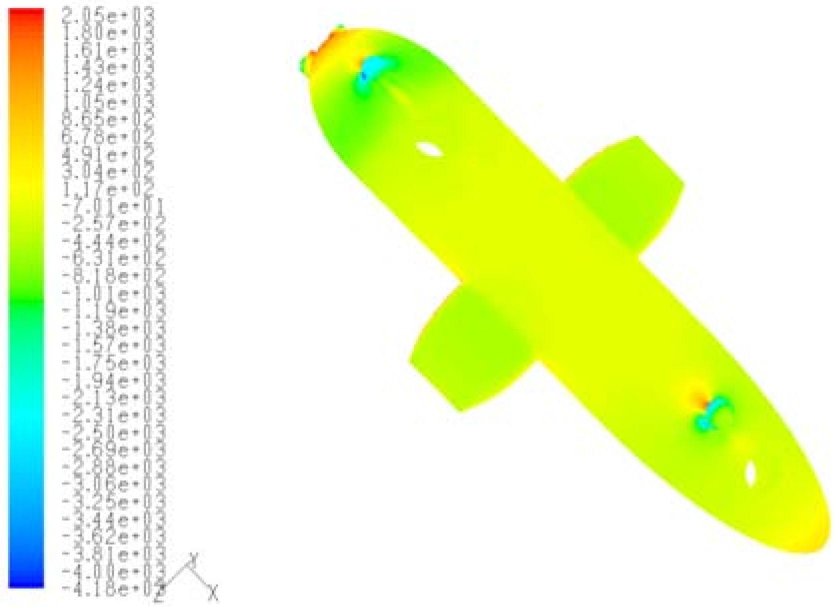

Figure 5.18 Pressure contours for fully appended configuration - 1

Total resistance on the body is seen in Table 5.3.

Table 5.3 Drag components for forward motion

	Friction drag (N)	Pressure drag (N)	Total drag (N)	Percentage (%)
Modem	0.09	2.81	2.90	9
Sonar	0.06	1.46	1.52	4.7
Camera	0.06	9.19	9.26	28.8
Wings	2.18	1.64	3.82	11.9
Tunnel – aft	-	1.56	1.56	4.8
Tunnel – forward	-	1.00	0.99	3.1
Hull	9.56	2.47	12.03	37.5
Total	11.95	20.13	32.08	

Even though extra drag due to appendages may seem insignificant, the cumulative effects of these appendages cause a significant increase in total drag force. Total drag is 14.02 N for bare hull, 16.84 for hull with wings and 32.07 N for the fully appended configuration which means that the drag value is twice as high as the bare hull case.

This increase is not only due to the extra drag of appendages, but also due to the distortion of the flow field. Therefore; one should pay extra attention to these protrusions and streamline them if possible.

Pathlines of the flow also provide interesting data for the designer. The appendages which distort the flow of the flow can be detected and modified if possible. For instance when Table 5.3 is examined, it is seen that the drag increase due to cameras is very high compared to other appendages. When pathlines which are given in Figures 5.19 and 5.20 are observed, it is seen that the protrusion of cameras are very significant and this results in separated flow and increased drag.

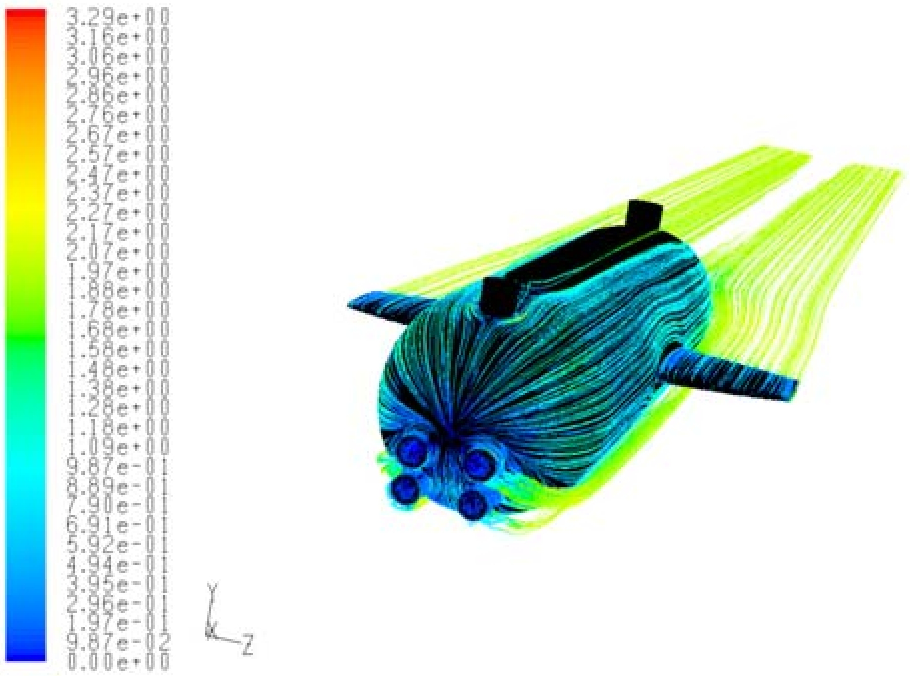

Figure 5.19 Pathlines for forward motion - 1

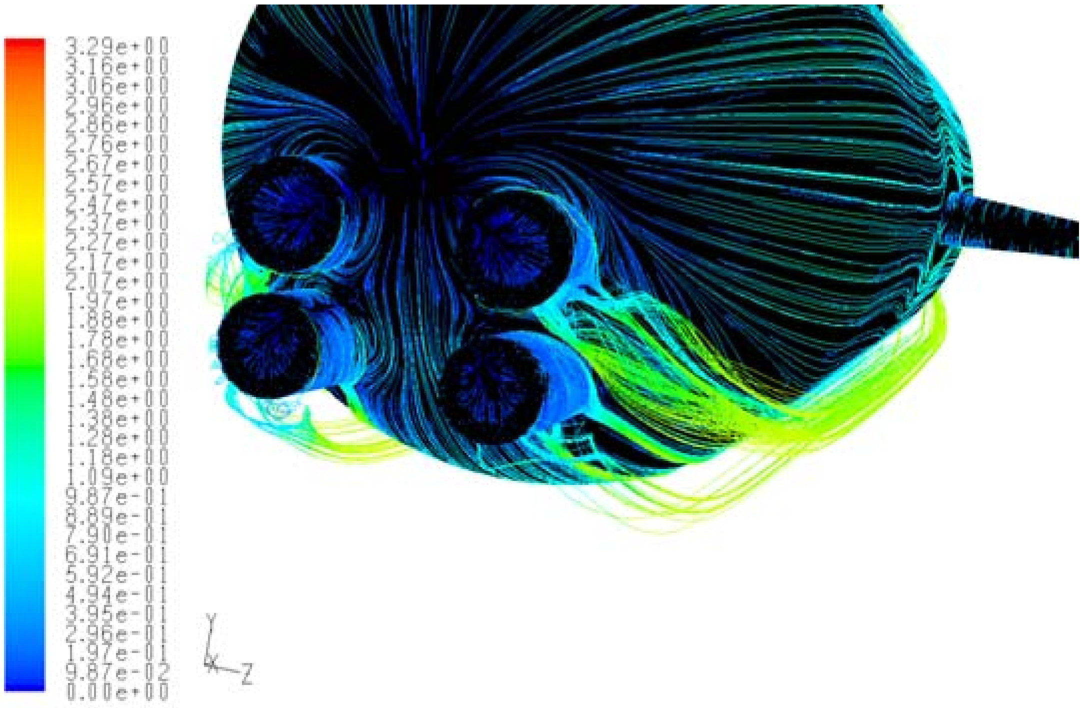

Figure 5.20 Pathlines for forward motion – 2

5.2.2 Vertical Motion

Vertical motion is achieved with two vertical thrusters that are placed inside a tunnel that passes throughout the body. In the project definition, no criteria were defined for vertical motion. Nevertheless, it is important to verify that the vehicle will at least be able to surface at a steady speed. For this purpose a vertical speed of 0.5 m/s is selected. The mesh which gives good resolution for forward motion is used again. This time the domain changes, however, a cube with a length of 5 m is chosen. The domain can be seen in Figure 5.21.

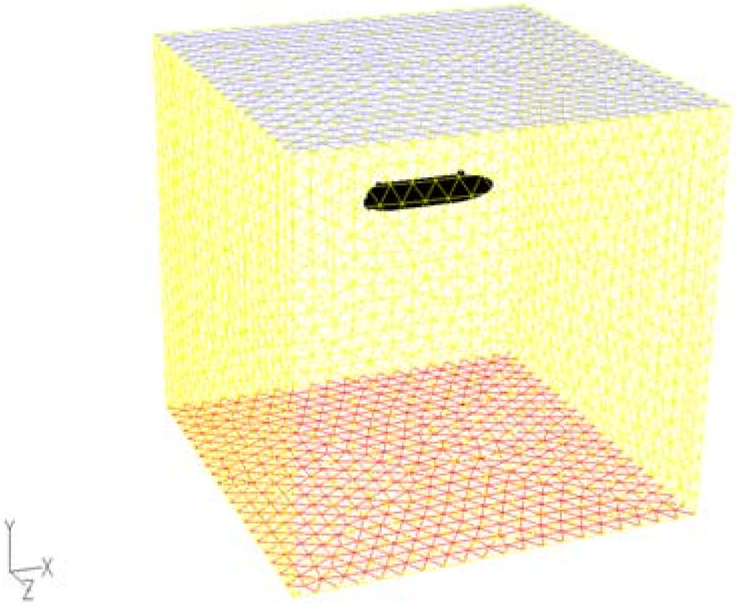

Figure 5.21 The domain used for vertical motion simulations

Solution parameters are similar to the previous simulations. Simulations are done by using the hull-wing configuration and the fully-appended configuration. Pressure, wall y^+ and pathline graphs of only fully-appended region will be provided here. Mesh details will not be given also since the same mesh for the forward motion is used.

Wall y^+ contours on the body are given in Figure 5.22. As seen from the figure, wall y^+ values are less than 1 all over the wall and mesh resolution is satisfactory. Pressure distribution on the body is seen in Figure 5.23.

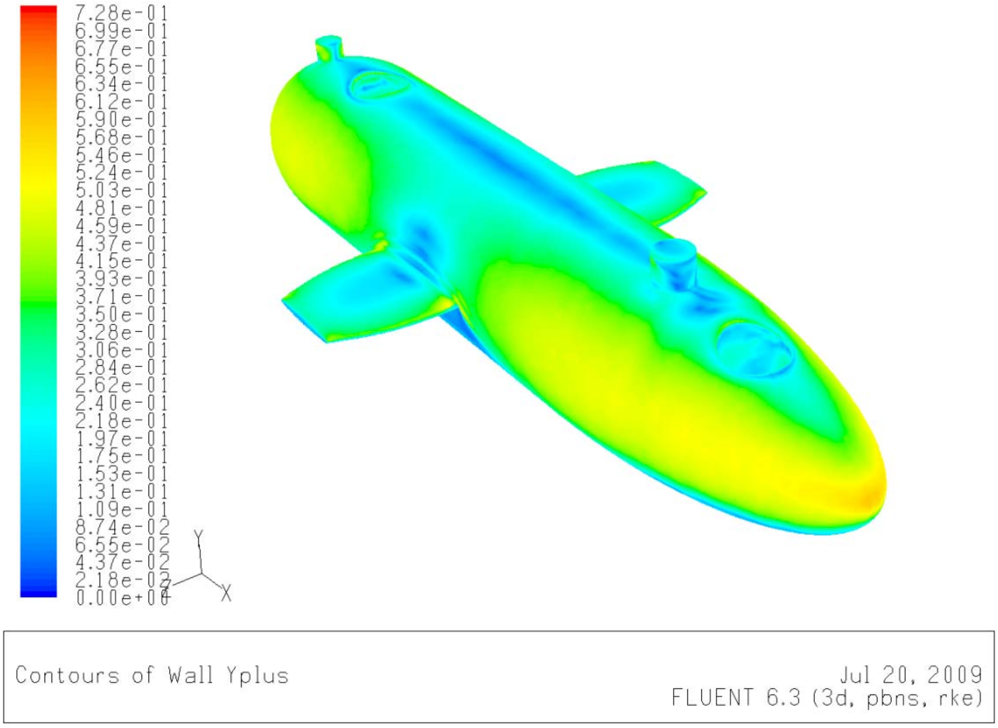

Figure 5.22 Wall y^+ contours for fully appended configuration

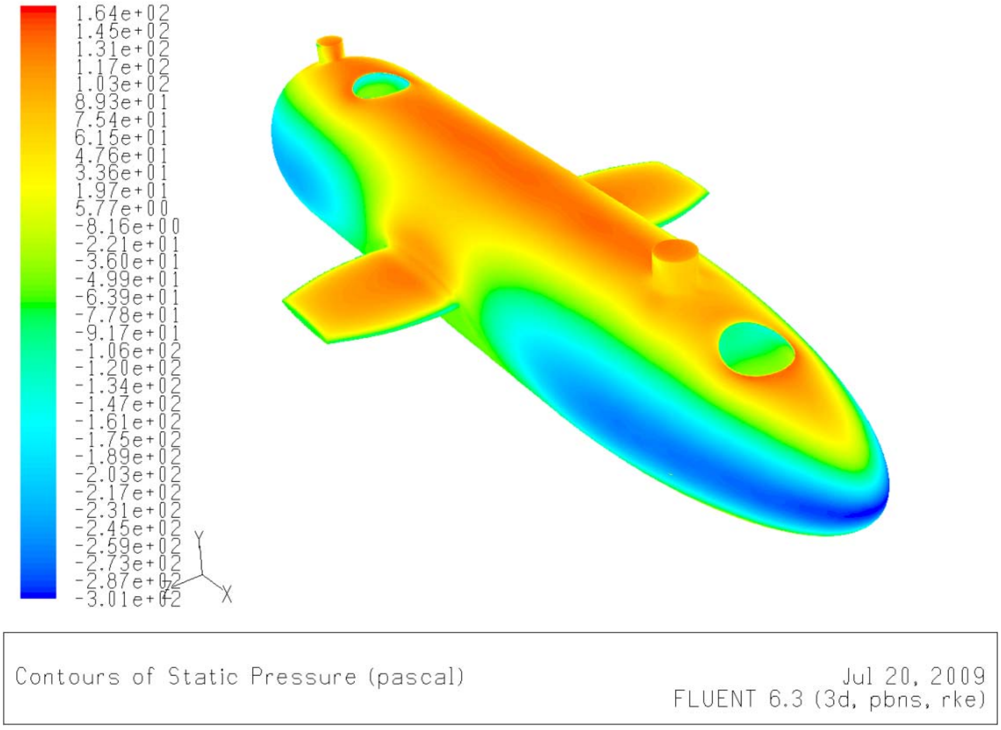

Figure 5.23 Pressure contours for fully appended configuration

Finally, pathlines for vertical motion are seen in Figures 5.24 and 5.25. From these figures, it is seen that appendages like cameras and wings distort the flow and cause separation. On the other hand, wings are useful for supporting the thrusters, providing rolling stability and creating a moment arm for forward thrusters. Therefore, the choice depends on the needs and priorities of the project group.

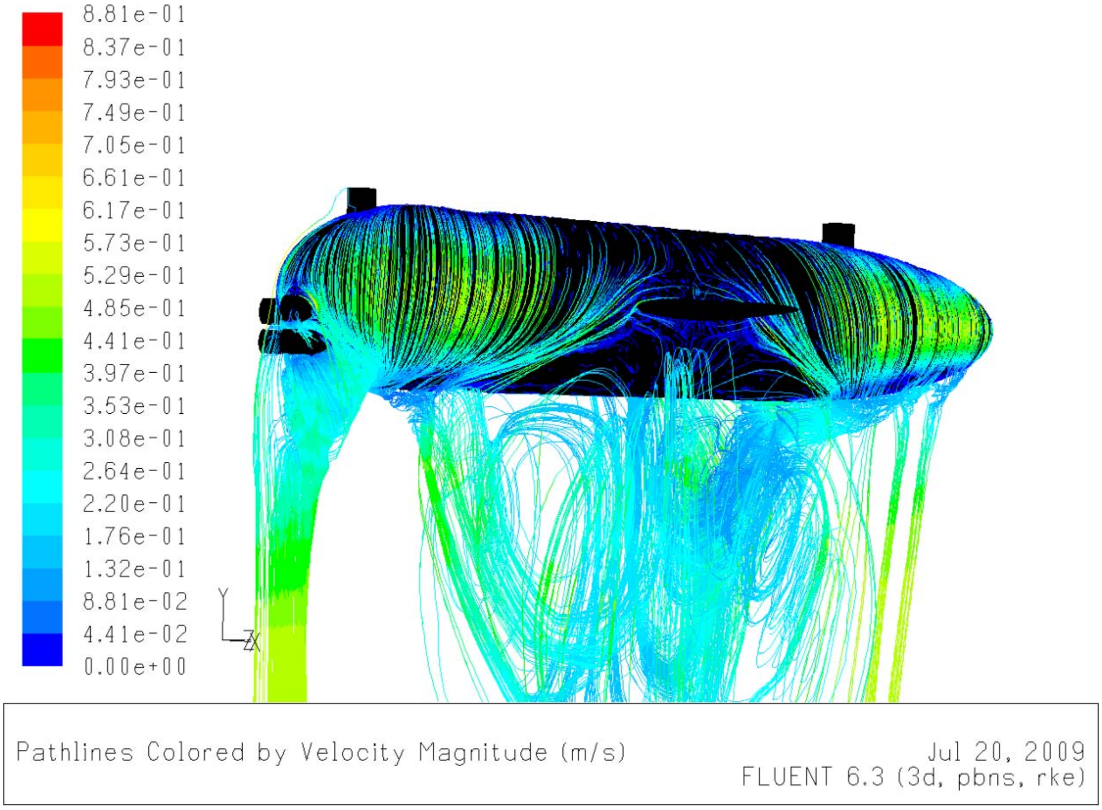

Figure 5.24 Pathlines for vertical motion - 1

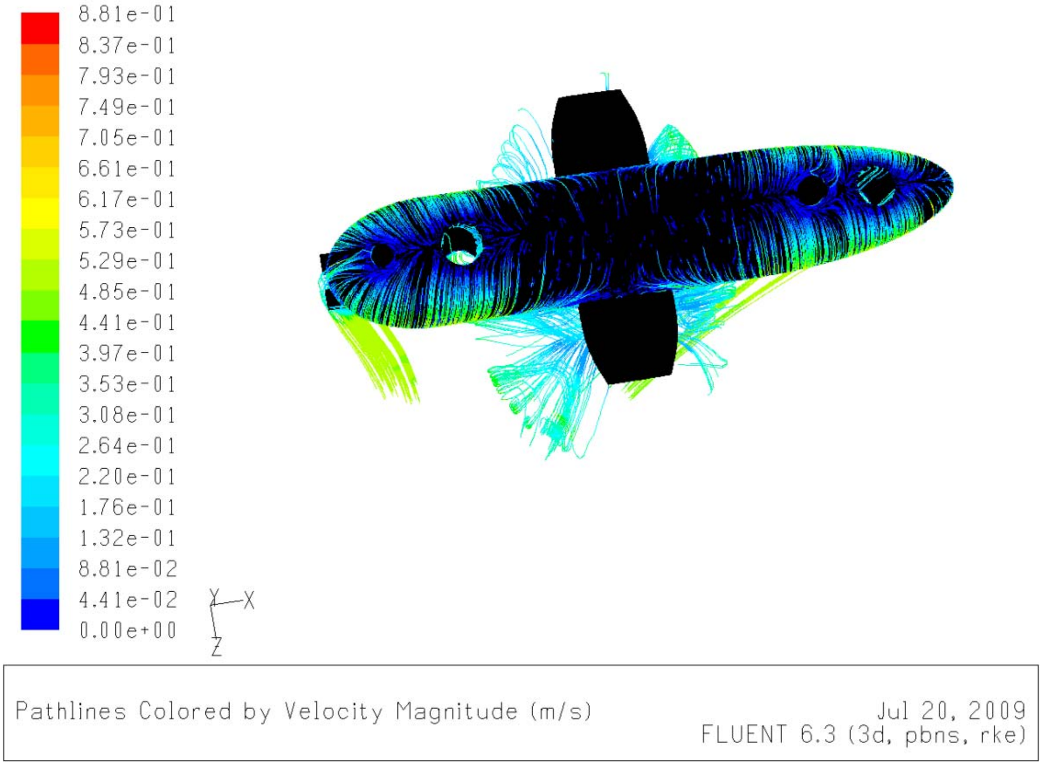

Figure 5.25 Pathlines for vertical motion – 2

Resistance predictions of hull-wings configuration and fully-appended configuration are almost equal. The resulting drag is about 53 N.

5.3 Thruster Selection

After determining the thrust requirements for forward and vertical motion, thruster selection can be done. For the 2 m/s forward motion of the fully-appended body, a resistance of 32 N is expected. BTD150 thrusters of Seabotix can give a continual bollard thrust of 2.2 kgf (21.6 N). Since two thrusters in parallel will be used for forward and vertical motion, a total of 43.2 N thrust is achieved which is probably sufficient for the speed criteria. BTD150 is a popular thruster for unmanned underwater vehicles. It is a podded propulsor so there is no need for sealed shafts to drive the motor. It should be noted that the demands of the electronics engineers in the group were also taken into account while selecting the thruster.

CHAPTER 6

MANUFACTURING AND TESTING

In this chapter of the thesis, information about the manufacturing and testing of the vehicle is provided. It should be noted that Barış Elektrik Endüstrisi Inc. is responsible from the manufacturing of the vehicle using composite materials; therefore, most of the efforts mentioned here are performed by them. Decisions such as determining the hull thickness, designing the mounting interface of devices and modifying the hull is done by them. Due to that reason, only an overview of the manufacturing process will be presented in this thesis. At this stage, only preliminary tests are performed; therefore, brief information is provided for tests as well.

6.1 Manufacturing

The manufacturing process consists of three steps: namely, manufacturing the model, manufacturing the mold and manufacturing the body. First of all a model that has the same shape of the body is manufactured with CNC machine. The model that was produced is seen in Figure 6.1. The cylindrical protrusions are used for the vertical tunnels later on.

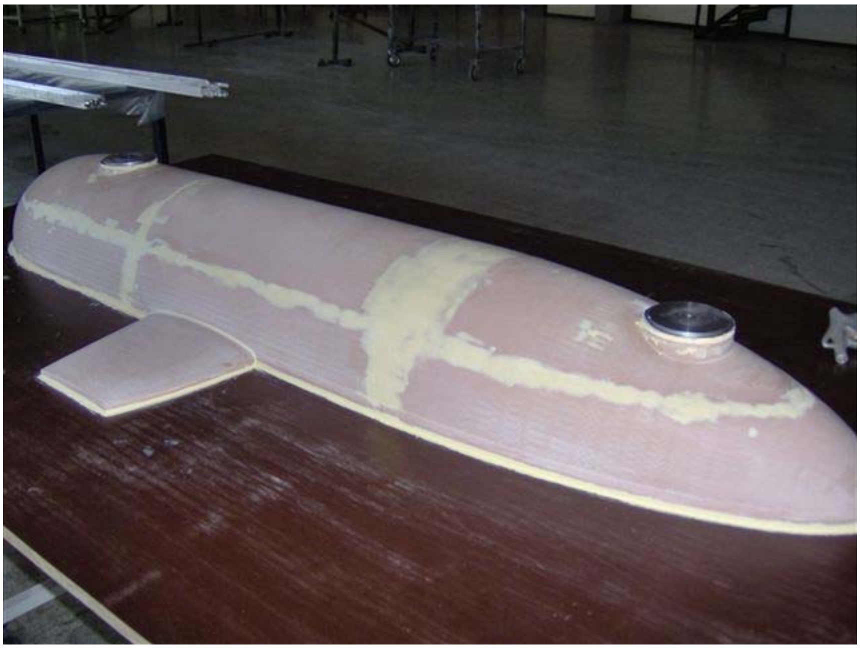

Figure 6.1 Model of the vehicle

The actual mold is obtained by using the model as the mold. The mold will be produced from glass-epoxy with vacuum bagging process. Lamination is done on the model as seen in Figure 6.2. The mold is the female counter-part of the vehicle and is seen in Figure 6.3.

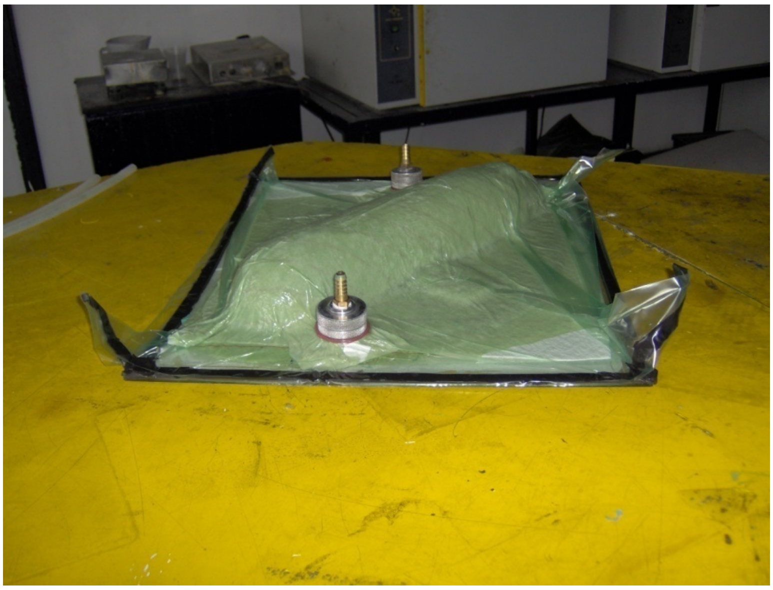

Figure 6.2 Mold of the vehicle (during production)

Figure 6.3 Mold of the vehicle (finished product)

This mold is used for producing the vehicle body. Similar to the previous process, fibers are laid on the mold, vacuum is applied and curing is done. Laying up the fibers is seen in Figure 6.4. After these steps, the raw vehicle body is obtained and it is processed to achieve the final design. Some of these processes are obtaining the walls of the pressure hull, fitting underwater connectors to those walls, piercing the necessary holes, providing a sealing system at the interface, manufacturing the mounting hardware of devices, placing the draw latches on the body, surface operations and painting. The final product is seen in Figure 6.5.

Figure 6.4 Hand lay-up process for the vehicle body

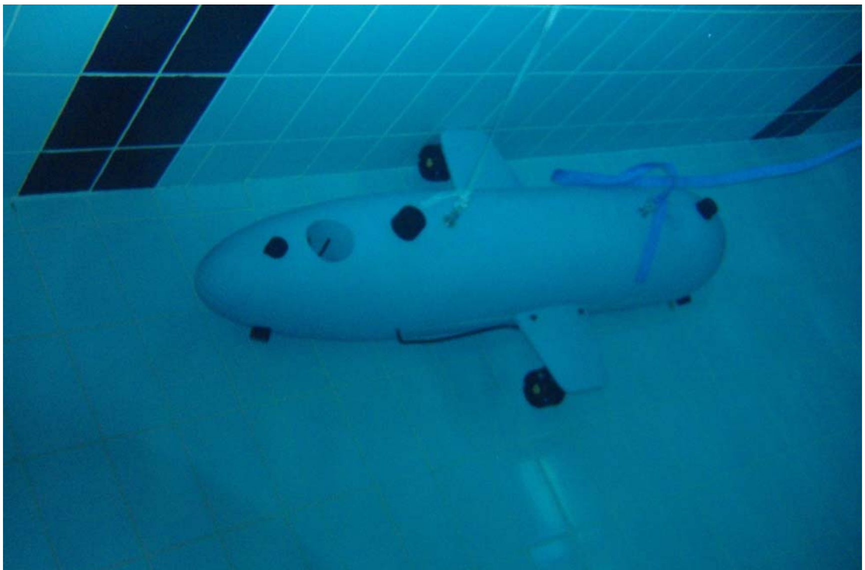

Figure 6.5 Vehicle body

6.2 Tests

Testing the vehicle is the final step in the project. In the scope of this project, tests that are or will be applied are leakage tests, heating tests, deep submergence tests and performance tests. It is obvious that before beginning performance tests, one should conduct leakage, heating and deep submergence tests and receive successful results.

The leakage test is a difficult step. Two types of leakage tests were performed. In the first one, vacuum is applied to the pressure hull and the vehicle is submerged in water. Vacuum is applied in order to simulate the effect of increased depth. 0.2 and 0.8 bars of vacuum is applied which correspond to water depths of 2 and 8 meters respectively. Initial trials were not successful. However, it was seen that leakage was lower at higher values of vacuum. It was assumed that the problem was insufficient compressive force provided by draw latches. As a result, additional latches were assembled to the vehicle and tests were conducted again. Leakage was reduced but still present. A final test was performed. This time four clamps were attached to the vehicle from the outside as seen in Figure 4.32 and the vehicle was submerged into the pool. The aim was to increase the compression force. The clamps proved to be helpful and no leakage was detected. It should be noted that these tests are performed for shallow water and the system has to be tested at deep submergence up to 100 meters.

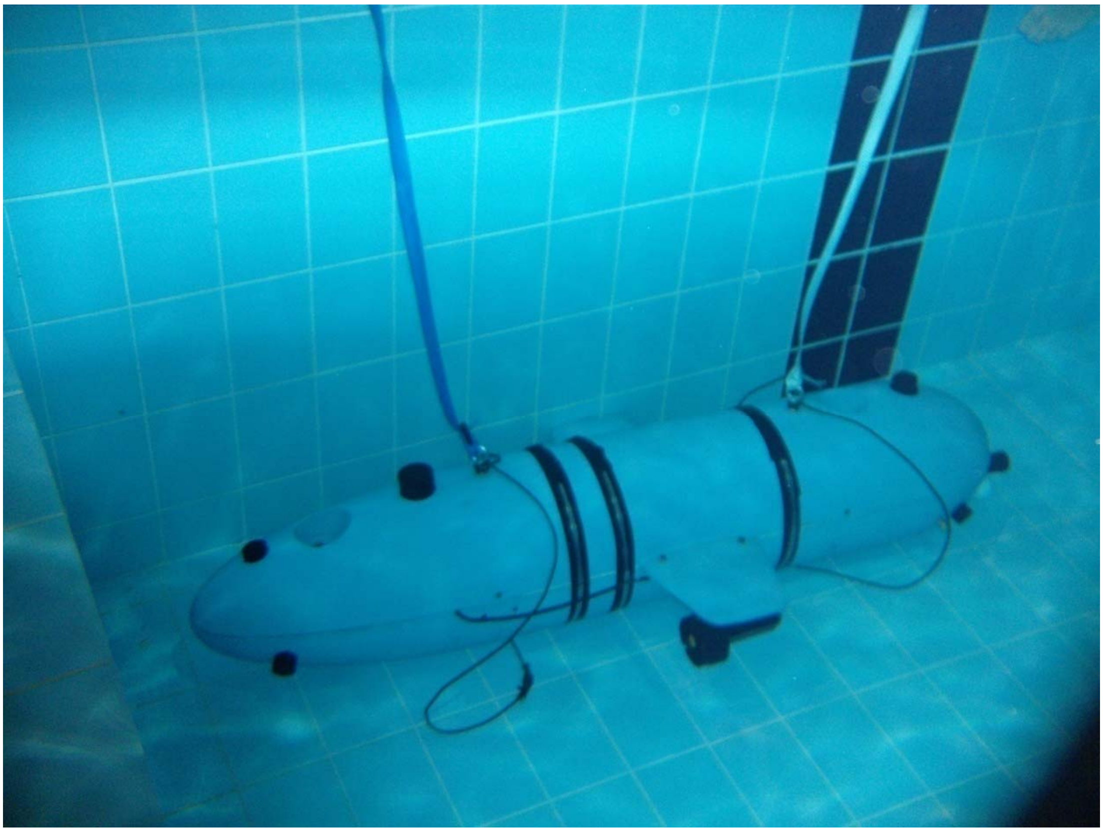

Figure 6.6 Leakage test at the pool

Initial heating tests were performed during the design step and results are presented in the previous part. In these tests a representative hull was used along with lamp as the heat sourse. Those results claim that no over-heating will occur inside the hull. However, it is important conduct these tests with actual system.

At present, leakage tests are successfully completed at the pool. Heating tests are being performed and their results will be received soon. Deep submergence test at sea and performance tests to check the maximum speed of the vehicle should be the next steps in the project.

CHAPTER 7

CONCLUSIONS AND DISCUSSIONS

7.1 Conclusions

The aim of this thesis study is to present the performance prediction simulations that were performed during the design of an unmanned underwater vehicle. First of all conceptual design of the hull is explained. Different hull shape examples and propulsion systems are investigated and appropriate selections are made. The dimensions of the hull are determined from the internal arrangement of devices. Besides the internal arrangement, it is decided to employ a floodable hull. Glass-epoxy is chosen as the hull material due to its high strength-to-weight ratio, ease of molding and high corrosion resistance. Vacuum bagging is chosen as the manufacturing method since it provides ease of manufacturing with relatively low cost compared to other RTM methods.

After the conceptual design of the hull, performance prediction analyses are done. The first set of analyses is about the heating problem of the watertight middle section (pressure hull). This section houses electronic equipments and has thicker walls to withstand the high hydrostatic pressure in deep submergence. Furthermore, glass-epoxy is known to be a poor thermal conductor. When the effects of thick walls and high thermal resistance of glass-epoxy are considered, it is inferred that the heat dissipation may not rejected from the pressure hull easily and the temperature inside the hull may increase. This increase should be avoided for the proper operation of electronic equipments. FLUENT is used for analyzing this heating problem. Due to computational resources, only two-dimensional unsteady analyses of the hull are performed for 2 hours (the expected operation time of the vehicle). Two different sections are analyzed with FLUENT. The results of these analyses revealed that the maximum temperature in the hull is below the maximum allowable value. Heating tests are also performed to check the validity of the analyses. A glass-epoxy pressure hull with a lamp inside as the heat source is immersed in water. A number of temperature sensors are placed in the pressure hull to record the temperature against time. The results of this test give close results to analyses. Results of the analyses and tests are presented in Chapter 3.

The second set of performance prediction analyses are about the forward and vertical motions of the proposed hull design. The most important speed requirement is the forward speed which is 2 m/s. Before analyzing whether the hull shapes satisfies this limitation, some validation studies are performed in Chapter 4. Series 58, which is a series of axisymmetric streamlined bodies, is chosen as the experimental reference. Three models of Series 58; namely, Model 4159, 4158 and 4154 are chosen for investigation in this thesis. Different mesh configurations with varying mesh densities in the boundary layer and along the body are generated for Model 4159. These mesh configurations are analyzed with different turbulence models and near wall modeling approaches. Moreover, the mesh is adapted to suitable wall y+ values depending on the mesh requirements of the turbulence model being used. The variation of total resistance coefficient in a Reynolds number range between 2x106 and 2.5x107 is obtained and compared with experimental data. Results revealed that realizable k – ε with EWT gives accurate results over the range of Reynolds numbers provided that the mesh is fine enough with wall y+ value around 1. The same conclusions are drawn from the analyses of Models 4158 and 4154 as well. Therefore, realizable k – ε turbulence model with EWT is used for the rest of the studies. Results of the validation studies are given in Chapter 4.

Forward motion of the vehicle at 2 m/s is analyzed using the realizable k – ε turbulence model with EWT. Three different body configurations with different appendages are used. The aim is to understand the effect of appendages on total drag force. Same body configurations are also analyzed for the vertical motion with a velocity of 0.5 m/s. Drag force values that are obtained from these analyses are used for the selection of an appropriate thruster for the vehicle. Results of forward and vertical motion analyses are given in Chapter 5.

.

In Chapter 6, manufacturing of the vehicle is given. It should be noted that manufacturing is done by a company; therefore, only an overview of the process is provided.

7.2 Future Work Recommendations

Studies performed in this thesis provide many beneficial recommendations for future unmanned underwater vehicle design projects.

Employing a floodable hull is beneficial in many aspects. First of all the watertight section is limited to a smaller volume which reduces the amount of sealing surfaces and the risk of leakage. Secondly, floodable sections provide room for equipments like pressure transducer which need to operate in water. Finally, the floodable hull increases the wetted surface area of the pressure hull and increases its heat rejection capabilities. As a result, the maximum temperature in the pressure hull reduces. This effect is demonstrated in Chapter 3 where two different models are used for heat transfer analyses. Second model includes the effect of flood water; hence, the maximum temperature in the pressure hull is found to be lower.

Even though preliminary heat transfer analyses performed in this thesis provide beneficial information, it is hard to rely on these data due to certain reasons. First of all, they are two-dimensional. Secondly, electronic equipments are not modeled in detail; instead, only simplified models are used. It may be a better choice to make use of three-dimensional analyses where components are modeled with more detail. Commercial programs like ICEPAK may also be useful for such analyses.

Although simple two-equation models like realizable $k-\varepsilon$ with EWT and $k-\omega$ SST provide accurate results for simple flows like the flow over a bare hull, their accuracy is questionable for more complex flows like the flow over the vehicle with appendages. Therefore, utilization of more complex turbulence models like Reynolds Stress Model (RSM) or Large Eddy Simulation (LES) approach should be considered.

The protrusions out of the body contribute to the total drag of the vehicle considerably as shown in Chapter 4. The largest contribution is from cameras in that they have significant extensions out of the body in the front end of the vehicle. High pressure values are experienced at this region due to stagnation of flow. Moreover, cameras disturb the flow in this region and cause separation as seen from pathlines of the flow. The combined effect of high pressure and separation cause a significant contribution from cameras. Locating cameras inside the hull is a remedy to this problem. The nose of the hull can be made to be transparent so that the cameras can work in the hull.

For vehicle design projects with higher demands on movement capabilities, it will be necessary to perform additional analyses. Maneuvering of the vehicle should be investigated for such cases. Developing the dynamic model of the vehicle is usually performed to solve this problem. Adding thrusters into the computational model is also an important issue. Thrusters affect the flow field and surface pressure distribution on the vehicle. Consequently, drag force values change considerable. It should be noted that thruster performance is also affected by the flow field. Due to that modeling the vehicle with thrusters helps the designer to investigate the performance of thrusters and enable to adjust thruster configuration.

REFERENCES

[1] Blidberg, D. R., *The Development of Autonomous Underwater Vehicles (AUVs); A Brief Summary*, IEEE International Conference on Robotics and Automation, Seoul, Korea, 2004.

[2] Langebrake, L. C. (2003), *AUV Sensors for Marine Research*, In: G. Griffiths (ed.), *Technology and Applications of Autonomous Underwater Vehicles,* CRC Press, p:245-246.

[3] Wernli, R. L., Christ, R. D., *The ROV Manual: A User Guide for Observation Class Remotely Operated Vehicles*, Elsevier Butteworth-Heinemann, 2007.

[4] Jalbert, J., Baker, J., Duchesney, J., Pietryka, P., Dalton, W., D.R. Blidberg, Chappell, S. G., Nitzel, R., Holappa, K., *Solar-Powered Autonomous Underwater Vehicle Development*, Proceedings of the 13th International Symposium on Unmanned Untethered Submersible Technology, Durham, NH, 2003.

[5] Hyakudome, T., Aoki, T., Tsukioka ,S., Yoshida, H., Ishibashi, S., Inada, T., Kabeno, T., Maeda, T., Hirokawa, K., Yokoyama, K., Tani, T., Sasamoto, R., Nasuno, Y., *Fuel Cell Underwater Vehicle URASHIMA*, 14th International Offshore and Polar Engineering Conference, Toulon, FRANCE, May 23-28, 2004.

[6] Küçük, K., *Modeling and Motion Simulation of an Underwater Vehicle,* MS Thesis in the Middle East Technical University, 2007.

[7] Wernli, R., *AUV Commercialization – Who's Leading the Pack?,* Oceans 2000, Providence, RI, 2000.

[8] Chance, T. S., Kleiner, A. A., Northcutt, J. G., *Reducing Deepwater Survey Costs: The Impact of Contrasting Technologies,* C & C Technologies, Inc.

[9] Department of the Navy (USA), *The Navy Unmanned Undersea Vehicle (UUV) Master Plan,* November 2004.

[10] Jolie, E. W., *A Brief History of U.S. Navy Torpedo Development*, NUSC Technical Document 5436, September 1978.

[11] Madhan, R., Desa, E., Prabhudesai, S., Sebastião, L., Pascoal, A., Desa, E., Mascarenhas, A., Maurya, P., Navelkar, G., Afzulpurkar, S., Khalap, S., *Mechanical Design and Development Aspects of a Small AUV-MAYA,* IFAC MCMC2006, Conference on Manoeuvring and Control of Marine Craft, Lisbon, Portugal, 2006.

[12] Bowen, A. D., Yoerger, D. R., Taylor, C., McCabe, R., Howland, J., Gomez-Ibanez, D., Kinsey, J. C., Heintz, M., McDonald, G., Peters, D. B., Fletcher, B., Young, C., Buescher, J., Whitcomb, L. L., Martin, S. C., Webster, S. E., Jakuba1, M. V., *The Nereus Hybrid Underwater Robotic Vehicle for Global Ocean Science Operations to 11,000m Depth,* OCEANS 2008, Vols. 1-4, p:1281-1290, 2008.

[13] Desset, S., Damus, R., Hover, F., Morash, J., Polidoro, V., *Closer to Deep Underwater Science with ODYSSEY IV Class Hovering Autonomous Underwater Vehicle (HAUV)*, IEEE Oceans 2005 Europe, Brest, FRANCE, 2005.

[14] Ohata, S., Ishii, K., Sakai, H., Tanaka, T., Ura, T., *Development of an Autonomous Underwater Vehicle for Observation of Underwater Structures*, Oceans 2005, Vol. 3, p:1928-1933, 2005.

[15] Georgiadesa, C., Nahon, M., Buehlera, M., *Simulation of an Underwater Hexapod Robot,* Ocean Engineering, Vol. 36, Issue 1, p:39-47, January 2009.

[16] Joubert, P., *Some aspects of submarine design Part 1. Hydrodynamics,* Defence Science and Technology Organisation, Technical Report, 2004.

[17] Gertler, M., *Resistance experiments on a systematic series of streamlined bodies of revolution for application to the design of high-speed submarines*, DTMB Report C-297, Bethesda, 1950.

[18] Bertram, V., Alvarez, A., *Hydrodynamic aspects of AUV design*, 5th Conf. Computer and IT Applications in the Maritime Industries (COMPIT), Leiden, pp.45-53, 2006.

[19] http://auvac.org/resources/browse/

[20] Cavallo, E., Michelini, R. C., Filaretov, V. F., *Conceptual Design of an AUV Equipped with a Three Degrees of Freedom Vectored Thruster,* Journal of Intelligent and Robotic Systems, Issue 39, p:365–391, 2004.

[21] Department of Defense, *Composite Materials Handbook Volume 3,* Department of Defense Handbook, 2002.

[22] Gay, D., Hoa, S. V., Tsai, S. W., *Composite Materials,* CRC Press, 2003.

[23] Balya, B., Senel, F., Miskbay, O., Parnas, L., *Comparison of Resin Transfer Molding Methods in Production of Composite Shell Structural Aerospace*

Components, 4. Ankara International Aerospace Conference, September 2007, Ankara.

[24] Yuh J., *Design and Control of Autonomous Underwater Robots: A Survey*, Autonomous Robots 8, 7-24 (2000).

[25] WS Atkins Consultants, *Best Practice Guidelines for Marine Applications of Computational Fluid Dynamics.*

[26] FLUENT 6.3 User's Guide.

[27] *Research Water Tunnels Specifications,* Rolling Hills Research Corporation.

[28] Gorski, J. J., *Drag Calculations of Unappended Bodies of Revolution,* Hydromechanics Directorate Research and Development Report, Naval Surface Warfare Center Carderock Division, 1998.